Digitized Theses
Digitized Special Collections

1978

X-ray Crystallographic Studies Of Optically Active Transition Metal Complexes

Richard George Ball

Follow this and additional works at: https://ir.lib.uwo.ca/digitizedtheses

NOTICE

AVIS

The quality of this microfiche is heavily dependent upon the quality of the original thesis submitted for microfilming Every effort has been made to ensure the highest quality of reproduction possible.

If pages are missing, contact the university which granted the degree.

Some pages may have indistinct print especially if the original pages were typed with a poor typewriter ribbon or if the university sent us a poor photocopy

Previously copyrighted materials (journal articles, published tests, etc.) are not filmed

Reproduction in full or in part of this film is governed by the Canadian Copyright Act, R.S.C. 1970, c. C-30. Please read the authorization forms which accompany this thesis.

La qualité de cette microfiche dépend grandement de la qualité de la thèse soumise au microfilmage. Nous avons tout fait pour assurer une qualité supérieure de reproduction

S'il manque des pages, veuillez communiquer avec l'université qui a conféré le grade.

La qualité d impression de certaines pages peut laisser à désirer, surtout si les pages originales ont été dactylographiées à l aide d un ruban usé ou si l'université nous a fait parvenir une photocopie de mauvaise qualité.

Les documents qui font déjà l objet d'un droit d'auteur (articles de revue, examens publiés, etc.) ne sont pas microfilmés.

La reproduction, même partielle, de ce microfilm est soumise à la Loi canadienne sur le droit d'auteur, SRC, 1970, c. C-30. Veuillez prendre connaissance des formules d'autorisation qui accompagnent cette thèse.

X-RAY CRYSTALLOGRAPHIC STUDIES OF OPTICALLY ACTIVE

TRANSITION METAL COMPLEXES

by

Richard George Ball

Department of Chemistry

Submitted in partial fulfillment

of the requirements for the degree of

Doctor of Philosophy

Faculty of Graduate Studies

The University of Western Ontario

London, Ontario

February, 1978

caveat illegitimi

ABSTRACT

In a study of the nature and extent of stereochemical interactions in optically active transition metal complexes, the structures of five complexes have been determined by X-ray crystallography. The absolute configurations of four of these were determined by the anomalous dispersion of X-rays. Intensity data were collected on an automated four-circle diffractometer and the structures were refined using full matrix least-squares techniques on F.

A Pt-diamine complex, $(-)_{280}$-cis-Dichloro(1-methyl-amino-2(S)-aminopropane)platinum(II), was examined for relationships between the observed chiroptical properties and the absolute configurations at the two asymmetric sites. The structure was refined to a conventional agreement factor of 0.035 using 3297 unique reflections for which $F^2 > 3\sigma (F^2)$. The complex is approximately square planar with an average Pt-Cl distance of 2.303(3) $\overset{o}{A}$ and an average Pt-N distance of 2.021(8) $\overset{o}{A}$. The absolute configuration of the chelate ring is δ and the N-methyl substituent is in the axial position.

The Pt(II) complex of a specific chiral sulphoxide displays high enantiotopic discrimination towards the co-ordination of selected prochiral olefins. Two of these complexes, containing coordinated olefins, were studied for interactions which could lead to the observed discrimination.

$(-)_{342}$-cis-Dichloro((S)-methyl p-tolylsulphoxide)

iv

(styrene)platinum(II). The structure refined to a final unweighted agreement factor of 0.029 using 2414 unique reflections for which $F^2 > 0$. The complex adopts a square planar coordination geometry, with the double bond of the olefin ligand at an angle of 77.6(6)$^\circ$ to the coordination plane. The absolute configuration at the olefin carbon atom, which becomes asymmetric upon coordination, is R. The configuration of the sulphoxide was confirmed to be S.

(+)$_{338}$-cis-Dichloro((S)-methyl p-tolylsulphoxide) (3-methyl-1-butene)platinum(II). The structure refined to a conventional agreement factor of 0.038 using 2820 unique reflections for which $F^2 > 2\sigma(F^2)$. The complex exhibits square planar coordination geometry with the double bond of the coordinated olefin tilted from the perpendicular by 5.7(6)$^\circ$. The absolute configuration at the asymmetric carbon atom of the olefin was determined to be S.

Rhodium(I) complexes of two optically active chelating phosphines give very high (70 - 100%) enantiomeric excesses in the catalytic asymmetric hydrogenation of selected unsaturated species. These complexes were examined for clues as to how an asymmetric environment about the metal atom is provided in order to give the necessary enantiotopic discrimination towards coordinating prochiral olefins.

(1,5-Cyclooctadiene)-(-)$_{589}$-2,3-bis(diphenylphosphino) butanerhodium(I) perchlorate, tetrahydrofuran solvate. The structure refined to a final conventional agreement factor of 0.040 using 6691 unique reflections for which $F^2 > 0$. The

cation is in a square planar configuration (if the diene is viewed as a bidentate chelating ligand) with average Rh-P and Rh-C distances of 2.271(4) and 2.24(1) $\overset{o}{A}$, respectively. The absolute configurations of the asymmetric carbon atoms of the phosphine were both determined to be S.

(Bicyclo[2.2.1]hepta-2,5-diene)-(+)$_{589}$-2,3-bis (diphenylphosphino)propanerhodium(I) perchlorate. The structure has been refined to an unweighted agreement factor of 0.092 using 4341 data for which $F^2 > 3\sigma(F^2)$. It has not proved possible to refine the structure completely as a result of crystal decomposition. The overall stereochemistry is square planar with average Rh-P and Rh-C distances of 2.28(4) and 2.19(9) $\overset{o}{A}$, respectively. The absolute configuration at the asymmetric carbon atom of the phosphine could not be confirmed using the anomalous dispersion technique; from chemical evidence it is assigned the R stereochemistry.

A program is described for a four-circle computer controlled diffractometer to aid in the optimization of the angular settings of a reflection.

ACKNOWLEDGEMENTS

The author wishes to express his appreciation and thanks to all those with whom he has worked during the years this research was carried out. Most especially to Nicholas Payne under whose aegis this time was rewardingly spent. R.F. Stepaniak and B.W. Davies as past coworkers, and D.H. Farrar, J.F. Richardson and D.W. Stephan as present colleagues are appeciated for their friendly help in pursuits both scientific and not. Other members of the chemistry department both here, and working for B. Bosnich at the University of Toronto, are thanked for helpful discussions and assistance.

TABLE OF CONTENTS

LIST OF PHOTOGRAPHIC PLATES

LIST OF TABLES

List of Tables continued

List of Tables continued

List of Tables continued

LIST OF FIGURES

List of Figures continued

NOMENCLATURE

The following is a list of the abbreviations and common names which have been used in this thesis.

Abbreviation	Chemical Name
Ac	acetyl
Anisyl	methoxyphenyl
Me	methyl
Ph	phenyl
^{i}Pr	isopropyl
COD	1,5-cyclooctadiene
NBD	norbornadiene (bicyclo 2.2.1 hepta-2,5-diene)
THF	tetrahydrofuran
Diop	2,3-0-isopropylidene-2,3-dihydroxy-1,4-bis(diphenylphosphino)butane
Chiraphos	2,3-bis(diphenylphosphino)butane
Prophos	2,3-bis(diphenylphosphino)propane

CHAPTER 1

INTRODUCTION

1.1 Preamble

The phenomenon of optical activity has been known and has received considerable investigation for more than a century. Despite this effort to understand the phenomenon, there are fundamental and important questions which remain unanswered.

A substance is optically active when it interacts differentially with plane polarized light, that is, the left and right circularly polarized components of plane polarized light are affected in a dissymmetric manner by passing through a medium which contains an optically active material (1). That a substance could be optically active was noticed more than a century and a half ago by Biot (2) and by 1848 Pasteur had concluded that for a substance to exhibit this anisotropic behavior towards plane polarized light the basic molecular structure must have a dissymmetry which gives the structure chirality (handedness) (3).

The concept of circular birefrigence (from which arises optical rotatory dispersion) and circular dichroism as tools for examining materials was not systematically applied until the 1890's when Cotton (4) studied the solutions of Cu(II) and Cr(III) (+)-tartrates. Early in this century Werner (5) established the principles of the

stereochemistry of metal complexes and showed the presence of optical activity in these inorganic systems was a consequence of the stereoisomerism.

The theoretical aspects of optical rotation and circular dichroism were first approached through quantum mechanical calculations around the 1930's. This period produced the one-electron theory of Eyring *et al.* (6), and the coupled oscillator model of Kirkwood (7). These were extended and reworked by Moffitt and others during the late 1950's (8), during which time the Cotton effects in d-d transitions of transition metal complexes began to be examined by Moffitt and others (9,10). While a detailed discussion of these various approaches to optical rotations and circular dichroism is well beyond the scope of the work in this thesis, these theories are the basis for the development of sector rules and the referenced literature contains the necessary details. Suffice it to say that optical activity is associated with electronic transitions' occurring in a chiral environment such that the scalar product of the electronic and magnetic dipole moments for the transition is nonzero (11).

1.2 Optical Activity in Transition Metal Complexes

Transition metal complexes exhibit optical activity with respect to the metal d-d transitions for a variety of reasons. The complex may be inherently dissymmetric with the site of asymmetry located at the metal atom as, for

example, in the square pyramidal complex $\left[C_5H_5Mo\right.$ $(CO)_2$ $\left.(C_6H_5CH(CH_3)N=CHC_5H_4N)\right]$ (12) or the dissymmetry may arise from contributions from the attached ligands. In this regard there are four generally accepted sources.

   i) A configurational contribution caused by a dissymmetric orientation of chelate rings about the metal atom, such as in the isomers of tris-(ethylenediamine)cobalt(III) (13).

   ii) A conformational effect arising from a preferred dissymmetric conformation of a chelate ring. A saturated five-membered chelate ring has two extreme conformations, as depicted in I and II, which are mirror images. If, due to stereochemical interactions, these two forms cannot interconvert then a dissymmetric molecule may be formed (14,15).
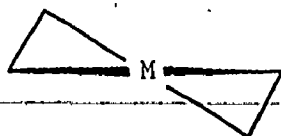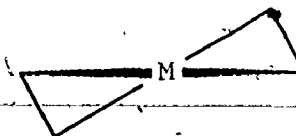
     I   II

iii) A vicinal effect which is ascribed to the presence

of asymmetric sites on the chelate rings (16).

iv) Donor atom vicinal effects arising from dissymmetric

ligating atoms. The dissymmetry of the donor atoms

can arise by substitution with dissimilar groups or,

potentially at least, by dissymmetric distortions of

these atoms about the metal atom (17).

These contributions may be affected by the presence and
distribution of asymmetric and symmetric unidentate ligands.
The usual ordering of these sources of dissymmetry with
respect to the magnitude of their observed optical rotatory
effect is configurational>conformational≥vicinal. These
characterizations of the contributions to optical activity
for transition metal complexes have been the basis for
extensive theoretical (10,18-22) and empirical studies
(23-30) attempting to relate the observed spectroscopic
properties to the absolute configuration and spatial
dispositions of the attached ligands.

X-ray crystallography is in principle capable of
unambiguously determining the absolute configuration of an
asymmetric complex (see section 1.7) and, to date, is the
only method which can accomplish this. The technique has
been used to examine many asymmetric complexes (31), and
some of these structural determinations have been used to
test predictions of the absolute configurations based on
information from circular dichroism studies. However,
despite modern advances which simplify the determination of

a crystal structure it is still a somewhat cumbersome and time consuming process to attempt for every optically active complex for which the absolute configuration is required. It is not surprising, therefore, that considerable effort has gone into attempts to find a single rule which will successfully relate absolute configurations and stereochemical relationships to observable circular dichroism effects. At the present time there is a plethora of such rules [1,10,18-30] all of which have serious restrictions on their generality.

1.3 Sector Rules and Optical Activity

. The development of sector rules has generally been predicated upon the one-electron theory of optical activity [6] and the general symmetry relations developed by Schellman [10]. To date the rules which have been developed are for correlation of the observed circular dichroism spectrum with the absolute configuration and stereochemical relationships for some specific types of complexes. Bosnich has formulated a sector rule [29] for ML_6 complexes possessing O_h zeroth - order microsymmetry about a metal atom with saturated chelate type ligands. Although successful for several cases this rule has been attacked by Richardson as having no theoretical basis [20]. Richardson, using semi-theoretical calculations, determined a set of sector rules which could be applied to various types of $Co(III)L_6$ complexes. In other papers Richardson [18,19]

has discussed the formulation of sector rules for tetragonal and pseudotetragonal complexes where the zeroth-order microsymmetry about the metal atom is D_{4h}. Mason has also proposed sector rules for the ML_6 and ML_4X_2 type complexes. For the ML_6 chromophore Mason asserts, contrary to Bosnich, that the contributions to the optical activity from the configurational effect, caused by the arrangement of the chelate rings, and the conformational effect, arising from a preferred dissymmetric conformation of the puckered chelate rings, must be considered under separate rules (32). For the ML_4X_2 complex having D_{4h} symmetry Mason provided experimental evidence (25) to support the sector rule developed by Schellman (10). Richardson using a semi-quantitative theoretical approach succeeded in developing a similar rule (18,19).

The application of these rules has been almost solely to first row transition metal complexes, in particular to Co(III) complexes of various substituted diamines (16) and the amino acid and peptide complexes of Cu(II) and Ni(II)(16). Indeed, Richardson has pointed out that for Pt(II) and Pd(II) complexes there is insufficient information available about relative energies for d-d excited states to apply a quantum mechanical approach to sector rules for these complexes (19).

To quote from one of the latter papers on this topic (29) "...a rational description of the observations

[structure - spectra relationships] has been given in terms of a general rule, but because of the number of uncertainties involved in its application it is of little practical value at the present time." Although this was said about a particular sector rule this statement sums up the current state of all the sector rules quite well and the field appears likely to remain at this impasse for some time yet. For this reason, among others, the emphasis in the research into optically active complexes has been shifting from spectra - structure relationships to the use of these complexes in asymmetric synthesis.

1.4 Asymmetric Synthesis

The goal of an asymmetric synthesis is to prepare one enantiomer of a chiral product using achiral reagents and an optically active catalyst or template molecule. This is a field of research which has been investigated by organic chemists for a hundred years but only in the last decade or so has it begun to capture the imagination of inorganic chemists. One of the aspirations of the researchers in this field is to mimic the ability of biological systems to routinely and rapidly prepare all manner of chiral species from simple achiral molecules.

A generalized mechanism for an asymmetric synthesis using a transition metal complex as a template molecule involves: i) the coordination of a chiral or prochiral (33) molecule to the asymmetric metal complex, and ii) the

stereospecific reaction of this coordinated chiral molecule with some substrate followed by the isolation of the resulting chiral product. These chiral or prochiral substrates are often unsaturated molecules since these can both be good ligands and provide sites for further reaction after coordination.

The study of metal coordinated olefins is one area of metal - unsaturated molecule interactions which has received an enormous amount of attention in the last three decades and has been the subject of several recent reviews (34-37). The extensive chemistry exhibited by these complexes includes carbonylation, hydrogenation, hydro-silation, isomerization and polymerization reactions which are often useful in commercial applications. Hence, considerable effort has been directed towards understanding the nature of the metal - olefin interaction and its role in these reactions.

1.5 The Metal - Olefin Bond

The Dewar - Chatt - Duncanson description (38,39) forms the basis for the most generally accepted model of the interaction between an olefin and a metal atom. In this theory a σ bond is formed by overlap of the filled π component of the olefin bond with an empty d hybrid orbital on the metal. Exactly which orbitals are involved and to what extent each contributes to this hybrid is a facet which has not yet been completely determined (40,41).

In addition to the σ bond a π bond is postulated to form from overlap of filled metal d orbitals/hybrids with the π* (antibonding) orbitals of the olefin.

In square planar Pt(II) complexes there are two d orbitals which have the appropriate symmetry to overlap with the olefin antibonding orbital and form the π bond. There is the d_{xy} orbital which lies in the xy plane (defined as shown) and the d_{xz} which is perpendicular
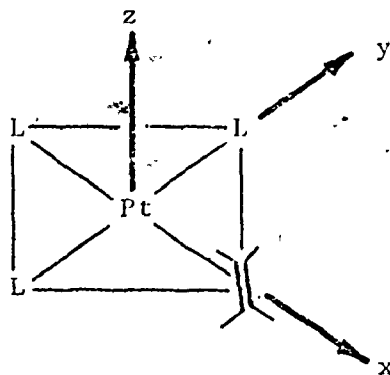
to this plane. Thus the olefin can rotate between two possible configurations, one in which the double bond is in the square plane and one in which it is perpendicular to this plane. The two d orbitals involved are not of the same energy, so there is a barrier to rotation between these two configurations. Experimental determination of the magnitude of this barrier from nmr studies (42) necessarily reflects all the steric as well as electronic contributions to this energy and this composite value is roughly 40 - 60 KJ mole^{-1}. Although this rotation about the metal - olefin σ bond is commonly observed in solution,

the solid state configuration of all square planar d^8
metal - olefin complexes have the olefin in the perpendicular
configuration (37). This observation has been rationalized
in that, on the basis of electronic considerations, the
perpendicular orientation is indeed the lowest energy
configuration (37,40).

Although facets of metal - olefin bonding such as
lengthening of the C-C bond (37) and bend back of the
olefin substituents (37), appear to be adequately ration-
alized within the current form of the D - C - D scheme.
others are not so well explained. For instance, the actual
mechanism of olefin rotation is not well understood (43)
nor are tilting (the pointing of the C-C vector away from
the metal atom) and sliding (the positioning of the C-C
bisector out of the mean coordination plane about the
metal) of coordinated olefins.

1.6 Asymmetric Metal - Olefin Complexes

When an olefin is dissymmetrically substituted at
one or both carbons involved in the double bond then these
atoms can be considered to be prochiral sites (33). If
such an olefin coordinates to a metal atom an asymmetric
unit, depicted in Figure 1.1a, is formed (44). The
dissymmetrically substituted carbon, now also coordinated
to the metal, has four different groups attached to it
and as such the absolute configuration at this chiral
center can be described as R or S using the rules of Cahn,
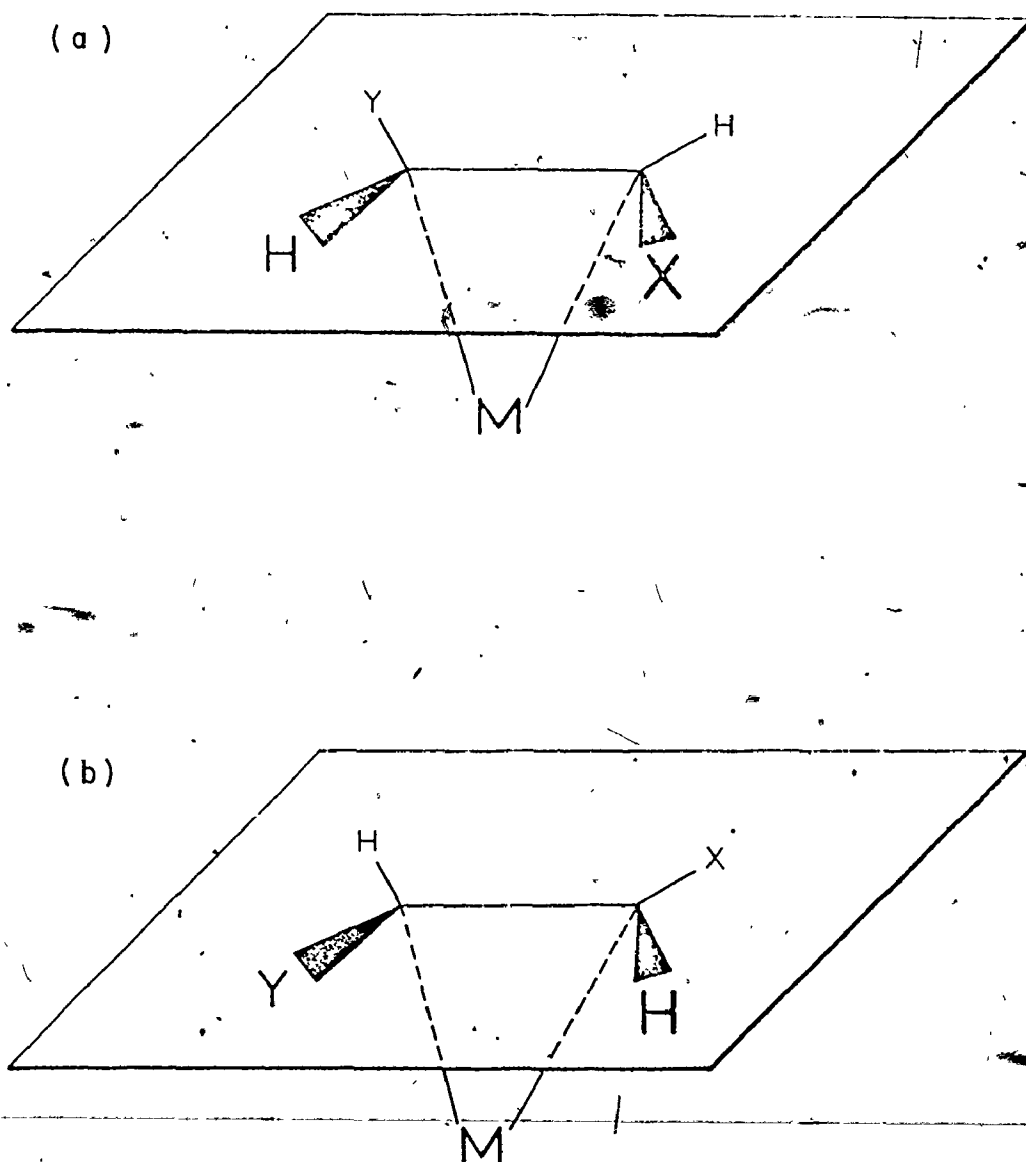
Figure 1.1 (a) Olefin coordinated in R,R configuration;
(b) coordinated olefin with S,S configuration

Ingold and Prelog (45). That such a prochiral olefin has two enantiotopically related faces is demonstrated in Figure 1.1b, where the olefin in Figure 1.1a has been rotated 180° about the carbon-carbon double bond and the result is to change the absolute configuration at the dissymmetrically substituted carbons from R to S . Thus if an asymmetric transition metal complex is going to be used as a template molecule in an asymmetric synthesis using prochiral olefins it must cause preferential coordination of one of the enantiotopic olefin faces with a high degree of specificity.

The attack of a variety of nucleophilic species upon a coordinated olefin is an example of a reaction using metal coordinated olefins in asymmetric synthesis. This type of reaction is the basis for several commercial metal - olefin processes including oxidation, carbonylation and alcoholysis (34). It is the coordination of the olefin to the metal atom which reduces the electron density around the double bond thereby rendering the olefin more susceptible to nucleophilic attack. For example, the stereochemistry of the reaction of diethylamine with 1-butene coordinated to Pt(II) in the S form has been determined by Paiaro (46) and was shown to occur with almost complete stereospecificity to yield (S)-2-butylamine with an optical purity of 95.5%. As shown by this reaction and others (34,47) the nucleophilic attack on monoolefins coordinated to Pt(II) occurs almost-exclusively exo with respect to the metal atom.

Thus if a chiral ligand coordinated to Pt can serve to induce preferential coordination of one of the enantiotopic faces of the prochiral olefin, a useful synthetic route is available for the asymmetric synthesis of a variety of products. Boucher and Bosnich (43) have developed a chiral sulphoxide ligand which can discriminate up to 75% with respect to a particular chirality for selected monoolefins. This is the highest discrimination available to date in these systems. Two Pt(II) complexes of this sulphoxide with different olefins coordinated have been examined crystallographically and the results are presented and discussed in Chapters 3-5.

To be able to design an asymmetric synthesis using the approach discussed above, it is necessary to control which diastereoisomer will be produced from the template complex and the incoming prochiral molecule. This task requires an intimate knowledge of factors such as electrostatic and steric interactions which can provide the necessary discrimination between diastereoisomers (48). At the present time this knowledge is in a rudimentary state and the information provided by the examination of stereotopic relationships and interactions in these complexes by X-ray crystallography may prove valuable in extending this knowledge.

Another area of asymmetric synthesis involving metal - olefin interactions which is receiving considerable attention of late is asymmetric hydrogenation using

homogeneous catalysts based on Wilkinson's complex
$(Rh(PR_3)_3Cl)$ but containing optically active phosphines
(49-52). The hydrogenation mechanism involving Rh(I) -
phosphine complexes has been extensively studied (53-56)
in achiral systems and appears to be reasonably well
understood. The general mechanism is discussed in more
detail in section 8.1.

The synthetic objective in these systems is to
preferentially coordinate one enantiotopic face of an
unsaturated substrate molecule to the metal catalyst where-
upon stereospecific hydrogenation of the substrate occurs.
Substrates commonly used are relatively small molecules
such as atropic, acrylic and cinnamic acids and substituted
styrenes. Currently research is being directed towards
studying how different phosphines, which incorporate
different sources of asymmetry, affect the coordination
preference for these substrates and therefore the optical
yields of the hydrogenation products. Examples of the
types of phosphines investigated include monodentate ones
with the P atom as the asymmetric site (49) as well as
seven- (52) and five-membered (57) chelating phosphines
having the asymmetric sites in the chelate ring. For a
chelating phosphine with the chiral center removed from
the P atoms there presumably is some mechanism for the
transmission of the asymmetry to the metal coordination
sphere. As will be discussed in Chapter 8 this transmission

is postulated to occur via a dissymmetric arrangement of the substituents on the P atoms. Two examples of chelating phosphines which show excellent ability to catalytically hydrogenate acrylic acid derivatives are (-)-2,3-bis (diphenylphosphino)butane and (+)-1,2-bis(diphenylphosphino) propane (57). To determine the absolute configurations of the Rh(I) complexes of these two ligands and to examine the metal - phosphine stereochemistry we undertook the crystallographic examination of both complexes. The results of this work are presented and discussed in Chapters 6-8.

1.7 Absolute Configurations and X-Ray Crystallography

The application of X-ray crystallography to determining the absolute configuration of molecules was not developed until the 1950's. At this time J.M. Bijvoet and his coworkers (58) made use of the correct expression for the total atomic scattering factor, f, which is in general complex, that is

$$f = f_o + f' + if'' \qquad 1.1$$

where f_o is the atomic scattering factor for a spherically symmetric atom for a radiation with a frequency much higher than that corresponding to any absorption edge, and f' and f'' are the real and imaginary components of the dispersion correction. The requirement for this form of the scattering factor expression arises from the nature of the interaction

between the incident X-radiation and the inner electrons of the atoms in the crystal (59). As the frequency of the X-rays falling upon the atoms approaches and passes through the absorption edge representing the natural frequency of the inner shell (K) electrons the phase of the co-vibrating electrons will deviate from π or zero (anomalous dispersion).

It had been determined in 1930 (60) that Friedel's law, which requires that the intensity for reflections related by a center of inversion be equal, was not always obeyed, but it wasn't until the scattering factor was formulated as a complex quantity that this observation could be incorporated into a method to solve absolute configurations. When a structure in which enantiomorphism is possible is solved by crystallographic techniques it is completely defined except for possible inversion (see section 2.3.1 (i)). With the proviso that there are atoms in the structure which will give rise to detectable anomalous dispersion then it is a relatively simple calculation which will show which of the two enantiomorphs gives rise to the observed intensity differences for the Bijvoet pairs of reflections (Bijvoet differences). Although this is not the only way to use anomalous dispersion effects to determine absolute configurations, see for example Okaya and Pepinsky (61), with the advent of automated diffractometers, having

quantum counters which can accurately measure the Bijvoet differences, it is the most common approach.

The determination of absolute configurations by crystallographic methods has been used increasingly widely over the last 25 years and is now a commonly accepted and practised technique for solving the problem of the absolute configuration of crystalline materials.

CHAPTER 2

THE X-RAY CRYSTALLOGRAPHIC EXPERIMENT USING DIFFRACTOMETER METHODS AND ITS APPLICATION TO THE STRUCTURE OF $(-)_{280}$-cis-DICHLORO(1-METHYLAMINO-2(S)-AMINOPROPANE)PLATINUM(II)

2.1 Introduction

The process of determining the structure of a crystalline material by the X-ray crystallographic method can be conveniently separated into three sections:

i) the determination of crystal symmetry and space group,

ii) the collection and processing of diffraction intensity data,

iii) and the solution and refinement of the molecular structure.

While each of these areas is common to a structural study, as the technique becomes more widespread in its use the procedures employed in each section may differ from laboratory to laboratory. Thus this chapter describes in detail the procedures followed, and where necessary the theory involved, for each of these stages in the structural determinations presented in this thesis. The experimental parameters for individual structures will be summarized in the chapters devoted to those complexes.

The application of the X-ray crystallographic experiment to the determination of the structure of cis-

dichloro(1-methylamino-2 (S)-aminopropane)platinum(II) is included in this chapter as a specific example of how the method is implemented in practice.

2.1.I Complex to be Examined

Analysis of the conformations of chelating ligands of the ethylenediamine type has indicated that these conformations are generally controlled by the nonbonding interactions associated with the puckered five-membered ring (14). Thus most C-substituted ethylenediamine ligands in octahedral complexes adopt a gauche conformation, with the substituent in the equatorial position and this arrangement appears to be favored by an energy of about 8 KJ mole^{-1} (14). Similar interactions are presumed to control the conformations of N-substituted ethylenediamine ligands and it would be expected that for monodiamine and *trans*-bisdiamine O$_n$ complexes of these ligands there should be smaller differences, on the order of 4 KJ mole^{-1}, between the free energies of the axial and equatorial isomers due to the decreased number of nonbonded intraligand interactions. Conformational energy minimization calculations on octahedral complexes of N-methylethylenediamine and N-methyl-1,2-diaminopropane have given a variety of results with respect to the energy differences of the axial and equatorial dispositions for the N-methyl groups (62,63). The later calculations indicate there should be a significant population of the axial isomer although the equatorial

disposition for the *N*-methyl group is preferred by about 2 KJ mole^{-1}. However, experimental investigations of the isomer populations in these systems (64,65) have not indicated the presence, at equilibrium, of significant amounts of the complexes containing the *N*-methyl substituent in the axial position. By contrast, for the square planar Pt(II) complexes of *N*-methylglycine a circular dichroism and ^{1}H nmr study (66,67) has shown the presence of the isomer with the *N*-methyl substituent axially disposed. Also, work by Bosnich and Sullivan (68) on a number of Pt(II) and (IV) complexes of *N*-methyl substituted 1,2-diaminopropane complexes showed there is little difference between the free energies of the axial and equatorial isomers (approximately 4 KJ mole^{-1}).

The two isomers of *cis*-dichloro(1-methylamino-2(*S*)-aminopropane)platinum(II) which contain the axial or equatorial arrangement of the *N*-methyl substituent have nearly identical linear absorption spectra but almost enantiomorphic circular dichroism spectra, an observation which was attributed to the change in the disposition of the methyl substituent at the nitrogen atom. The system represents a relatively simple model for studying the effect on the circular dichroism of the complex due to the conformation at an asymmetric donor atom. Thus we felt that the determination of the molecular structure and absolute

configuration of the two isomers would provide a good correlation between the observed stereotopic relationships and the circular dichroism spectra of the complexes.

2.2 Experimental Procedures

2.2.1 Crystal Selection

A representative crystal is selected from a sample of the compound. The one chosen should have clean, well-developed faces and be of an appropriate size for the experimental conditions. The effect of crystal size and shape on the measurement of reflections by photographic and diffractometer methods has been extensively discussed (69,70) and an optimum choice for the types of complexes examined in this thesis would be an equidimensional crystal of approximately 0.25 mm in cross-section. The chosen crystal is examined with plane polarized light as a preliminary determination of crystal quality. A crystal lattice which is single will alternately extinguish and transmit the polarized light every $90°$ if the symmetry of the lattice is not isotropic. Thus the appearance of areas of the crystal which do not extinguish at the same time is usually indicative of macroscopic twinning of the crystal lattice. In order to discover the symmetry of the lattice and unit cell parameters a photographic examination is undertaken employing the Weissenberg and precession techniques.

2.2.2 Photographic Study

A geometrical requirement for Weissenberg photo-
graphy (70) is a crystal rotating about a direct lattice
vector which is coincident with the camera spindle axis.
This technique provides a photographic record, albeit
distorted, of the reciprocal lattice layers perpendicular
to the rotation vector, that is, for a crystal rotating
about b the layers $h0l$, $h1l$, $h2l$, etc. can be recorded.
Interpretation of these photographs is often not trivial
but the procedures are well described in a variety of texts
(for example 70) and need not be detailed here.

Precession photography (70,71) complements the
Weissenberg technique by permitting recording of that portion
of the reciprocal lattice inaccessible to the Weissenberg
method when the same crystal mount is used. For precession
photography the crystal must rotate about a reciprocal lattice
vector, and the reciprocal lattice image recorded by the
precession technique is a direct magnification with no
distortion of the geometrical relationships between
reciprocal lattice points. This simplifies and increases
the accuracy of the measurement of the crystal lattice
parameters from these photographs.

An examination of these photographs with respect
to reflection intensities and any systematic absences
permits the determination of the elements of symmetry
present in the crystal lattice. Often this is an unambiguous

assignment particularly when optically active compounds are being investigated since it is necessary that these compounds crystallize in acentric space groups. For example the two monoclinic space groups $P2_1$ and $P2_1/m$ (72), display the same systematic absences and both belong to the Laue symmetry class $2/m$. If the reflection intensities are not sufficiently different to remove the mirror symmetry then the two space groups could not be distinguished by the photographs alone. However an optically active complex would necessarily crystallize in the acentric space group $P2_1$ thereby eliminating $P2_1/m$ as a possibility.

The precession photographs are usually chosen for measurement of interplanar spacings and angles to permit a more accurate determination of the unit cell parameters (71) than could be obtained from the Weissenberg photographs. Measurement of the crystal density and calculation of Z, the number of formula units per unit cell (91), permits comparison of the number of equivalent positions available in the unit cell with the number of molecules present to occupy those positions and hence determination of any site symmetry imposed on these molecules.

Once the space group and unit cell dimensions have been determined from the photographic study a new crystal is chosen for the collection of intensity data, which in this laboratory is carried out by an automated four-circle diffractometer.

The crystal data for *cis*-dichloro(1-methylamino-2

(S)-aminopropane)platinum(II) are summarized in Table 2.4.

2.2.3 Collection of Data

The data for the structures comprising this thesis were all collected on a Picker Corporation FACS-1 diffractometer (Plate) controlled by a Digital Equipment Corporation PDP8-L computer using a variety of different software systems, some based on the original Busing and Levy programs (73,74) and some written locally by the author (Chapter 9).

The crystal chosen for data collection is cemented to a thin glass fiber using fast drying epoxy resin and this fiber is in turn cemented into a brass holder. This unit is then secured into either a eucentric or fixed (x,y,z translations only) goniometer head which is subsequently transferred to the diffractometer.

The geometrical conditions of a four-circle diffractometer experiment are illustrated in Figure 2.1. The first objective is to determine the matrix which will relate the a^*, b^*, c^* axes of the reciprocal cell to the x,y,z axial system of the diffractometer. This is accomplished by first manually centering the crystal with the aid of a microscope until it appears to lie at the point of intersection of the $\phi, \chi, 2\theta$ circles. The crystal is then oriented with respect to the diffraction plane such that a lattice plane, usually axial, of known hkl values is in a

TABLE 2.1

CRYSTAL DATA FOR cis-$Cl_2Pt(CH_3NHCH_2CHCH_3NH_2)$

Formula	$C_4H_{12}Cl_2N_2Pt$
Fw	354.15
Crystal Description	Pale yellow equidimensional blocks
Systematic absences	$h00$ for h odd, $0k0$ for h odd, $00l$ for l odd
Laue symmetry	mmm
Crystal system	Orthorhombic
Space group	$P2_12_12_1$
Cell constants	$a = 10.488(3)$ Å $b = 11.034(4)$ $c = 7.432(2)$
Cell volume	860.21 Å^3
Density (calculated)	2.734 g cm^{-3}
(observed)	$2.706(1)$ g cm^{-3}
Density measured by	Neutral bouyancy in $C_2H_4Br_2$ and CH_2I_2
Z	4
Symmetry constraints	None
Crystal faces (12)	$\{110\}$, $\{101\}$, $\{001\}$
Crystal dimensions	$0.24 \times 0.21 \times 0.18$ mm
$\mu(MoK_{\alpha_1})$	162.06 cm^{-1}

PHOTOGRAPHIC PLATE

The Picker FACS-1 Four-Circle Diffractometer
Employed in this Study
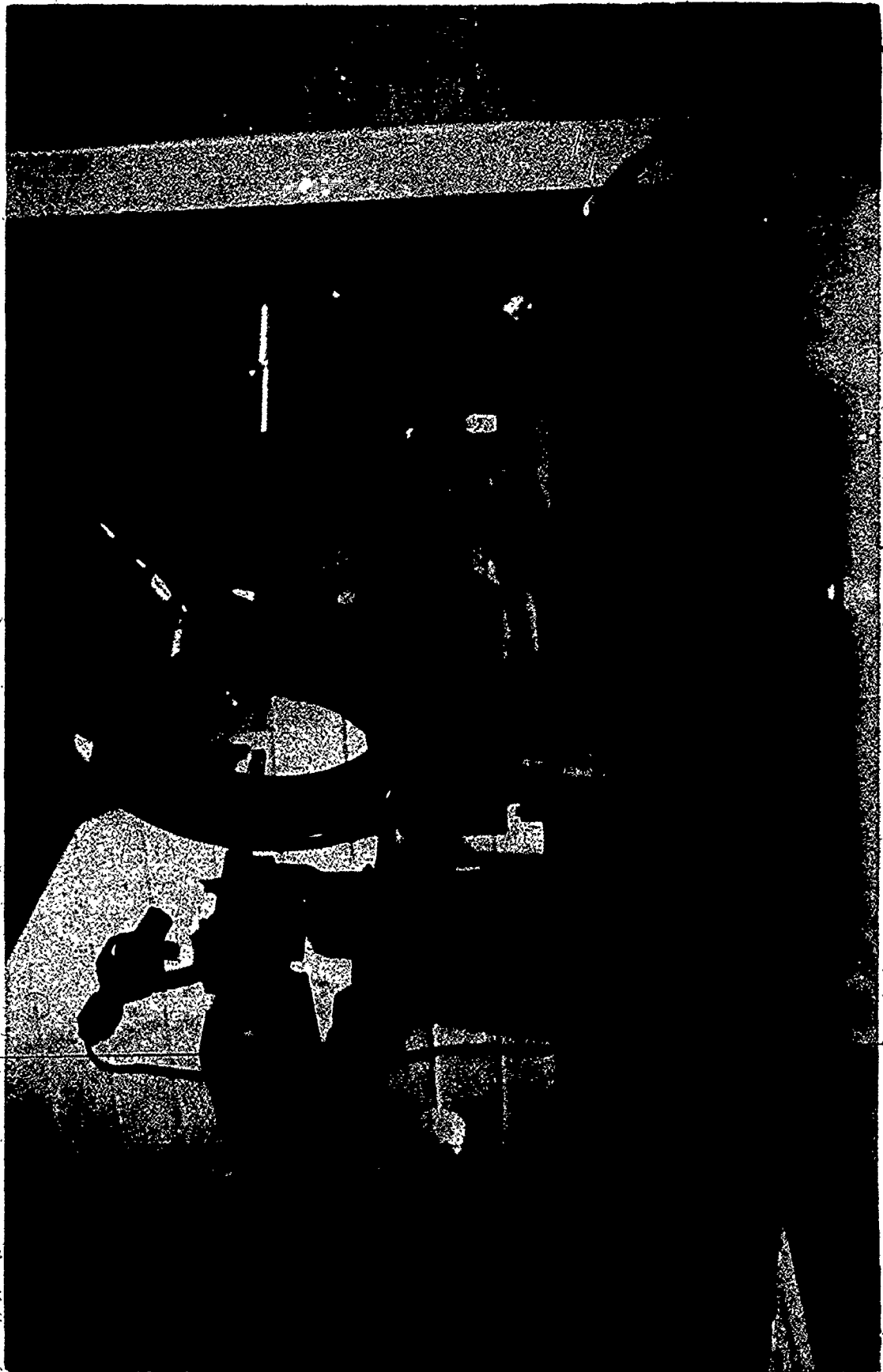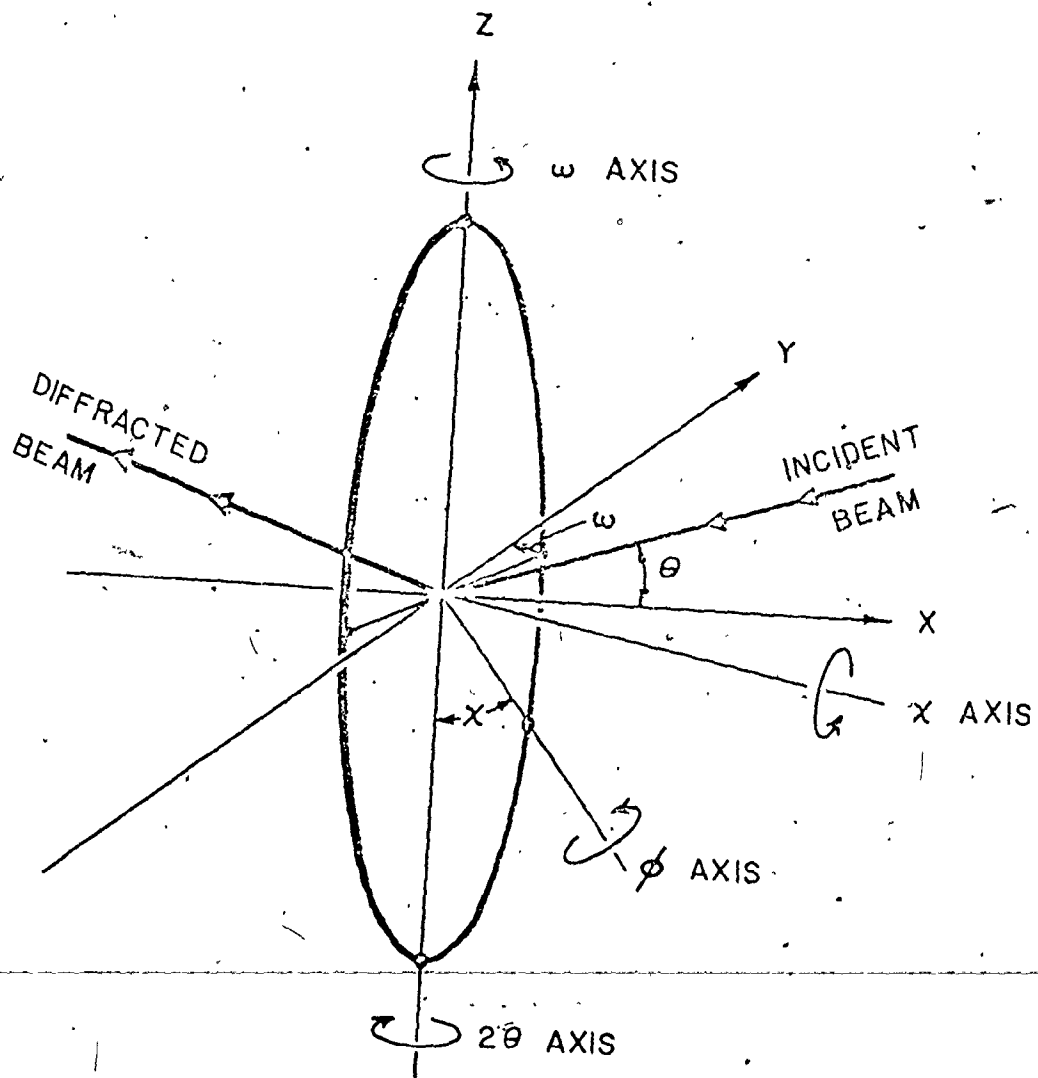
Figure 2.1 Geometry of a four-circle diffractometer

position to diffract. Location of a second reflection on
another axis by the same method is followed by the calculation
of the requisite matrix using the unit cell parameters
determined from the photographic study and the angular
positions for these two reflections (73). Confirmation of
the correct labelling for the axes is made by comparison of
the calculated and observed 2θ values for axial reflections
and a comparison of the relative intensities for a series of
reflections on the films and on the diffractometer.

The next step is to confirm the accuracy of the
positioning of the crystal at the center of the diffractometer,
that is, the point of intersection of the three independent
diffractometer circles 2θ, χ and ϕ . This is accomplished
by determining as precisely as possible the angular values
of a specific reflection measured at the following four
equivalent positions:

i) 2θ, ω, χ, ϕ ii) -2θ, ω, χ, ϕ

iii) 2θ, ω, $\chi+180°$, ϕ iv) -2θ, ω, $\chi+180°$, ϕ

Mathematical manipulation of the values for the angles at
these four settings allows determination (75) of the presence
of any errors in the translational centering of the crystal
as well as any discrepancy in the positioning of the X-ray
source relative to the center of the diffractometer.

The crystal is now examined to determine if it is
of sufficient quality to warrant continuing with the experi-
ment. This is most easily accomplished by centering a

reflection accurately in the middle of the counter aperture
and recording an ω scan profile of the peak using a narrow.
source and a wide counter aperture. The width of the peak
at half-height is a measure of the crystal mosaicity with
acceptable values ranging from 0.05 to 0.10° (69). If the
crystal lattice is appreciably twinned this will normally
result in marked asymmetry of the peak or in partial or
complete splitting of the peak. Should examination of the
peaks for a selection of axial and off axial reflections
indicate acceptable quality the process of aligning the
crystal is continued, if not a new crystal is found and
the evaluation process is repeated.

The procedure of centering a reflection involves
careful adjustment of the various diffractometer angles in
order to position the reflection accurately in the diffraction
plane and on the sphere of reflection. This whole process
can be automated to a great extent and the computer programs
written to handle reflection centering can adequately cope
with most types of peaks arising from crystals which are
suitable for data collection. However there are different
approaches to the problem and two such methods, compared in
Chapter 9, exemplify this point. The basic method used in
this laboratory is to use the Kα radiation peak (69), as
generated from a narrow source, and center the reflection
using a pinhole aperture which is as small as possible and
yet still allows a significant counting rate (not less than
about 20 cps). The incident radiation is filtered using an

appropriate metal foil chosen so that its X-ray absorption edge will strongly attenuate the Kß radiation peak (76).

Once a suitable crystal is found the diffractometer is used to measure the unit cell constants to a greater degree of precision than obtained by the measurement of photographs. A selection of the more intense reflections, chosen from the regions of reciprocal space from which the diffraction intensity data will be garnered, are carefully centered using the procedure described above and detailed in Chapter 9. The angular settings for all the centered reflections are used as input to the non-linear least-squares program PICKTT*. The parameters varied are the unit cell constants, the three orientation angles relating the unit cell axes to the diffractometer coordinate system and the angle zero for the diffractometer angle χ to account for any systematic error in the centering with respect to this angle. Also calculated are the estimated standard deviations for the parameters which were varied.

Having completed this initial phase the experimenter may now proceed to collect the intensity data necessary to solve the structure. The procedure followed to collect this data is dependent both on the diffractometer used and the crystal chosen.

Our diffractometer hardware includes a scintillation counter connected to a pulse height analyser which is adjusted to accept 90% of the X-ray energies symmetrically disposed about the Kα energy level. The diffractometer is

---

* This and other programs used in this work are described in Appendix 1.

also set up such that if the counting rate exceeds approximately 10^4 cps copper foil attenuators, with accurately determined attenuation factors, are automatically inserted between the crystal and the counter to prevent coincidence losses during the counting process.

The set of crystal dependent parameters for which the conditions are determined by the crystallographer include: (i) the number and types of data to be collected; (ii) scan type, range and speed; (iii) X-ray source intensity, collimator and counter aperture size; and (iv) the method of monitoring crystal and data quality over the course of data collection. The approach used to determine the conditions for the structures reported here is detailed below.

The number of data collected must be sufficient to uniquely determine the structure. Which data are collected, in terms of hkl, depends on the symmetry elements present in the space group. The presence of this symmetry renders some classes of reflections equivalent (77) thereby decreasing the number of unique data which can be collected. However, it is advantageous to collect sufficient reflections made equivalent by symmetry elements present so that some statistical analyses can be made to evaluate the magnitude of the errors in the final measured intensities. For acentric space groups, in which optically active complexes crystallize, the data collected will also include Bijvoet pairs if this method is going to be used to determine the absolute configuration of the structure. The data are collected in

shells of 2θ, each containing approximately the same number of reflections, for specified hkl ranges.

The reflections are scanned by the $\theta-2\theta$ moving crystal - moving counter method (69) with background counts taken at the high and low angle scan limits. The scan range is initially determined by scanning through a selection of representative peaks and picking 2θ values which encompass the full peak and give relatively equal background values. This range is automatically corrected for $\alpha_1-\alpha_2$ dispersion of the $K\alpha$ radiation which is a function of $\tan\theta$ (78). The scan speed is chosen to give good counting statistics, to minimize the exposure time of the crystal to X-radiation and to maximize the number of data which can be collected in a given time.

The take-off angle for the X-ray source is adjusted to give 80-90% of the maximum intensity of a strong low angle reflection. The choice of collimators and counter aperture size is dictated by the size of the crystal (69). For crystals of approximately 0.25 mm on a side 1 mm collimators are used and an aperture large enough to prevent vignetting of the peak (4 x 4 mm).

The crystal quality and machine fluctuations are monitored by repeatedly measuring a set of standard reflections (usually 100-200). A visual record is also made by means of a strip chart recorder. If these checks indicate a significant deterioration of the crystal,

a collection is halted and a new crystal is found from which to collect the remaining data.

Table 2.2 presents the conditions used for data collection in the structural determination of the title complex. A drawing of the crystal used is given in Figure 2.2.

2.2.4 Data Reduction

The term data reduction refers to the process of applying the necessary corrections to the measured intensities in order to accurately transform them into the square of the structure factor modulus

$$I \propto |F|^2$$

Corrections are applied for Lorentz, polarization, background, decay and absorption effects. The magnitude of these effects and the method of application of the corrections is dependent on the geometrical configuration of the diffractometer used to collect the intensity data. For the Picker diffractometer used in this research the data reduction is handled by the program WOFACV.

The Lorentz correction is applied because the time required for a reflection to pass through the sphere of reflection is not constant but varies with 2θ such that the correction is an inverse function of $\sin 2\theta$. Thus those reflections with $\theta \neq 45°$ will be more intense than they should be.

TABLE 2.2

EXPERIMENTAL CONDITIONS ASSOCIATED WITH DATA COLLECTION

Radiation	MoK$\bar{\alpha}$
Wavelength	0.71073 $\overset{\circ}{A}$
Take-off angle	2.0°
% of intensity available	90%
Tube Kv,mA	40, 18
Filter	Nb foil (0.07 mm) prefilter
Temperature	19°C
Collimator size	1.0 mm
Aperture size	4 x 4 mm
Crystal-counter distance	32 cm
Mean ω scan width	0.07°
No. and 2θ range of centered reflections	24, $18 < 2\theta < 38^\circ$
Scan range; speed	0.8° for $0 < 2\theta < 45^\circ$, 1.0° $2\theta > 45^\circ$; 1° min^{-1}
Miller index range	$0 \leq h \leq 19$, $0 \leq k \leq 20$, $-14 \leq l \leq 14$
2θ shells	3-45°, 45-55°, 55-65°, 65-75°
Background count time	10s for $2\theta < 65^\circ$, 20s for $2\theta > 65^\circ$
Standards	02$\bar{1}$, 040, 021, 0$\bar{4}$0, 020, 004; recorded every 200 reflections.
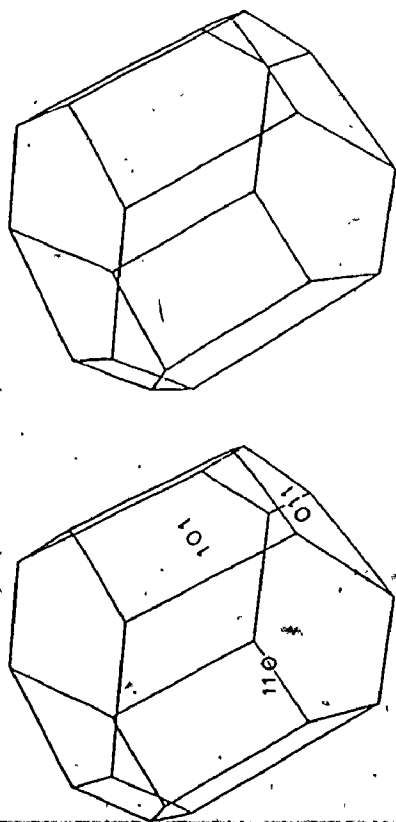
Figure 2.2 Stereoview of crystal

The correction for polarization is also 2θ dependent and arises from the reduction of those electric vectors of the X-radiation which are perpendicular to the reflecting plane (79) thereby decreasing the observed intensity. The background contribution to the intensity is approximated by a linear relation between the high and low angle background counts taken at the scan limits.

The integrated intensity, I, is calculated from

$$I = CT - 0.5(B_1 + B_2)(t_c/t_b) \qquad\qquad 2.1$$

and the estimated standard deviation on I from

$$\sigma(I) = \left[CT + 0.25 \ (t_c/t_b)^2 \ (B_1 + B_2) + (pI)^2 \right]^{1/2} \qquad 2.2$$

where CT is the integrated peak count obtained in time t_c, B_1 and B_2 are the background counts obtained in time t_b and I is the intensity. The factor, p, is the so-called 'ignorance' factor and is included to account for both variations in the counting statistics and to prevent over weighting the more intense reflections (80).

The standard reflections are examined for a systematic decrease or increase in the intensities which would indicate a decay in the crystal quality or an alteration of crystal mosaicity. If the change is uniform for each of the standards then a correction can be applied to the measured intensity as a function of when the reflection was measured in order to minimize the effects of the change over the

course of data collection.

To correct for absorption of the X-ray beam as it passes through the crystal the analytical approach of De Meulenaer and Tompa (81) or the Gaussian integration method can be used. These techniques are fully described in reference 82 and are available in the program AGNOST. Which approach is chosen depends on the crystal size, shape and absorption coefficient. Trials using both techniques are run to determine which method will give the faster correction in terms of computer time, while maintaining an acceptable level of accuracy. In this laboratory the absorption correction is usually applied after the structure has been solved and refined to a point where it can be determined that the structural analysis can be carried to completion.

The results of the data reduction process applied to the data collected in section 2.2.3 are presented in Table 2.3.

Having determined a set of $|F_{hkl}|$ values by the above procedures it becomes the task of the crystallographer to find a trial structure for which the calculated values of the structure factor, F_c, will agree with the observed one, F_0. This process of finding the correct structural model is referred to as structure solution and refinement and will now be dealt with in more detail in reference to the structure of *cis*-dichloro(1-methylamino-2(S)-amino-propane)platinum(II).

TABLE 2.3

RESULTS OF DATA REDUCTION

Number of measured intensities	4920
Average standard change	+7%; intensity data uncorrected
The 'p' factor	0.02
Distribution of measured intensities	$-3426 > 3\sigma(I)$ $2\sigma(I) < 401 < 3\sigma(I)$ $\sigma(I) < 437 < 2\sigma(I)$ $656 < \sigma(I)$
Absorption correction method	Gaussian; 14x14x14 grid
Data absorption corrected	3827; $I > 2\sigma(I)$
Maximum, minimum transmission coefficients	0.147, 0.120
Pairs of equivalent reflections, and the symmetry relationship	119; $h0l$, $h0\bar{l}$
R factor for averaging equivalent reflections: nonabsorption corrected absorption corrected	0.035 0.032

2.3 The Crystal and Molecular Structure of $(-)_{280}$-cis-Dichloro(1-methylamino-2(S)-aminopropane)platinum(II)

2.3.1 Structure Solution and Refinement.

The major problem which must be overcome to solve a crystal structure is the assigning of phases to the $|F_{hkl}|$ quantities derived from the intensity data (83). The need for a phase arises from the structure factor equation (84)

$$|F_{hkl}| = (A^2_{hkl} + B^2_{hkl})^{1/2} \qquad 2.3$$

which implies

$$F_{hkl} = A_{hkl} + iB_{hkl} \qquad 2.4$$

and the phase angle α is defined by

$$\alpha_{hkl} = \tan^{-1}(B_{hkl}/A_{hkl}) \qquad 2.5$$

Thus when the $|F|$ quantities are measured experimentally the signs of A and B in equation 2.5 are unknown which makes the phase angle indeterminate. There is a variety of methods available to the crystallographer to solve this problem and one of the most powerful and commonly used techniques is the Patterson synthesis (85).

i) Patterson Methods

Using the Patterson synthesis to solve the structure circumvents the lack of knowledge regarding the phases for

the reflections since the $|F_{hkl}|^2$ quantities are used as
the coefficients in the calculation of the Fourier series
(83). The map generated from the Patterson synthesis has
peaks corresponding to the interatomic vectors between all
the atoms in the unit cell. The symmetry of the Patterson
function is that of the Laue group to which the space group
belongs. This arises because the space group translational
symmetry elements are altered to the nontranslational ones
(86) in accordance with the loss of information in using
the F^2 values as the coefficients. Thus, Patterson functions
are centrosymmetric, even for acentric space groups, since
any pair of atoms giving rise to a vector UV will also give
the vector VU. As a consequence of Friedel's law the
magnitude of these two peaks will be the same except when
the equality between F_{hkl}^2 and $F_{\bar{h}\bar{k}\bar{l}}^2$ is broken by the contri-
bution to the diffracted ray of atoms having an absorption
edge in the vicinity of the wavelength of the incident X-
radiation.

The peaks due to vectors between the heavier atoms
in the cell are usually readily identifiable since the peak
height, in the zeroth - order approximation, is proportional
to the product of the atomic numbers of the two atoms
involved. (86).

A Patterson synthesis calculated using the program
FORDAP resulted in the determination of the positional
parameters for the Pt and two Cl atoms.

ii)   Refinement Procedures

The crystallographic coordinates for the atoms located in the Patterson map are used as input to the first cycle of least-squares refinement carried out by the program WOCLS. We use this program to implement full matrix least-squares refinement on F by minimizing the function

$$\Sigma w (|F_o| - |F_c|)^2$$

where $|F_o|$ and $|F_c|$ are the observed and calculated structure factor amplitudes, respectively, and the weighting factor w is given by

$$w = 4F_o^2 / \sigma^2 (F_o^2) \qquad\qquad 2.6$$

In every structure included in this thesis the scattering factors, which describe the X-ray scattering power of the atoms in the molecule as a function of λ^{-1} sin θ, were those for the neutral atoms as listed by Cromer and Waber (87). The H atom scattering factors were taken from Stewart, Davidson and Simpson (88). The f' and f'' terms describing anomalous dispersion, as determined by Cromer and Liberman (89), were included in the calculations for the heavy atoms in the molecule as specified in the table summarizing the conditions for the final refinement.

The atomic parameters refined during the first cycle were the x,y,z positional parameters and isotropic thermal parameters (the form of the equation for the

isotropic and anisotropic thermal parameters is listed in Appendix 2) for the Pt and two Cl atoms. This refinement was based on the *hkl* data only. The residuals R_1 and R_2, defined by

$$R_1 = \Sigma ||F_o| - |F_c|| / \Sigma F_o; \quad R_2 = (\Sigma w(|F_o| - |F_c|)^2 / \Sigma w(F_o)^2)^{1/2};$$

are a means of testing how closely the structure factors for the trial structure approximate those measured experimentally (90,91) and were 0.102 and 0.111, respectively, after the first cycle. The remaining six nonhydrogen atoms were located by a difference Fourier synthesis. Using the quantities $|F_o| - |F_c|$ as the coefficients in the Fourier series and the calculated phases from the heavy atoms, results in an electron density map from which the contributions for the atoms already located are subtracted. This approach makes the subsequent location of the remaining atoms progressively easier. Two cycles of least-squares refinement of the positional and anisotropic thermal parameters for these nine atoms using the absorption corrected data resulted in $R_1 = 0.038$ and $R_2 = 0.033$.

iii) Location and Treatment of H Atoms

The twelve H atoms present in the molecule were evident in a difference Fourier synthesis as peaks of positive electron density in geometrically feasible positions. Idealized positional coordinates were computed, assuming tetrahedral coordination about both the N and C atoms, with

an N-H and C-H distance of 0.95 $\overset{o}{A}$. Two cycles of least-squares refinement, with the H atom contributions included but not refining their parameters, resulted in R_1 and R_2 values of 0.0357 and 0.0283 which represents a significant, in terms of Hamilton's R factor ratio test (92), improvement in R_2. In an attempt at a refinement of the positional parameters of these atoms it was found that the geometry of the six nonmethyl H atoms was acceptable while the methyl H atoms refined to positions yielding an unacceptable. geometry. Also the change in the R factor produced by refining the H atom positional parameters showed no significant improvement from the model with idealized positions. Accordingly, the H atoms were included in further calculations as fixed atoms in idealized positions each with an iso-tropic thermal parameter of 1.0 $\overset{o}{A}{}^2$ greater than that of the atom to which it is bonded.

      iv)   Extinction

       Extinction is an attenuation of the diffracted X-rays, not arising from absorption, which has two contri-butions referred to as primary and secondary extinction (93, 94). Primary extinction is a result of destructive inter-ference from multiply reflected rays which differ in phase by odd multiples of π. The effect is most noticeable for reflections from planes in a perfect crystal or, in the case of a real crystal, by the perfect blocks in the mosaic. If the size of these perfect blocks is small enough (95) then primary extinction effects are considered to be negligible.

It has not proved possible to correct for primary extinction in practice although it is theoretically possible to do so if the thickness of each of the contributing blocks is known (94,95). Secondary extinction occurs within the mosaic blocks when the incident beam is internally reflected by the first planes encountered which therefore prevents the deeper planes from receiving the same amount of incident energy. This reflection occurs with no particular phase relationship to the incident radiation since the blocks are optically independent. Zachariasen has suggested (95) that in general the effects of primary extinction are negligible for most real crystals while the effects of secondary extinction can be corrected for during the least-squares refinement of the structure. However, questions have arisen (96) about the value of this approach to correcting for secondary extinction and indeed as to whether primary extinction can be generally considered to be negligible.

Extinction effects are most noticeable for the intense reflections (low λ^{-1} · sin θ values) and refinement of an extinction parameter (95) results in better agreement between F_o and F_c for these reflections. During the last cycles of refinement the value obtained for the extinction coefficient was $2.51(9) \times 10^{-6}$ which corresponds to a maximum change in F_o of 2.8%.

v) Determination of Absolute Configuration

During the determination of the initial solution from the Patterson function an assumption was made as to which enantiomer of the model was present. Since the Patterson function is by its very nature centrosymmetric (section 2.3.2(i)) the vector used to solve for the heavy atom position could, equally as likely be the one centrosymmetrically related to that chosen. Therefore at some point in the structure determination one of the two enantiomeric models must be eliminated.

For the work done in this laboratory the approach used is to solve and refine the structure to a point such that the refinement is close to convergence. This model is then converted to its enantiomer, by inverting the positional parameters through the origin, and both models are refined under identical conditions for an additional cycle. For this structure the refinement for model A gave $R_1 = 0.038$ and $R_2 = 0.033$ while the enantiomeric model, B, had $R_1 = 0.049$ and $R_2 = 0.046$. Accordingly model A was used in the final refinement. After completion of the refinement procedure the enantiomeric model is again tested by refining it to convergence. The converged residual indices for model A were $R_1 = 0.0352$ and $R_2 = 0.0277$ while the alternative model, B, had values of $R_1 = 0.0471$ and $R_2 = 0.0426$. When comparing these indices Hamilton's R factor ratio test (92) is used and, for the values observed, the hypothesis that the second model is correct may be rejected at a confidence

level of greater than 0.995. In addition to using a
comparison of the weighted agreement factors two other
methods are commonly used to decide on the correctness of
the chosen model. Firstly, an examination of the geometries
of the two models for any gross discrepancies may indicate
an incorrect assignment of chirality (97-100). This
approach is of particular value when strongly anomalously
scattering atoms in the structure are aligned along polar
directions of the space group. Secondly, the observed and
calculated structure factors, based on the final refined
atomic parameters, can be compared for those Bijvoet re-
flection pairs with large contributions from the anomalously
scattering atoms. These reflections should show good agree-
ment if the structure is the correct enantiomer. Table 2.4
lists such a selection of structure amplitudes for reflec-
tions differing by more than 14%.

When a complex contains a site of known absolute
configuration then solving the structure such that this
chirality is preserved necessarily means that the correct
absolute configuration at all the chiral sites in the
molecule will be specified. For (+)-1-methylamino-2-
aminopropane the asymmetric C atom is presumed to be S
since the absolute configuration of the precursor is known
(66). Thus, that the model finally chosen on the basis of
the Bijvoet absorption edge technique also gives the S
absolute configuration at the chiral C atom supplies
additional evidence that the correct structure has been

TABLE 2.4

Determination of Absolute Configuration

h	k	l	$F_c(hkl)$	F_o Relationship	$F_c(hk\bar{l})$
1	10	2	19.34	<	25.29
2	6	4	29.51	<	34.06
3	2	6	19.82	<	24.52
7	4	1	18.56	<	21.76
9	6	1	20.04	<	23.11
2	2	8	17.15	>	13.02
6	6	6	16.01	<	18.46
7	3	6	16.53	<	20.65
1	1	3	61.71	<	70.91
4	5	6	22.00	<	25.17
6	2	2	34.41	>	29.41
6	4	1	37.87	>	32.39
14	3	4	18.45	<	21.20
1	4	4	18.99	≈	22.00
2	4	6	16.15	≈	13.59
3	8	2	13.99	>	17.54
3	6	6	19.27	≈	16.57
7	3	2	15.12	>	17.34

determined.

vi). Final Refinement

A summary of the conditions for the final cycles of refinement is presented in Table 2.5. Three cycles of full matrix least-squares refinement were used to converge the model with final residuals of $R_1 = 0.0352$ and $R_2 = 0.0277$. During the final cycle no parameter shift exceeded 0.01 of its estimated standard deviation indicating that the refinement had converged. Tables 2.6 and 2.7 list the final atomic positional and thermal parameters and the final derived H atom positional and thermal parameters, respectively. Structure factor amplitudes are listed in Appendix 3.

Upon completion of the refinement procedure a statistical analysis of the data is performed to examine how R_2 varies in terms of $|F_0|$, diffractometer setting angles χ and ϕ, $\lambda^{-1} \sin \theta$, and various combinations of Miller indices. There should be no correlation between any of these quantities and R_2 although we commonly see higher R_2 values for the reflections having low F_0 values. These increased R_2 values are usually around 10% but are based on a smaller number of observations than the values determined for the more intense data. Any correlations in this analysis may represent an inadequate weighting scheme or gross errors in the observed data which must be rationalized or corrected for, if they will affect the model. A difference Fourier synthesis is calculated from the final structure factors,

TABLE 2.5

CONDITIONS AND RESULTS FOR FINAL FULL MATRIX LEAST-SQUARES REFINEMENT CYCLE

Unique Observations	3297
Variables	83
Ratio (observations/variables)	39.7
Agreement factors R_1	0.0352
R_2	0.0277
Error on an Observation of Unit Weight	1.92 e
Maximum (parameter shift/esd)	0.01
Number of Anisotropic atoms	9
Number of H atom contributions included	12
Anomalous Scatterers	3; Pt, 2 x Cl
Extinction Coefficient	$2.51(9) \times 10^{-6}$
Remaining difference Fourier peak: a) Electron density	$0.53(13)$ e$\overset{o}{A}^{-3}$
b) Fractional coordinates	0.252, 0.057, 0.127
c) Associated with	Pt atom

Final Atomic Positional and Thermal Parameters*

TABLE 2.6

Atom	x	y	z	U11	U22	U33	U12	-U13	U23
Pt	1713.8(3)	1279.3(3)	1289.6(4)	222(1)	218(1)	295(1)	-4(1)	4(1)	-5(1)
Cl(1)	3598(2)	1719(2)	2778(3)	333(11)	456(13)	616(13)	-34(10)	-132(10)	-49(11)
Cl(2)	2258(2)	2473(2)	-1125(3)	475(11)	393(11)	473(12)	-80(9)	114(12)	125(12)
N(1)	85(6)	782(6)	68(8)	325(37)	324(37)	391(37)	-50(31)	-14(31)	111(28)
N(2)	1063(6)	175(5)	3269(8)	304(32)	257(30)	396(42)	28(27)	-33(27)	86(27)
C(1)	-776(6)	100(6)	1279(13)	261(32)	278(34)	411(39)	-42(29)	17(43)	60(43)
C(2)	96(8)	-645(7)	2484(10)	412(45)	296(41)	399(44)	-23(38)	-32(38)	47(34)
C(3)	-1750(10)	-646(9)	277(12)	483(55)	585(63)	675(60)	-193(64)	12(57)	-5(49)
C(4)	546(9)	835(10)	4862(10)	627(64)	679(72)	288(44)	-14(58)	-8(43)	-52(43)

*Estimated standard deviations in this and other tables are given in parentheses and correspond to the least significant digits.

The thermal ellipsoid is given by $\exp[-(B_{11}h^2 +B_{22}k^2 +B_{33}l^2 +2B_{12}hk +2B_{13}hl +2B_{23}kl)]$ and $U_{ij}=B_{ij}/(2\pi^2 a_i^* a_j^*)$ Å^2. The quantities

given in the table have been multiplied by 10^4.

TABLE 2.7

Derived Hydrogen Atom Positional* and Thermal Parameters

Atom	x	y	z	B
H1N(1)	-343	1489	-346	4.72
H2N(1)	289	285	-942	4.72
H1C(1)	-1220	667	2009	4.42
H1C(2)	506	-1258	1797	4.95
H2C(2)	-387	-1013	3417	4.95
H1N(2)	1758	-307	3671	4.46
H1C(3)	-2358	-955	1105	7.12
H2C(3)	-2162	-155	-592	7.12
H3C(3)	-1330	-1303	-307	7.12
H1C(4)	1205	1282	5433	6.14
H2C(4)	-111	1378	4487	6.14
H3C(4)	195	268	5698	6.14

*The positional parameters have been multiplied by 10^4.

over the full asymmetric unit for any remaining electron

density. The largest peak had an electron density of 0.53

(13) e$\mathring{A}^{-3}$ and was located 1.1 $\mathring{A}$ from the Pt atom. This

peak was not felt to have any chemical significance with

respect to the structure, and is probably due to series

termination effects (83) in the calculation of the Fourier.

2.3.3 Structure Description

A perspective view of a single molecule drawn by

the program ORTEP is shown in Figure 2.3 and includes the

atom numbering scheme. Table 2.8 contains selected inter-

atomic bond distances and angles with errors calculated

using the program ORFFE. The molecule exhibits square

planar coordination about the Pt atom with the two *cis* Cl

atoms, Cl(1) and Cl(2), 2.306(2) and 2.299(2) $\mathring{A}$,

respectively, from the metal atom. These distances and the

Cl(1)-Pt-Cl(2) angle of 92.27(8)° represent a normal

geometry for this moiety (101). The mean Pt-N distance is

unexceptional at 2.021(8) $\mathring{A}$ and the bond distances and

angles for the chelating ligand range from 1.479(9) = 1.521

(11) $\mathring{A}$ and from 105.5(6) - 113.8(6)° which are normal ranges

of values (102).

The five-membered chelate ring adopts the gauche

conformation, with δ absolute configuration. The methyl

group on C(1) is disposed equatorially with respect to the

plane of the ring, while the methyl substituent on N(2)

adopts the axial position making the absolute configuration
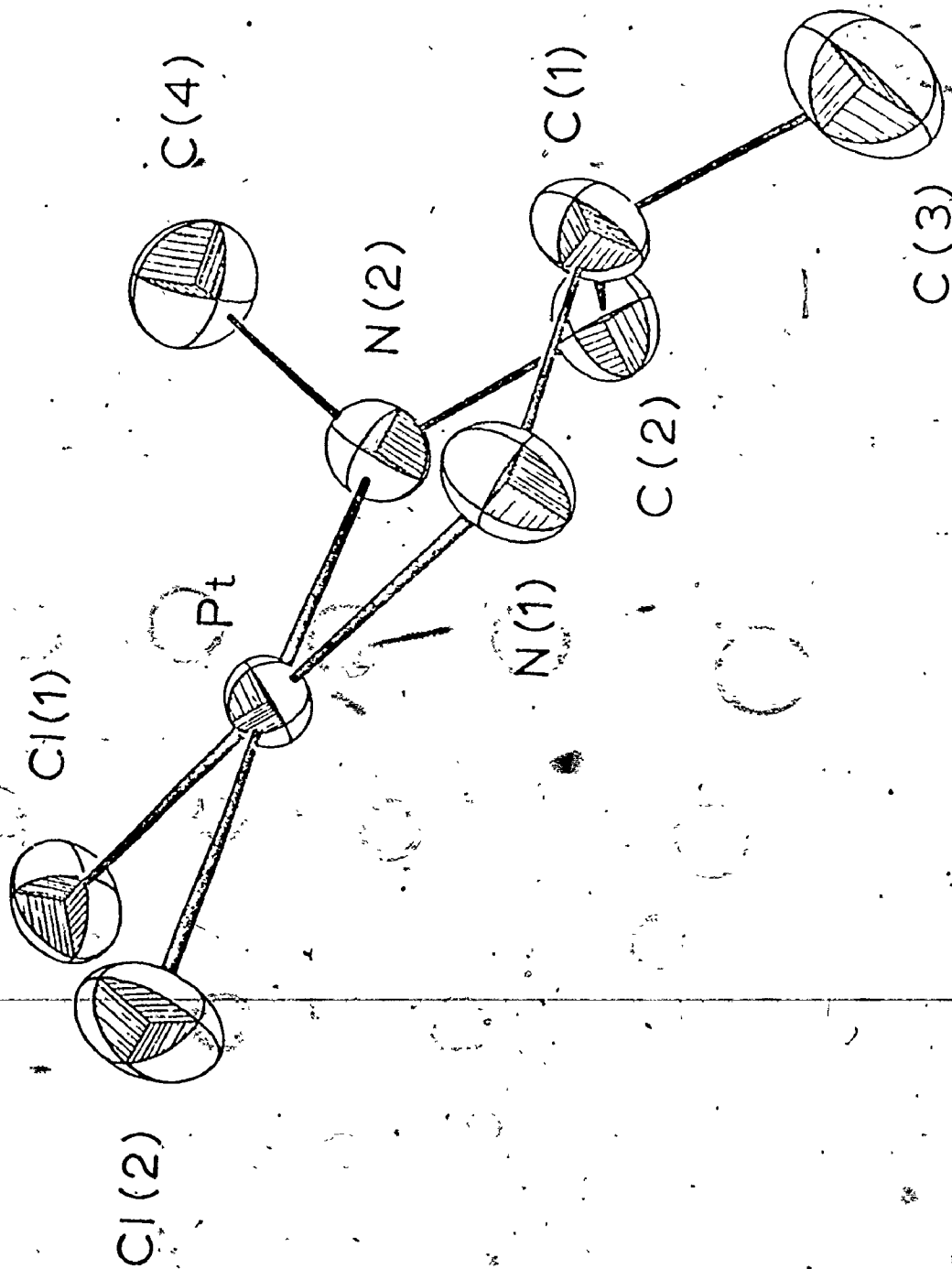
Figure 2.3 Perspective view of molecule including the atom numbering scheme

TABLE 2.8

SELECTED INTRAMOLECULAR BOND DISTANCES (Å) AND BOND ANGLES (deg)

Distances

Pt-Cl(1)	2.306(2)	N(2)-C(2)	1.479(9)
Pt-Cl(2)	2.299(2)	N(2)-C(4)	1.493(10)
Pt-N(1)	2.013(6)	C(1)-C(2)	1.521(11)
Pt-N(2)	2.028(6)	C(1)-C(3)	1.508(12)
		C(1)-N(1)	1.484(9)

Angles

Cl(1)-Pt-Cl(2)	92.27(8)	Pt-N(2)-C(2)	108.2(4)
Cl(1)-Pt-N(2)	93.84(18)	N(1)-C(1)-C(2)	105.5(6)
N(1)-Pt-N(2)	83.12(24)	N(1)-C(1)-C(3)	112.8(8)
N(1)-Pt-Cl(2)	90.75(18)	N(2)-C(2)-C(1)	108.3(6)
Pt-N(1)-C(1)	112.2(5)	C(3)-C(1)-C(2)-N(2)[a]	175.6(7)
Pt-N(2)-C(4)	113.8(5)		

[a] A clockwise rotation of C(3) through the indicated angle superimposes it on N(2) when looking from C(1) to C(2).

at this asymmetric centre S. The dihedral angle between
the normals to the planes formed by Pt, N(1), C(1) and Pt,
N(2), C(2) is 20.4(4)$^{\circ}$. Some least-squares planes and
selected atom displacements from these planes are presented
in Table 2.9.

Figure 2.4 shows the content of a unit cell and
serves to illustrate the packing between molecules in the
crystal. There appears to be no unusual intramolecular
contacts with the distance of closest approach being 2.50
$\overset{o}{A}$ between H2N(1) and H3C(4), and with the shortest Pt-Pt
interaction being 4.950(1) $\overset{o}{A}$.

2.3.4 Discussion

The absorption and circular dichroism spectra for
(-)-cis-dichloro-(1-methylamino-2(S)-aminopropane)platinum
(II) are presented in Figure 2.5 (68). The absorption
spectrum is very similar to that of cis-$\left[\text{Pt}(R\text{-pn})\text{Cl}_2\right]$
which was analysed (103) according to the ordering of the
metal d orbitals depicted in Figure 2.6.

TABLE 2.9

SELECTED WEIGHTED LEAST-SQUARES PLANES

Atoms of Plane 1 and Their Displacements from the Plane $(\overset{\circ}{A})$ [a]

Pt	-0.0002(3)		C(1)	-0.13
Cl(1)	0.011(2)		C(2)	0.53
Cl(2)	0.0015(22)		C(3)	0.39
N(1)	0.073(7)		C(4)	-1.31
N(2)	0.013(6)			

Atoms of Plane 2 and Their Displacements from the Plane $(\overset{\circ}{A})$

Pt	-0.0228		C(1)	-0.18
Cl(1)	0.005(2)		C(2)	0.48
Cl(2)	-0.004(2)		C(3)	0.32
N(1)	0.035(7)		C(4)	-1.36
N(2)	-0.026(6)			

Plane Equations of the Form $Ax + By + Cz - D = 0$

	A	B	C	D
Plane 1	4.64	-8.65	-3.24	-0.730
Plane 2	4.73	-8.58	-3.26	-0.686

[a] Displacements without esd's refer to atoms not included in the calculation of the plane
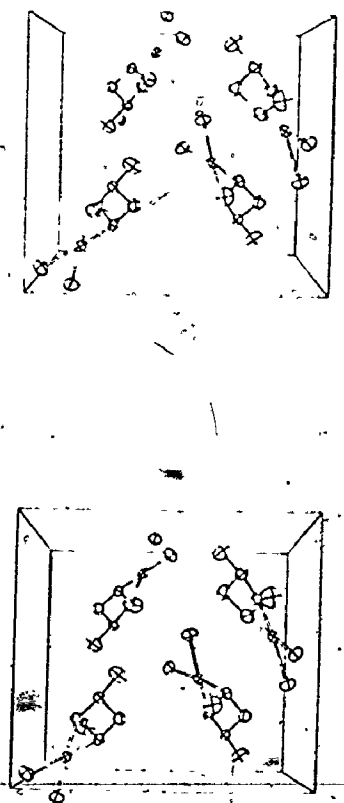
Figure 2.4 Stereoview of a unit cell contents. The a axis runs from left to right, with b vertical

Figure 2.5 Absorption and solution and solid state
circular dichroism spectra of $(-)_{280}$-
$[Cl_2Pt(CH_3NHCH_2CHCH_3NH_2)]^*$ (——); CD
solution spectrum of $[Pt(S-pn)Cl_2]$ (----)
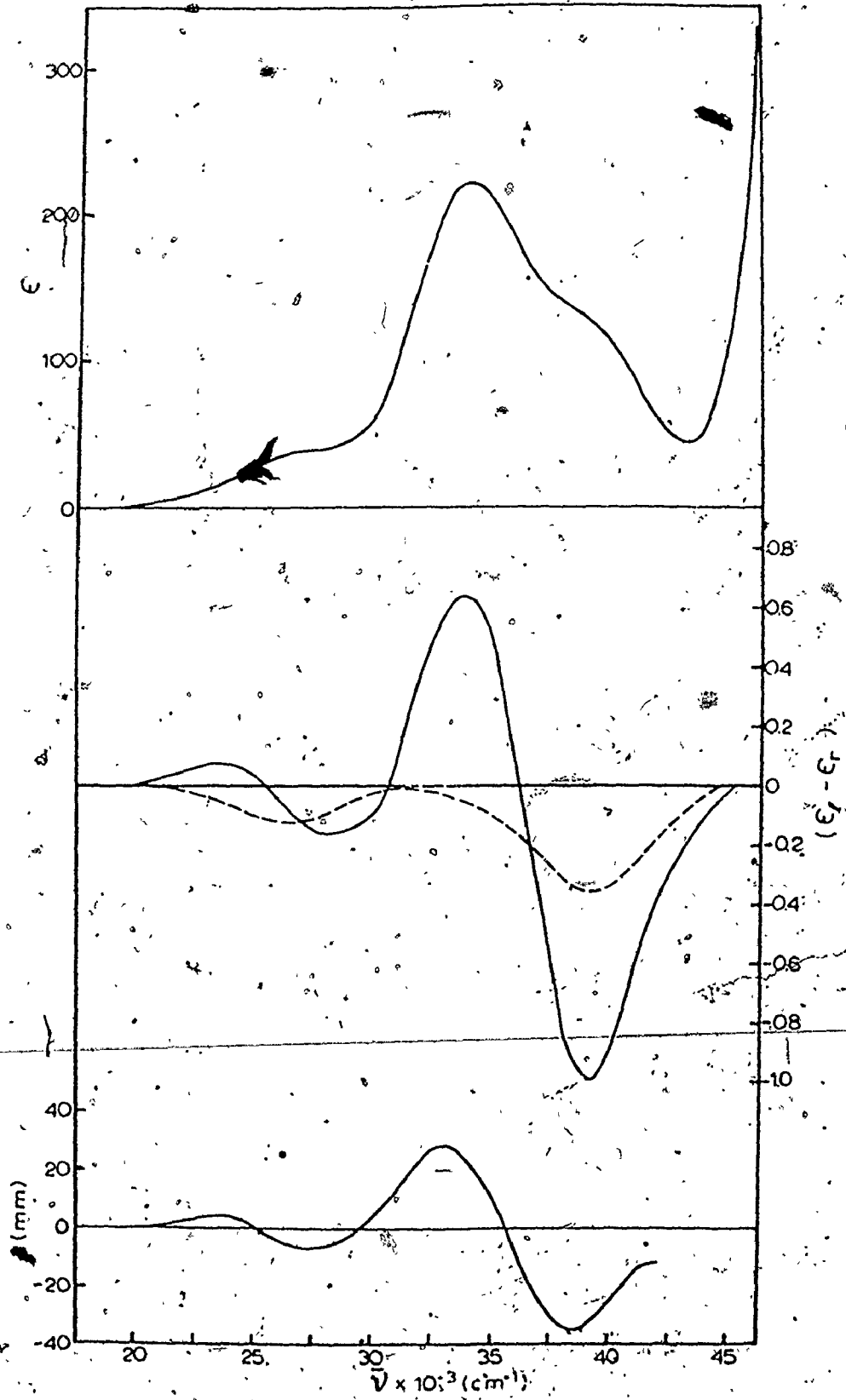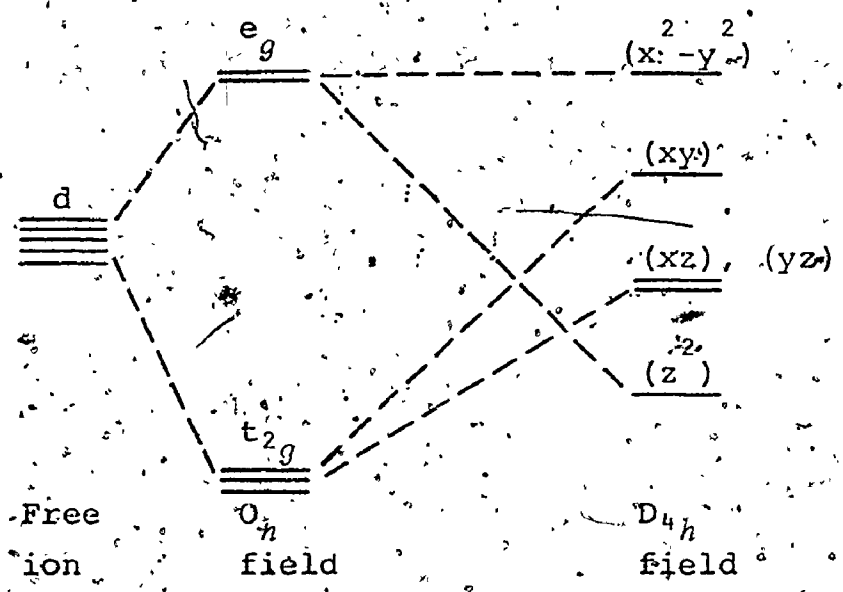
Figure 2.6 Relative ordering for Pt d-orbitals in square planar complexes.

This ordering assignment is based on the polarized crystal and magnetic circular dichroism spectra for $[PtCl_4]^{2-}$ (104), recent quantum mechanical calculations on this anion (105) and the determination of the relationship between crystal field strength and the d-d transitions for the complexes of the series $[Pt(NH_3)_n Cl_{4-n}]^{(n-2)+}$ (106). Using this relative ordering the absorption maxima at 33,000 and 36,500 cm are the $^1A_1 \rightarrow {}^1A_{2g}$ ($d_{xy} \rightarrow d_{x^2-y^2}$) and $^1A_1 \rightarrow {}^1E_g$ ($d_{xz,yz} \rightarrow d_{x^2-y^2}$) magnetic dipole, spin-allowed transitions, respectively. The broad absorption around 27,000 cm^{-1} is assigned to the singlet-triplet state transitions. The circular dichroism associated with the two spin-allowed transitions has been assigned in two ways (68): either the two CD bands are due

to the $^1A_{2g}$ and ^1E_g transitions separately or the two

absorptions arise from the split ^1E_g components with the

$^1A_{2g}$ transition being superimposed on the 33,000 cm^{-1}

band.

In the molecule *cis*-dichloro(1(S)-methylamino-2

(S)-aminopropane)platinum(II) the sources of dissymmetry

are restricted to a conformational contribution arising

from the five-membered chelate ring being in the δ con-

figuration, vicinal contributions from the two asymmetric

centers of the coordinated diamine (S at both the carbon and

nitrogen atoms), and lastly there could be a contribution

from the dissymmetric distortion of the donor atoms out of

the square plane about the metal atom. A similar complex,

cis-$[Pt(S$-pn$)Cl_2]$, would have the same sources of dissymmetry

except for the vicinal contribution from the asymmetric

nitrogen atom. Although the structure of this latter complex

has not been determined crystallographically it is presumed

to be structurally similar to the *N*-methyl analogue examined

in this chapter. The stereospecificity of the 1,2-pro-

panediamine ligand for an equatorial disposition of the C-

methyl group as a result of the non-bonded interactions

(section 2.1) would require the chelate ring to adopt the

δ configuration for an S absolute configuration at the

asymmetric carbon atom. It might also be expected that the

S-pn complex would have similar distortions of the donor

atoms. This similarity of structure has been used (68) to

propose that the contribution to the circular dichroism of the Pt(II) complex from the S-pn unit would be almost constant despite the presence of the N-methyl substituent.

In the circular dichroism spectra of the two isomers of the 1-methyl-2(S)-aminopropane complex it is observed (68) that for the isomer having N(2) in the S absolute configuration (axial methyl) the spectrum is almost enantiomorphic to that for the isomer with the R absolute configuration at N(2) (equatorial methyl). If the contribution from the S-pn chelate ring is a constant then it can be concluded that the spatial disposition of the N-methyl group, resulting in an R or S configuration at N(2), exerts a dominating influence on the circular dichroism spectra of these complexes. Similar effects have been noticed and conclusions drawn for the octahedral complexes of Co(III) containing trans-diamines of the N-methylethylenediamine and N-methyldiaminopropane types (27,66) and a rule was developed by Mason (25) to relate the signs of the CD bands for the d-d transitions to the disposition of the groups at the secondary nitrogen atom.

It was intended to continue this study by examining the structure of the complex containing the equatorial N-methyl group. Unfortunately the crystals of this isomer are not of good enough quality to permit a crystallographic study. This precludes a comparison of the geometries of the two isomers with the observed circular dichroism spectra.

2.4 Summary

This chapter was written to serve two purposes. Firstly, to acquaint the reader with the technique of crystallography as practised in this laboratory so that an informed opinion could be made as to the reliability of the work presented in this thesis. Secondly, to present the structure and absolute configuration of one isomer of *cis*-dichloro(1-methylamino-2(*S*)-aminopropane)platinum(II). In this latter regard it was shown that both chiral sites in the molecule have the *S* absolute configuration thus constraining the *N*-methyl group to be axially disposed. This information proved that the isomer which was slightly preferred at equilibrium (68) was the axial isomer.

CHAPTER 3

THE CRYSTAL AND MOLECULAR STRUCTURE AND

ABSOLUTE CONFIGURATION OF (-)$_{342}$-cis-DICHLORO(METHYL p-

TOLYLSULPHOXIDE)(STYRENE)PLATINUM(II)

3.1 Introduction

As was discussed in Chapter 1 a good deal of effort
has been expended in the last three decades to elucidate the
nature of the metal - olefin interaction and how this can
be used to influence the chemistry of these complexes. One
area which has been just recently investigated is that of
optically active metal - olefin complexes (34,107) and their
uses in asymmetric synthesis.

For monoolefin platinum(II) complexes, nucleophilic
addition to the coordinated olefin appears to occur
exclusively exo to the metal atom thereby giving rise to a
stereospecific product (34,46,47). Thus a prochiral olefin
coordinated to a platinum atom by only one of its enantio-
meric faces would, upon reaction with a nucleophile, give
an enantiomerically pure product.

The approach used by Paiaro (46,108) was to form
the Pt(II) complex of a monodentate amine containing an
asymmetric carbon atom which was to supply the necessary
discrimination towards the incoming prochiral olefins.
These complexes gave very low diastereoisomeric discrimina-
tion, but, by changing the amine to a chiral sulphoxide in

which the sulphur atom is asymmetric, as done by Boucher

and Bosnich (43), the discrimination towards which

chirality of a coordinated olefin was preferred was

observed to range from 52 to 75%. It was with a view to

determining the steric interactions which occurred when one

face of the olefin coordinated to the metal atom that the

structural studies presented in Chapters 3 and 4 were

initiated.

3.2 Experimental

Pale yellow crystals of (-)$_{342}$-*cis*-dichloro((S)-
methyl p-tolylsulphoxide)(styrene)platinum(II), $[Cl_2(CH_3(O)$
$S(C_6H_4CH_3))Pt(C_6H_5HC=CH_2)]$, were kindly supplied by H. Boucher

and B. Bosnich. From preliminary Weissenberg and precession

photography the crystals were found to be orthorhombic having

Laue symmetry mmm with systematic absences $h00$ for h odd,

$0k0$ for k odd and $00l$ for l odd.. These unambiguously

determine the space group to be $P2_12_12_1$, D_2^4, No. 19 (72).

The crystal and space group data are summarized in Table

3.1.

The crystal chosen for data collection (Figure 3.1)

was mounted with $[001]$ offset approximately ten degrees

from coincidence with the diffractometer ϕ axis. Cell

constants and an orientation matrix were obtained from a

least-squares refinement of the setting angles for 26

intense, carefully centered, reflections having 2θ between

15 and 48°. Prefiltered CuK$_{\alpha_1}$ radiation was used, $\lambda=1.54056$ Å,
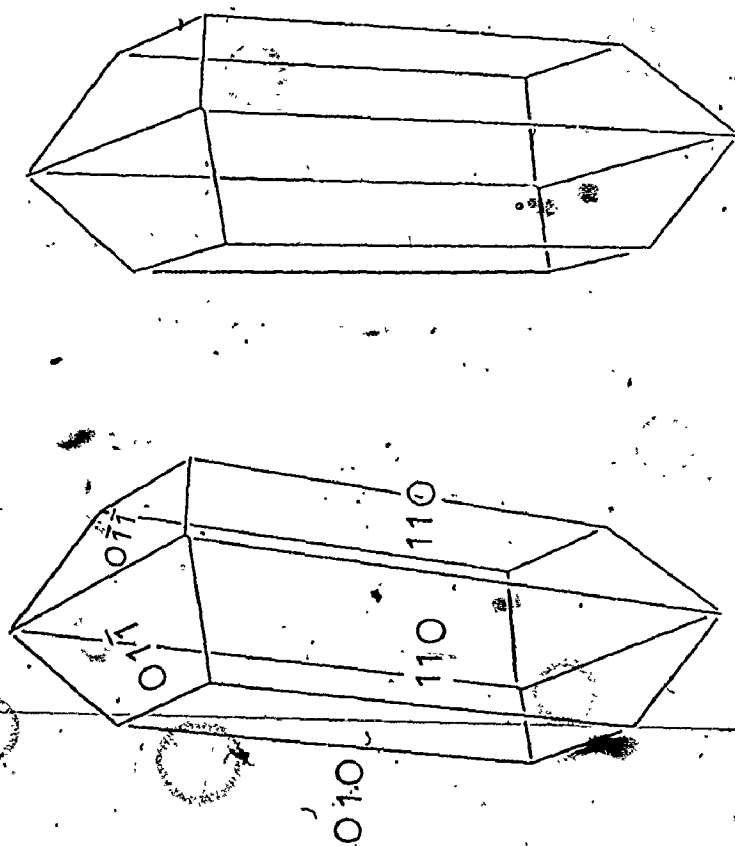
Figure 3.1. Stereoview of crystal

TABLE 3.1

CRYSTAL DATA FOR cis-$Cl_2[CH_3(O)S(C_6H_4CH_3)]Pt(C_6H_5HC=CH_2)$

Formula	$C_{16}H_{18}Cl_2OPtS$
Fw	524.38
Crystal description	Pale yellow prismatic crystals
Systematic absences	$h00$ for h odd, $0k0$ for $00l$ for l odd
Laüe symmetry	mmm
Crystal system	Orthorhombic
Space group	$P2_12_12_1$
Cell constants	$a = 11.633(4)$ Å $b = 15.055(5)$ $c = 9.776(3)$
Cell volume	1712.1 Å^3
Density (calculated)	2.03 g cm^{-3}
(observed)	$2.04(1)$ g cm^{-3}
Density measured by	Neutral bouyancy in aqueous ZnI_2
Z	4
Symmetry constraints	None
Crystal faces (10)	{110}, {110}, {001}
Crystal dimensions	$0.04 \times 0.06 \times 0.19$ mm
$\mu(CuK_{\alpha 1})$	189.9 cm^{-1}

at an ambient temperature of 20°C. Table 3.2 summarizes the conditions for data collection. The measurement of standard reflections during data collection and crystal mosaicity, by the ω scan technique, before and after data collection indicated no significant decomposition of the crystal quality had occurred. The intensity data were processed and the value for the empirical parameter p in equation 2.2 was chosen to be 0.01 from a statistical examination of the variations in the standard reflections. The results of the data reduction are presented in Table 3.3.

3.2.1 Structure Solution and Refinement

The solution and preliminary refinement of the structure were carried out using the 2224 data with $F^2 > 3\sigma(F^2)$. The positional parameters for the Pt atom were determined from a three-dimensional Patterson synthesis. Two cycles of least-squares refinement, followed by structure factor and Fourier synthesis calculations revealed the positions of the remaining 20 non-hydrogen atoms. Refinement of atomic parameters was carried out by full matrix least-squares techniques on F as detailed in Chapter 2.

One cycle of full matrix least-squares refinement on the molecule with the two phenyl rings constrained as rigid groups (D_{6h} symmetry, C-C=1.392 $\overset{\circ}{A}$ (109)) and varying the positional and anisotropic thermal parameters for the

TABLE 3.2

EXPERIMENTAL CONDITIONS ASSOCIATED WITH DATA COLLECTION

Radiation	CuK_{α}
Wavelength	1.54184 Å
Take-off angle	1.8°
% of intensity available	90%
Tube Kv,mA	40,16
Filter	Ni foil (0.18mm) prefilter
Temperature	20°C
Collimator size	1.0 mm
Aperture size	4 x 4 mm
Crystal-counter distance	32 cm
Mean ω scan width	0.08°
No. and 2θ range of centered reflections	26; $15 < 2\theta < 48°$
Scan range; speed	1.2°; $1°\,min^{-1}$
Miller index range	$0 \leq h \leq 13$, $-17 \leq k \leq 17$, $0 \leq l \leq 11$
2θ shells	$0-70°$; $70-110°$
Background count time	20s
Standards	002, 00$\bar{2}$, 040, 0$\bar{4}$0, 200, $\bar{2}$00; recorded every 200 observations

TABLE 3.3

RESULTS OF DATA REDUCTION

Number of measured intensities	2448
Average Standard Change	-1%, intensity data uncorrected
The 'p' factor	0.01
Distribution of measured intensities	$83 < \sigma(I)$ $\sigma(I) < 71 < 2\sigma(I)$ $2\sigma(I) < 71 < 3\sigma(I)$ $2223 > 3\sigma$
Absorption correction method	Analytical
Data absorption corrected	2448
Maximum, minimum transmission coefficients	0.768, 0.576
Pairs of equivalent reflections and the symmetry relationship	75; $hk0$, $h\bar{k}0$
R factor for averaging equivalent reflections: nonabsorption corrected absorption corrected	— 0.019

Pt, S, Cl, O and C atoms of the olefin resulted in values of $R_1 = 0.053$ and $R_2 = 0.075$. At this point the enantiomorphic structure was refined under identical conditions to R_1 and R_2 values of 0.042 and 0.0556 respectively. Accordingly, this second model was used in the subsequent calculations.

Of the eighteen H atoms present in the molecule, fourteen were evident in a difference Fourier synthesis, in geometrically feasible locations. The four which were not clearly discernable comprised one of the tolyl methyl group and the three olefinic H atoms. Idealized positional coordinates were computed, assuming sp^2 and sp^3 coordination geometries about the appropriate C atoms and an H-C bond distance of 0.95 $\overset{o}{A}$ for all the H atoms except those of the olefin. The H atoms were assigned isotropic thermal parameters 1.0 $\overset{o}{A}{}^2$ greater than those of the atoms to which they are bonded. The contributions for the H atoms were calculated and included in two cycles of refinement. A difference Fourier showed peaks in reasonable positions for two of the three olefinic H atoms while the third, coordinated to $C(2)$, remained a poorly defined smear of electron density. Two further cycles of full matrix least-squares refinement with the group constraints removed, allowing the C atoms of the phenyl rings to be refined as individual atoms assigned anisotropic thermal parameters, and the recalculated contributions from the H atoms included,

resulted in R_1 and R_2 values of 0.0249 and 0.0285 respectively.
At this point the third H atom of the olefin still could not
be adequately defined, so Fourier synthesis were calculated
over the appropriate region as a function of $\lambda^{-1} \sin \theta$.
This approach was taken to try and determine if the reason
for the difficulty in finding the H atom was its nearness
to the much heavier Pt and O atoms of the molecule. The
results of these calculations were inconclusive and this H
atom was not included in the final model. An attempt to
refine the H atom parameters did not result in a significant
improvement in the model and accordingly further refinement
included the contributions and did not refine any parameters
of the H atoms.

After recalculation of the non-olefinic H atom
positions the model was refined for three cycles using all
2414 data with $F^2 > 0$. The conditions and results of the
final cycle are presented in Table 3.4. A statistical
analysis of R_2 in terms of $|F_o|$, diffractometer setting
angles χ and ϕ, and $\lambda^{-1} \sin \theta$ showed no unusual trends. The
largest remaining peak on a total difference Fourier synthesis
calculated from the final structure factors was 0.52(15)
$eÅ^{-3}$ located 1.46 Å from the S atom and not chemically
significant. The data showed no evidence for secondary
extinction. Final positional and thermal parameters for
the non-H atoms are given in Table 3.5, and H atom para-
meters in Table 3.6. Structure factor amplitudes are
included in Appendix 3.

TABLE 3.4

CONDITIONS AND RESULTS FOR FINAL FULL MATRIX LEAST-SQUARES
REFINEMENT CYCLE

Unique Observations	2414
Variables	190
Ratio (observations/variables)	12.7
Agreement factors R_1	0.0292
R_2	0.0268
Error on an Observation of Unit Weight	1.86 e
Maximum (parameter shift/esd)	0.006
Number of Anisotropic atoms	21
Number of H atom contributions included	17
Anomalous Scatterers	4; Pt, 2 x Cl, S
Remaining Difference Fourier Peak: a) Electron density	0.52(15) e$\mathring{A}^{-3}$
b) Fractional coordinates	0.325, 0.240, -0.280
c) Associated with	S atom

2

1.0 2.8 2.5

3.2 2.2

3.6

1.1 4.0 2.0

1.8

1.25 1.4 1.6

4

TABLE 6.11

SELECTED WEIGHTED LEAST-SQUARES PLANES[a]

Plane 1   A = 0.624   B = -14.7   C = 5.35   D = -6.64[b]

C(21)	0.000(5)	C(24)	0.003(6)
C(22)	0.003(6)	C(25)	0.001(7)
C(23)	-0.005(7)	C(26)	-0.002(6)
		P(1)	0.242

Plane 2   A = -3.01   B = 0.951   C = 9.84   D = -0.674

C(31)	0.009(5)	C(34)	-0.006(8)
C(32)	-0.005(6)	C(35)	0.016(7)
C(33)	0.002(7)	C(36)	-0.015(6)
		P(1)	-0.006

Plane 3   A = 3.47   B = -16.9   C = 1.33   D = -4.88

C(41)	0.014(5)	C(44)	0.014(7)
C(42)	-0.007(6)	C(45)	0.004(7)
C(43)	-0.010(7)	C(46)	-0.016(6)
		P(2)	0.060

Plane 4   A = -0.544   B = -7.09   C = 8.61   D = -4.52

C(51)	-0.009(5)	C(54)	-0.010(7)
C(52)	0.011(6)	C(55)	0.007(7)
C(53)	-0.003(7)	C(56)	0.005(7)
		P(2)	0.181

Dihedral Angles (Deg) between Planes

Plane	Plane	Angle		Plane	Plane	Angle
1	2	57.80		2	3	81.90
1	3	24.98		2	4	28.12
1	4	30.40		3	4	53.83

TABLE 3.6

Derived Hydrogen Atom Positional* and Thermal Parameters

Atom	x	y	z	B
H1C(1)	2054	688	126	6.94
H1C(2)	3153	-294	1678	7.33
H1C(12)	1371	1725	-1002	6.74
H1C(13)	1688	3102	-2082	7.27
H1C(14)	3550	3705	-2071	7.27
H1C(15)	5007	2968	-956	7.22
H1C(16)	4675	1682	185	6.61
H1C(22)	1470	2915	2299	6.09
H1C(23)	1286	4291	1210	6.17
H1C(25)	4632	4748	1622	6.18
H1C(26)	4871	3390	2735	5.47
H1C(3)	4021	1938	5483	6.42
H2C(3)	3211	2740	5217	6.42
H3C(3)	2700	1795	5407	6.42
H1C(4)	3239	5932	891	7.82
H2C(4)	3153	5373	-440	7.82
H3C(4)	2047	5616	367	7.82

*The positional parameters have been multiplied by 10^4.

3.2.2 Determination of Absolute Configuration

The absolute configuration of the molecule, determined by the Bijvoet absorption edge technique, was confirmed by refinement of both models, including H atom contributions, to convergence. The chosen model has residuals of $R_1 = 0.0292$ and $R_2 = 0.0268$ while the enantiomeric structure gave agreement factors of $R'_1 = 0.0442$ and $R_2 = 0.0472$. The R factor ratio test (92) applied to R_2 shows that the alternate model may be rejected at less than the 0.005 significance level assuming no systematic errors in the data. Further illustration that the correct model was chosen is given in Table 3.7, which lists a selection of structure amplitudes for the chosen model for which $F_c(hkl)$ and $F_c(h\bar{k}l)$ differ by more than 25% based on the final positional parameters.

3.3 Molecular Structure

Some interatomic distances and selected bond angles are given in Table 3.8. A perspective view of a single molecule showing the atom numbering scheme is presented in Figure 3.2. A stereoview of the molecule including H atoms is shown in Figure 3.3.

The inner coordination sphere of the Pt atom is of square planar geometry, with the double bond of the olefin ligand approximately perpendicular to the plane. The angle between the olefin and the Pt-Cl(1)-Cl(2) plane is 77.6(6)$^\circ$.

TABLE 3.7

DETERMINATION OF ABSOLUTE CONFIGURATION

h	k	l	$F_c(hkl)$	F_o Relationship	$F_c(h\bar{k}l)$
1	4	3	12.15	<	19.16
1	6	2	31.12	>	23.35
1	6	5	14.42	<	22.76
2	7	1	19.60	>	10.07
2	2	2	37.80	<	53.30
4	5	2	21.77	>	15.03
4	2	2	10.21	<	17.43
5	3	2	17.39	>	12.60
5	5	4	17.83	<	24.81
6	3	1	29.29	<	39.11
2	13	5	13.22	>	9.13
2	10	3	18.41	>	12.34
3	2	7	20.52	<	28.79
3	7	8	9.62	<	15.09
4	5	8	13.01	>	7.88
5	5	6	11.73	<	7.17
2	8	2	12.78	>	17.46

TABLE 3.8

SELECTED INTRAMOLECULAR BOND DISTANCES (Å) AND BOND ANGLES (deg)

Distances

Pt-Cl(1)	2.301(2)	S-O	1.461(5)
	2.320(2)^a	S-C(3)	1.757(8)
Pt-Cl(2)	2.297(2)	S-C(21)	1.787(7)
	2.308(2)^a	C(1)-C(2)	1.360(11)
Pt-S	2.252(2)	C(1)-C(11)	1.488(12)
Pt-C(1)	2.219(9)		1.555(11)^b
Pt-C(2)	2.188(8)	C(4)-C(24)	1.508(10)

Angles

Cl(1)-Pt-Cl(2)	87.67(9)	C(2)-C(1)-C(11)	128.0(9)
Cl(2)-Pt-S	91.10(8)	Pt-C(1)-C(11)	113.2(5)
Cl(1)-Pt-C(1)	84.4(2)	C(2)-C(1)-HC(1)	138.6
Cl(1)-Pt-C(2)	91.9(2)	C(1)-C(2)-HC(2)	117.9
C(1)-Pt-C(2)	35.9(3)		

^{a}Averaged over thermal motion, assuming Cl "riding" on Pt.

^{b}Averaged over thermal motion assuming independent motion.
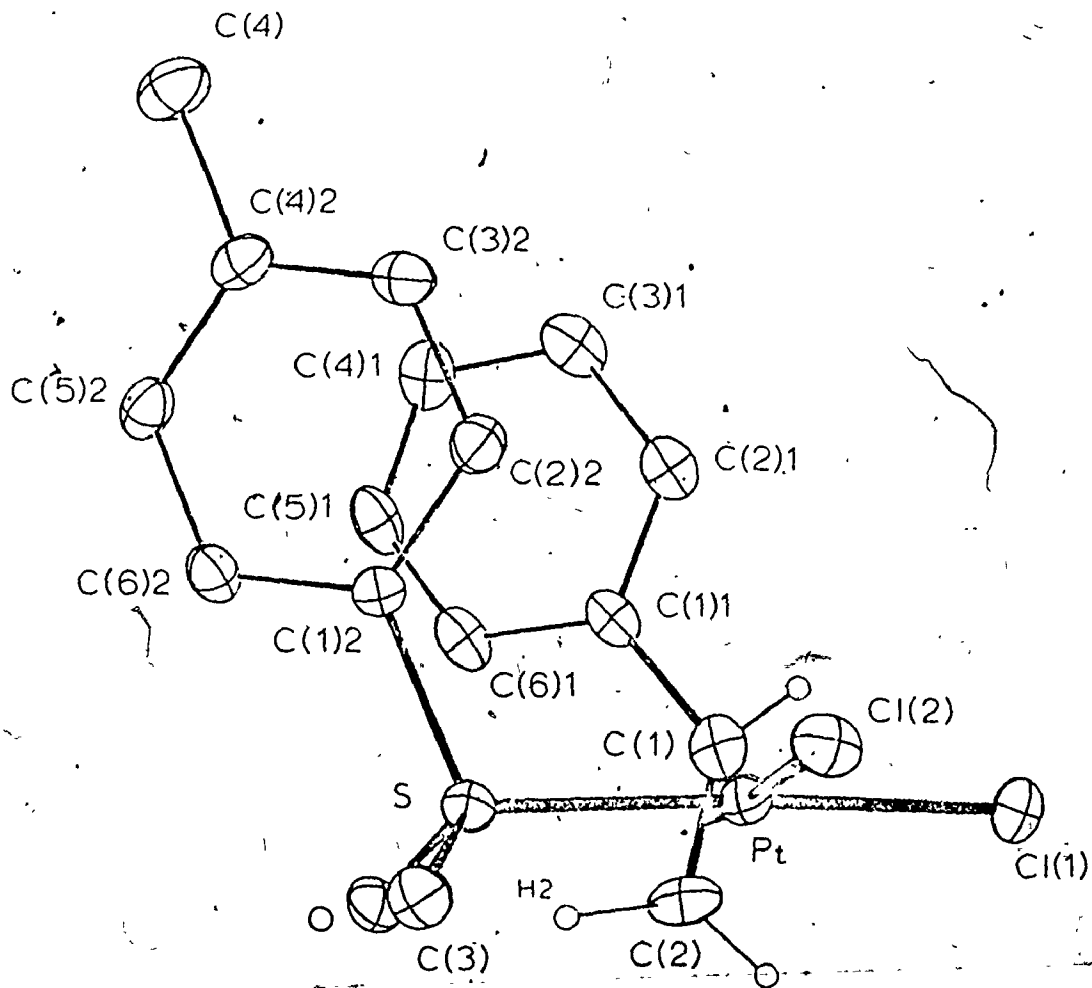
Figure 3.2 Perspective view of molecule showing the atom numbering scheme
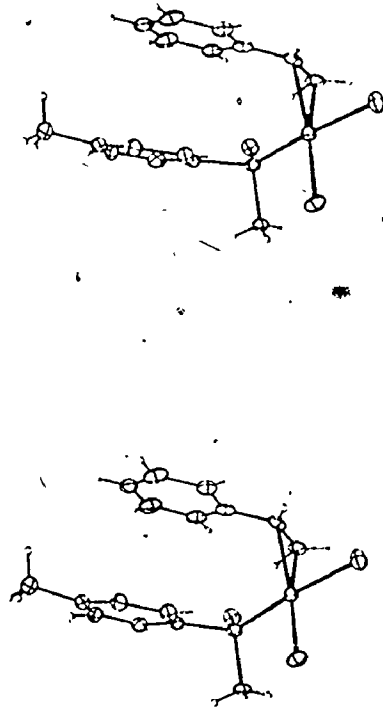
Figure 3.3 Stereoview of the molecule. The thermal
parameters of the H atoms have been reduced
for clarity

A twist of this magnitude is commonly observed in Pt - olefin structures (110). The two Pt-C distances to the olefin differ by 2.6 σ, a difference, which while not unequivocal, does suggest a dissymmetric coordination of the two carbon atoms to the metal atom and may well arise from both electronic and steric effects of the olefin substituent. The olefin C-C double bond distance of 1.360(11) Å is consistent with the range of values reported for other double bonds in Pt - olefin structures (110). The olefin coordinates such that the absolute configuration at C(1) is R.

The asymmetric sulphoxide ligand has the S absolute configuration which is consistent with the R designation of free (+)-methyl p-tolylsulphoxide (111). The structures of free (+)-methyl p-tolylsulphoxide and a related sulphoxide (112) compare favourably with the internal structure of the coordinated sulphoxide in this structure. As might be expected, the bond distances to the S atom are somewhat shorter in the coordinated ligand compared to the free molecule, resulting from a reduction of electron density on the S atom upon coordination to the Pt atom.

The Pt-Cl bond distances are Pt-Cl(1)=2.301(2) and Pt-Cl(2)=2.297(2) Å. Correction of these distances for thermal motion, assuming a model in which the Cl atoms 'ride' upon the Pt atom, gave 2.320(2) and 2.308(2) Å, distances within the normal range (110,113). These values lie on

the borderline of being significantly different (1.4 σ uncorrected for motion, 4.2 σ corrected), and reflect the assessment that both the styrene and sulphoxide ligands have similar *trans* influences.

The two benzene rings in the molecule overlap in an interesting fashion. Weighted least-squares planes for the ring atoms were calculated, and the results are presented in Table 3.9. The planes of the rings are almost parallel, Figure 3.3, with an angle between the plane normals of 5.68 degrees. For example, the atoms of the styrene benzene ring lie between 3.36 Å and 3.62 Å, from the mean plane of the sulphoxide benzene ring. The mean value for the atom to ring separation is 3.49(3) Å, a distance strongly reminiscent of the 3.4 Å separation between sheets in the structure of graphite. The mean C-C distance in the two phenyl rings is 1.37(3) Å, and the internal angles range from 117.6(9) to 121.8(10) degrees. The average displacement of ring atoms from the least-squares planes is 0.009(7) Å.

As shown by the diagram of a unit cell contents in Figure 3.4 there appears to be no unusual interaction between molecules in the crystal. The closest intramolecular interaction is 2.44 Å between the H atom on C(12) of the styrene phenyl ring and the H atom on C(26) of the sulphoxide. The closest intermolecular Pt-Pt and Pt-Cl distances are 5.777(1) and 5.471(2) Å respectively.

This experiment has successfully determined the

TABLE 3.9

SELECTED WEIGHTED LEAST-SQUARES PLANES

Plane 1 and Displacements from the Plane, Å *

Pt	0.0028(3)		C(1)	0.8166
Cl(1)	-0.0838(24)		C(2)	-0.4985
Cl(2)	-0.0066(23)			
S	-0.0656(21)			

Plane 2 and Displacements from the Plane, Å

C(21)	-0.0110(84)		C(24)	-0.0197(82)
C(22)	0.0017(84)		C(25)	0.0129(88)
C(23)	0.0122(84)		C(26)	0.0079(96)

Plane 3 and Displacements from the Plane, Å

C(11)	0.0091(77)		C(14)	0.0092(98)
C(12)	-0.0116(87)		C(15)	-0.0105(98)
C(13)	0.0027(99)		C(16)	-0.0021(92)

Plane Equations of the Form AX + BY + CZ - D = 0

	A	B	C	D
Plane 1	4.437	-9.949	6.319	-1.604
Plane 2	2.041	-6.682	-8.591	3.600
Plane 3	2.701	-7.653	-8.107	1.783

*Displacements without esd's refer to atoms not included in the calculation of the plane.
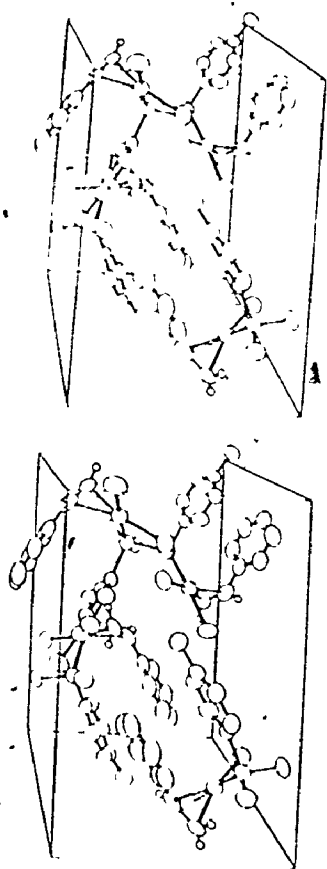
Figure 3.4 Stereoview of a unit cell contents. The b axis runs from
left to right, with c vertical

structure of the preferred diastereoisomer of *cis*-dichloro(methyl *p*-tolylsulphoxide)(styrene)platinum(II) to be *R* at the styrene when the sulphoxide is *S*. It is postulated that the reason the styrene prefers to coordinate in this fashion is to allow the phenyl rings of the olefin and the sulphoxide to get within range of an attractive and therefore stabilizing interaction. This structure has also confirmed that the absolute configuration of (+)-methyl *p*-tolylsulphoxide is *S* (*R* when the sulphoxide is uncoordinated).

To further examine the nature of the stereotopic relationships in these chiral olefin - chiral sulphoxide complexes of Pt(II) it was felt that an additional complex should be examined. The 3-methyl-1-butene analog of the styrene complex had been prepared (43) and found to display a high diastereoisomeric discrimination (66%) in solution and it could be crystallized as a diastereoisomerically pure solid. The results of the structural investigation of that complex are presented in Chapter 4.

CHAPTER 4

THE CRYSTAL AND MOLECULAR STRUCTURE AND ABSOLUTE CONFIGURATION OF (+)$_{338}$-cis-DICHLORO(METHYL p-TOLYL-SULPHOXIDE)(3-METHYL-1-BUTENE)PLATINUM(II)

4.1 Introduction

The structural analysis of the title complex was undertaken in order to compare it to the structure of the analogous complex containing styrene as the coordinated olefin (Chapter 3). As in the case of the styrene complex it was observed that the diastereoisomeric discrimination for the complex containing a specific chirality at the olefin was quite high (2:1 as compared to 3:1 for the styrene derivative (43).). For the styrene complex there are indications that an unexpected attractive interaction between the phenyl rings of the styrene and sulphoxide contributes to the observed discrimination (which is discussed in detail in Chapter 5) while we felt it unlikely that there would be any such unexpected interactions in the methyl-butene complex.

4.2 Experimental

The crystals of (+)$_{338}$-cis-dichloro((S)-methyl p-tolylsulphoxide)(3-methyl-1-butene)platinum(II), [PtCl$_2$ {CH$_3$(O)S(C$_6$H$_4$CH$_3$)}{(CH$_3$)$_2$CHCH=CH$_2$}], were kindly provided by H. Boucher and B. Bosnich. Preliminary Weissenberg and

precession photography showed the crystals to be monoclinic with Laue symmetry 2/m. The systematic absences observed, 0k0 for k odd, and the requirement of an acentric space group for an optically active molecule, determined the space group to be $P2_1$, C_2 , No. 4 (72).

The crystal chosen for data collection (Figure 4.1) was mounted on a diffractometer in a nonspecific orientation with [010] approximately 28° from coincidence with the diffractometer ϕ axis. Cell constants and an orientation matrix were obtained from a least-squares refinement of the setting angles for 18 intense, carefully centered reflections with $20 < 2\theta < 50^\circ$. Prefiltered Cu $K\alpha_1$ radiation was used, $\lambda =$ 1.54056 $\overset{o}{A}$, at an ambient temperature of 20°. The crystal data are summarized in Table 4.1.

The conditions used for data collection are given in Table 4.2. The measurement of standard reflections over the course of data collection and an examination of ω scans for several intense, low-angle reflections before and after data collection, showed no significant degradation of crystal quality had occurred.

The intensity data were processed as previously described and the value for p, in equation 2.2, was chosen to be 0.02. The results of the data reduction are presented in Table 4.3.
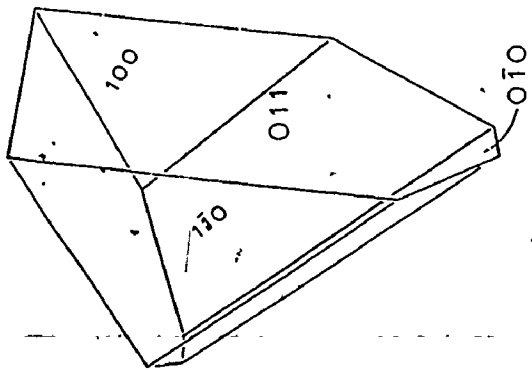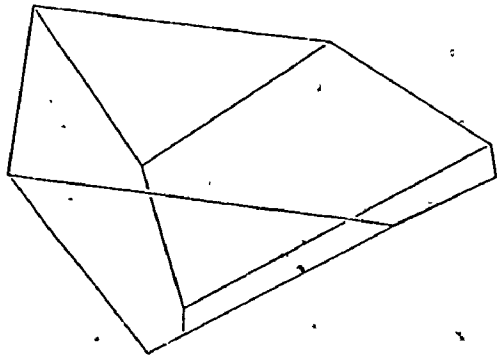
Figure 4.1 Stereoview of crystal

TABLE 4.1

CRYSTAL DATA FOR cis-$[PtCl_2\{CH_3(O)S(C_6H_4CH_3)\}(CH_3)_2CHCH=CH_2]$

Formula	$C_{13}H_{20}Cl_2PtSO$
Fw	490.36
Crystal description	Translucent white triangular blocks
Systematic absences	$0k0$ for k odd
Laue symmetry	$2/m$
Crystal system	Monoclinic
Space group	$P2_1$
Cell constants	$a = 10.556(2)$ Å $b = 10.488(2)$ $c = 7.941(2)$ $\beta = 107.72(1)^{\circ}$
Cell volume	837.51 Å^3
Density (calculated)	1.944 g cm^{-3}
(observed)	$1.950(2)$ g cm^{-3}
Density measured by	Neutral bouyancy in hexane and 1,2-dibromotetra-fluoroethane
Z	2
Symmetry constraints	None
Crystal faces (7)	$\{100\}$, $\{110\}$, $\{0\bar{1}1\}$, (010)
Crystal dimensions	$0.23 \times 0.20 \times 0.10$ mm
$\mu(CuK_{\alpha_1})$	187.4 cm^{-1}

TABLE 4.2

EXPERIMENTAL CONDITIONS ASSOCIATED WITH DATA COLLECTION

Radiation	$CuK_{\bar{\alpha}}$
Wavelength	1.54184 Å
Take-off angle	2.3°
% of intensity available	90%
Tube Kv,mA	40; 16
Filter	Ni foil (0.018mm) prefilter
Temperature	$24^\circ C$
Collimator size	1.0 mm
Aperture size	4 x 4 mm
Crystal-counter distance	33 cm
Mean ω scan width	0.10°
No. and 2θ range of centered reflections	18, $20 \leq 2\theta < 50^\circ$
Scan range; speed	1.2° for $2\theta < 70^\circ$, $K_{\alpha_1} - 0.8^\circ$ to $K_{\alpha_2} + 0.6^\circ$ for $2\theta > 70^\circ$.
Miller index range	$-12 \leq h \leq 12$, $-13 \leq k \leq 13$, $0 \leq l \leq 9$
2θ shells	$0-70^\circ$, $70-110^\circ$, $110-130^\circ$
Background count time	10s for $2\theta < 110^\circ$, 20s for $2\theta > 110^\circ$
Standards	020, $\bar{1}00$, $0\bar{2}0$, 100, 001, $\bar{1}02$; recorded every 175 reflections

TABLE 4.3

RESULTS OF DATA REDUCTION

Number of measured intensities	3099
Average Standard change	+0.46%; intensity data uncorrected
The 'p' factor	0.02
Distribution of measured intensities	$2980 > 3\sigma(I)$ $2\sigma(I) < 51 < 3\sigma(I)$ $\sigma(I) < 32 < 2\sigma(I)$ $36 < \sigma(I)$
Absorption correction method	Analytical
Data absorption corrected	3088 with $F^2 > 0$
Maximum, minimum transmission coefficients	0.838, 0.661
Pairs of equivalent reflections, and symmetry relationship	211; $hk0$ and $\bar{h}k0$
R factor for averaging equivalent reflections: nonabsorption corrected	6.0%
absorption corrected	3.6%

4.2.1 Structure Solution and Refinement

The structure solution and preliminary refinement employed the 1553 data with $k>0$ and $F^2>3\sigma$ (F^2). The positional parameters for the Pt atom were determined from a three-dimensional Patterson synthesis. A series of three least-squares refinements and difference Fourier synthesis calculations revealed the positions of the remaining 17 non-hydrogen atoms. From the results of a single crystal X-ray structural study on a similar complex (Chapter 3) we knew the absolute configuration of the sulphoxide ligand to be S and this enabled the choice of the correct hand for the model from the beginning. Refinement of atomic parameters was carried out by full matrix least-squares techniques on F as described in Chapter 2.

One cycle of full matrix least-squares refinement on the molecule, with the phenyl ring constrained as a rigid group (D_{6h} symmetry, C-C 1.392 $\overset{o}{A}$) with individual atomic isotropic temperature factors, and varying the positional and anisotropic thermal parameteres for the non-group atoms resulted in values of $R_1 = 0.0493$ and $R_2 = 0.0611$. Using the 2980 absorption corrected data with $F^2>3\sigma(F^2)$ two cycles of refinement, varying the positional and anisotropic thermal parameters for all non-hydrogen atoms, gave R_1 and R_2 values of 0.0393 and 0.0487, respectively.

Of the twenty H atoms in the molecule, all were located in regions of positive electron density by a

difference Fourier synthesis. The locations determined for
the non-olefinic H atoms compared favorably to idealized
positions computed assuming appropriate sp^3 and sp^2 co-
cordination geometries at the C atoms, and C-H bond lengths
of 0.95 Å. The H atoms were assigned isotropic thermal
parameters 1.0 Å^2 greater than those of the atoms to which
they are bonded. Rather than constrain the olefinic H
atoms to an artificial model it was decided to refine their
positional coordinates keeping the isotropic thermal para-
meters constant. Two cycles of refinement on this model
gave acceptable geometries for the two H atoms on C(1), but
H1C(2) refined to a position 1.42 Å distant from C(2).
Accordingly it was decided to fix the H atoms for the final
cycles with H1C(2) moved to a position 0.95 Å from C(2).
The model was converged using all data for which $F^2 > 2\sigma(F^2)$.
The conditions and results of the final cycle are presented
in Table 4.4.

A statistical analysis of R_2 in terms of $|F_o|$,
diffractometer setting angles χ and ϕ, and $\lambda^{-1} \sin \theta$ showed
no unusual trends. A difference Fourier synthesis calculated
from the final structure factors contained no features of
chemical significance. The highest peak, located 1.73 Å
from the Pt atom has an electron density of 1.1(3) eÅ^{-3}
and is not apparently chemically significant. An examination
of F_o and F_c showed no evidence for secondary extinction.
Structure factors calculated for those reflections with

TABLE 4.4

CONDITIONS AND RESULTS FOR FINAL FULL MATRIX LEAST-SQUARES REFINEMENT CYCLE

Observations used	3031; $F > 2\sigma(F)$
Variables	162
Ratio (observations/variables)	18.7
Agreement factors R_1	0.0377
R_2	0.0449
Error on an Observation of Unit Weight	2.6 e
Maximum (parameter shift/esd)	0.95
Number of Anisotropic atoms	17
Number of H atom contributions included	20
Anomalous Scatterers	4; Pt, 2xCl, S
Remaining Difference Fourier Peak: a) Electron density	$1.1(3)\ e\mathring{A}^{-3}$
b) Fractional coordinates	$-0.16,\ 0.30,\ 0.34$
c) Associated with	Pt atom

$F^2 < 2\sigma$ (F^2) showed only four reflections for which F_o - F_c exceeded 3σ. Final positional and thermal parameters for the non-H atoms are given in Table 4.5, those for the H atoms are in Table 4.6. Structure factor amplitudes are included in Appendix 3.

4.2.2 Determination of Absolute Configuration

To confirm that the correct choices for the absolute configuration of the asymmetric sites were made, we compared F_o and F_c for all reflections with calculated Bijvoet differences exceeding 5%. The agreement factor for this comparison $R_{Bij} = \Sigma|\overline{F}_o - F_c|/\Sigma F_o = 0.0453$ is quite good. A comparison of $F_c(hkl)$ and $F_c(h\overline{k}l)$ values for reflections exhibiting Bijvoet differences in excess of 20% based on the final model is presented in Table 4.7. The R factor ratio test (92) was also applied after refining the chosen model and its enantiomer under identical conditions. For a refinement using 171 variables and 2980 data agreement factors R_2 of 0.0453 and 0.0661 were obtained for the two structures. This indicates the first model, containing the sulphoxide in the same absolute configuration determined in Chapter 3, is preferred at a significance level of greater than 99.5%.

Final Atomic Positional and Thermal Parameters*

TABLE 4.5

Atom	x	y	z	U11	U22	U33	U12	U13	U23
Pt	-738.5(3)	3000	1842.0(4)	391(2)	365(2)	321(2)	-23(3)	122(1)	-13(3)
Cl(1)	1091(3)	4296(3)	2094(4)	497(14)	557(16)	612(17)	-154(12)	117(13)	7(14)
Cl(2)	26(3)	2658(3)	4861(4)	681(16)	852(31)	333(12)	-122(14)	59(12)	16(1)
S	-2388(2)	1629(2)	.1668(3)	479(13)	419(12)	342(12)	-68(10)	185(11)	-21(10)
O	-3328(8)	1428(8)	-186(10)	620(46)	735(53)	318(37)	-190(41)	155(35)	-90(35)
C(1)	-1027(10)	2810(14)	-979(12)	654(57)	510(95)	302(43)	-109(61)	184(42)	-2(51)
C(2)	-1880(10)	3807(10)	-744(15)	489(57)	403(56)	439(59)	-25(45)	95(49)	40(46)
C(3)	-1724(13)	5227(11)	-948(19)	652(72)	420(60)	754(87)	-21(55)	135(68)	190(61)
C(4)	-2358(19)	5969(14)	228(26)	1276(144)	523(82)	1190(148)	245(87)	407(122)	-83(89)
C(5)	-2436(17)	5514(17)	-2918(25)	974(115)	928(119)	888(120)	-74(92)	-5(98)	482(98)
C(6)	-1668(13)	146(10)	2476(18)	747(77)	315(51)	810(91)	86(51)	485(73)	96(54)
C(7)	-5866(11)	3079(26)	6143(16)	602(60)	1148(116)	687(73)	91(115)	322(57)	-312(139)
C(11)	-3322(9)	2063(10)	3083(13)	869(48)	482(55)	320(49)	-28(41)	107(41)	-3(42)
C(12)	-4323(10)	2938(21)	2421(14)	609(54)	641(69)	498(53)	146(92)	233(46)	185(102)
C(13)	-5135(11)	3292(12)	3429(17)	516(57)	697(127)	703(81)	192(59)	188(57)	34(64)
C(14)	-4972(10)	2736(11)	5059(14)	425(46)	565(96)	437(53)	7(46)	156(42)	-120(49)
C(15)	-3957(11)	1877(12)	5685(14)	528(52)	740(79)	312(53)	27(55)	189(48)	2(52)
C(16)	-3426(10)	1526(12)	4704(14)	480(56)	639(69)	333(54)	103(51)	123(46)	67(52)

*Estimated standard deviations in this and other tables are given in parentheses and correspond to the least significant digits.

The thermal ellipsoid is given by $\exp\{-(B_{11}h^2 +B_{22}k^2 +B_{33}l^2 +2B_{12}hk +2B_{13}hl +2B_{23}kl)\}$ and $U_{ij}=B_{ij}/(2\pi^2 a_i{}^*a_j{}^*)$ Å^2. The quantities

given in the table have been multiplied by 10^4.

TABLE 4.6

Derived Hydrogen Atom Positional* and Thermal Parameters

Atom	x	y	z	B
H1C(1)	-170	3181	-812	4.80
H2C(1)	-1299	1795	-1477	4.80
H1C(2)	-2713	3452	-764	4.35
H1C(12)	-4456	3291	1294	5.19
H1C(13)	-5794	3924	3007	5.72
H1C(15)	-3835	1502	6811	4.77
H1C(16)	-2510	932	5412	4.56
H1C(3)	-810	5428	-656	5.61
H1C(4)	-2069	6829	285	8.15
H2C(4)	-3296	5930	-256	8.15
H3C(4)	-2089	5604	1375	8.15
H1C(5)	-2452	6407	-3105	8.41
H2C(5)	-1907	5136	-3610	8.41
H3C(5)	-3282	5164	-3276	8.41
H1C(6)	-2343	-499	2131	5.32
H2C(6)	-985	-45	1968	5.32
H3C(6)	-1328	178	3713	5.32
H1C(7)	-5828	3970	6350	7.07
H2C(7)	-6755	2836	5522	7.07
H3C(7)	-5583	2638	7243	7.07

*The positional parameters have been multiplied by 10^4.

TABLE 4.7

DETERMINATION OF ABSOLUTE CONFIGURATION

hkl	$F_c(hkl)$	F_o Relationship	$F_c(h\bar{k}l)$
$\bar{4}40$	3.42	<	6.29
440	3.42	>	6.29
021	19.25	>	11.14
$\overline{89}2$	5.35	<	7.01
$\overline{53}6$	8.43	>	6.10
$\overline{13}2$	23.77	<	30.35
$\bar{4}74$	6.84	>	8.72
661	3.17	<	4.03
$\bar{9}17$	8.70	>	6.35
$\bar{4}34$	15.31	>	11.64
$\overline{38}0$	5.54	<	6.84
$\bar{9}83$	5.16	>	3.97
265	7.70	>	5.94
$9\bar{1}1$	6.95	<	5.37
$\bar{1}58$	6.36	<	7.76
$\bar{6}56$	7.55	<	9.19

4.3 Molecular Structure

A perspective view of a single molecule showing the atom numbering scheme is presented in Figure 4.2. A stereoview of the molecule including H atoms is shown in Figure 4.3. Selected interatomic distances and angles are given in Table 4.8. A diagram of the molecules in a unit cell is presented in Figure 4.4 and illustrates apparently normal packing with no unusual interactions between molecules in the crystal. The closest intermolecular contact is 2.34 Å between H1C(15) and the O atom of the molecule related by a unit cell translation along z. The nearest Pt-Pt and Pt-Cl intermolecular distances are 6.418(1) and 7.266(3) Å, respectively.

The inner coordination sphere of the Pt atom is of square planar geometry with the double bond of the olefin ligand approximately perpendicular to the square plane. The angle between the Pt-Cl(1)-Cl(2) plane and the olefinic bond is 84.3(6)°. This twisting of the olefin away from the perpendicular is a commonly encountered phenomenon (110). The olefin C atoms are displaced by 0.681 and -0.744 Å from the mean coordination plane of the Pt atom, Table 4.9. The Pt-C distances to the olefin are Pt-C(1) = 2.175(9) and Pt-C(2) = 2.211(11) Å. The C-C double bond distance of 1.43(2) Å is within the range commonly seen for coordinated double bonds (37,110).

Figure 4.2 Perspective view of molecule showing the atom numbering scheme
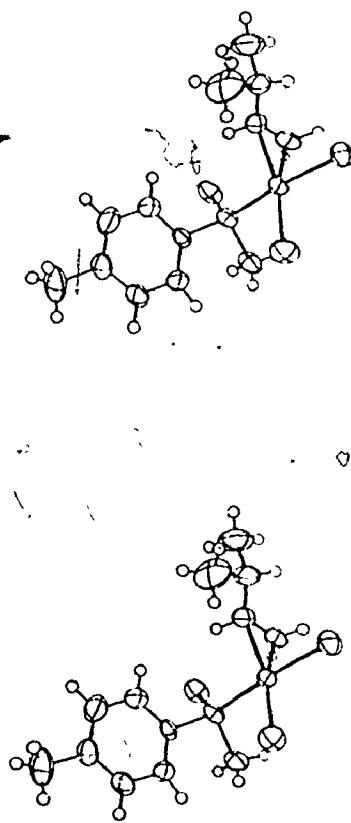
Figure 4.3 Stereoview of molecule. The thermal
parameters of the H atoms have been
reduced for clarity

TABLE 4.8

SELECTED INTERATOMIC BOND DISTANCES (Å) AND ANGLES (deg)

Distances

Pt-Cl(1)	2.313(3)	C(7)-C(14)	1.50(1)
	2.326(3)[a]		
Pt-Cl(2)	2.312(3)	C(1)-C(2)	1.43(2)
	2.330(3)[a]	C(2)-C(3)	1.51(1)
Pt-S	2.235(3)	C(3)-C(4)	1.52(2)
Pt-C(1)	2.175(9)[b]	C(3)-C(5)	1.54(2)
Pt-C(2)	2.211(11)		
S-O	1.466(7)	C(1)-H1C(1)	0.956(11)[b]
S-C(6)	1.766(11)	C(1)-H2C(1)	1.42(14)
S-C(11)	1.771(9)		

Angles

Cl(1)-Pt-Cl(2)	89.20(11)	C(1)-C(2)-C(3)	128(1)
S-Pt-Cl(2)	89.09(10)	C(2)-C(3)-C(4)	111(1)
C(1)-Pt-Cl(1)	89.9(3)	C(2)-C(3)-C(5)	105(1)
C(2)-Pt-Cl(1)	93.5(3)	H1C(1)-C(1)-H2C(1)	124
Pt-S-O	116.3(3)	H1C(1)-C(1)-C(2)-C(3)	23(1)[c]
Pt-S-C(6)	107.6(4)	H2C(1)-C(1)-C(2)-H1C(2)	16(1)
Pt-S-C(11)	111.7(3)		

[a] Distance corrected for Cl "riding" on Pt.

[b] Errors estimated from last cycle in which H atoms were refined.

[c] A positive angle indicates a clockwise rotation of atom 1 about the atom 2-atom 3 bond to superimpose its image on atom 4.
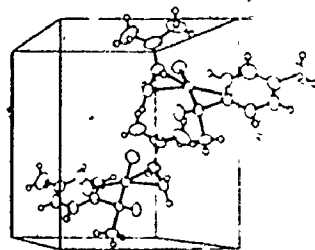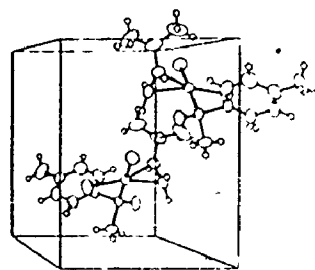
Figure 4.4   Stereoview of a unit cell contents
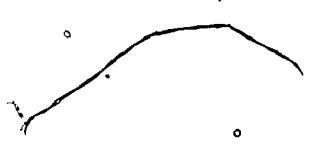
TABLE 4.9

WEIGHTED LEAST-SQUARES PLANES AND DISPLACEMENTS (Å) OF ATOMS THEREFROM[a]

Plane 1: $5.53x + 7.76y + 1.93z - 0.363 = 0$

C(11)	-0.003(10)	C(14)	-0.011(10)
C(12)	-0.011(19)	C(15)	0.005(12)
C(13)	0.016(13)	C(16)	0.003(12)

Plane 2: $6.58x - 8.07y + 2.56z + 3.37 = 0$

Pt	-0.0003(2)	S	0.063(3)
Cl(1)	0.087(3)	C(1)	0.681
Cl(2)	-0.000(3)	C(2)	-0.744

[a]Displacements without esd's refer to atoms not included in the calculation of the plane.

The initial refinement of the olefinic H atoms allowed an estimate of the bendback angle α, defined as the angle between the normals of the planes of the substituents (37). The value determined was $154(8)^\circ$, with the error estimated from the last cycle of refinement in which the H atom parameters were varied. This angle compares favorably to values reported for a number of other structures (37).

The Cl-Pt-Cl angle of $89.20(11)^\circ$ and the Pt-Cl distances of 2.313(3) and 2.312(3) $\overset{o}{A}$, to Cl(1) and Cl(2) respectively, represent a normal geometry for square planar Pt complexes containing *cis* Cl ligands opposite weak *trans* influence ligands (110,113,114). The Pt-S distance of 2.235(3) $\overset{o}{\cdot A}$ is somewhat shorter than observed in the styrene complex but both values are consistent with the range of Pt-S and Pd-S distances observed in other structures (115). The $S-C(sp^2)$, and $S-C(sp^3)$ distances of 1.771(9) and 1.766(11) $\overset{o}{A}$ respectively are similar to values normally observed for coordinated sulphoxide ligands as is the S-O distance of 1.466(7) $\overset{o}{A}$ (115).

The absolute configuration of the sulphoxide ligand is *S* as expected from the structural results of the styrene complex (Chapter 3), which contains the same ligand. The asymmetric C atom of the olefin is also in the *S* absolute configuration, in contrast to the *R* absolute configuration observed for that in the styrene complex.

With the completion of this structure we now have
two closely related systems, the styrene and methyl-butene
complexes of Chapters 3 and 4, for studying the interactions
which produce a given diastereoisomer of the Pt-sulphoxide -
olefin complex. The geometrical features of these two
complexes will be discussed in Chapter 5 in order to compare
the metal - olefin and olefin - chiral sulphoxide interactions
in light of the current theories regarding these complexes.

CHAPTER 5

DISCUSSION OF THE RESULTS OF CHAPTERS 3 AND 4

When a prochiral olefin, namely one which is dissymmetrically substituted at one or both carbon atoms, coordinates to a metal atom it may do so through either of two enantiotopic faces resulting in either R or S absolute configurations at the substituted carbon atoms (section 1.6). If the metal atom is already part of an asymmetric complex two diastereoisomers may be formed which are not necessarily of equal thermodynamic stability. This implies that discrimination between the two enantiotopic faces of the olefin is possible to an extent dependent on the degree of interaction between an asymmetric site in the complex and the dissymmetric olefin. For the styrene complex, the diastereoisomer ratio at equilibrium is 75:25 in favour of the complex with the olefin in the R configuration and the sulphoxide in the S absolute configuration, while, for the complex with 3-methyl-1-butene the ratio observed is 2:1 in favour of the S olefin and S sulphoxide. In this chapter the reasons for this are examined in the light of the results presented in Chapters 3 and 4'.

5.1 Diastereotopic Discrimination

As a prochiral olefin approaches the Pt atom to form a bond, the positioning of the olefin with respect to the sulphoxide may occur in several ways.
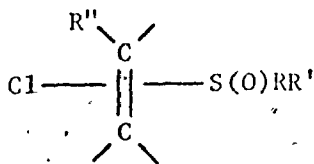
Ia
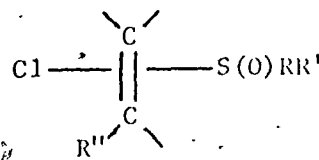
IIa
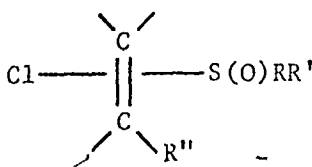
Ib
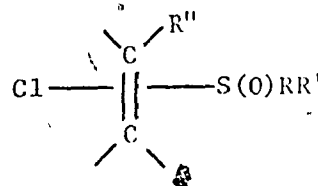
IIb

Orientations Ia and IIa result from coordination of each of
the two enantiotopic faces of the olefin to the Pt atom.
Ib and IIb are isomers generated from Ia and IIa respectively,
by rotation about the metal - olefin bond. The difference
in energy between structures Ia and IIa is presumably low
(as indicated by a study of molecular models) since the
olefin substituent is remote from the asymmetric sulphoxide
ligand.

However, the energies of Ib and IIb can be very
different depending on the nature and extent of the inter-
actions between the sulphoxide ligand and the substituent

on the olefin. If there are strong interactions in either Ib or IIb there will be a net bias for an S or R form of the olefin in the final complex.

A variety of factors can serve to determine any difference in thermodynamic stability of two diastereoisomers. Craig *et. al.* (47) have examined the problem of interpreting this discriminatory energy in terms of intermolecular forces which include long-range (5 $\overset{o}{A}$ and greater) dispersive, inductive and permanent multipole components as well as the short-range (typical of intramolecular contacts) repulsive interactions. The authors (47) felt that the short-range interactions were, energetically, an order of magnitude greater than those attributed to long-range forces.

The energy requirements for discrimination between diastereoisomers can be derived (43) simply from the equation

$$\Delta G_{DIS} = G_R - G_S = \Delta G^0 - RT\ln K \qquad 5.1$$

Where ΔG^0 is zero, T is temperature and K is the equilibrium constant for the equilibrium

$$\left[\text{complex } (S\text{- olefin})\right] \overset{K}{\rightleftharpoons} \left[\text{complex } (R\text{- olefin})\right]$$
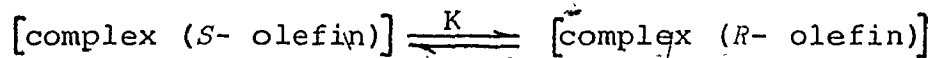
Thus a discrimination energy of approximately 2.4 KJ mole^{-1} will result in a 75:25 diastereoisomer ratio favoring the R- olefin complex. The diastereoisomer ratios, in solution, for these complexes range from 1:1 (no discrimination) to 3:1 (43,107,116) depending on the system involved. However, upon crystallization some of these systems can be induced to

form diastereoisomerically pure products (43,107,116). This extra discrimination energy comes, presumably, from crystal packing forces enhanced by the removal of degrees of rotational freedom for the interacting chiral moieties.

In the configuration observed in the solid state for the styrene complex the positioning of the styrene ligand with respect to the sulphoxide (Figure 3.2) is not what might be expected based on simple steric interactions between two bulky groups. Orienting the styrene ligand such that the phenyl ring would be closer to the apparently less bulky *cis* Cl atom would appear to lessen the nonbonded contact between the sulphoxide and styrene ligands. In the methyl-butene complex the substituent on the olefin is observed to be remote from the sulphoxide (Figure 4.2). One is thus required to consider why the styrene ligand does not rotate about the metal - olefin σ bond to a configuration similar to that for the methyl-butene complex.

The energy barrier to rotation about the Pt-olefin bond axis is generally accepted to be about 40 - 60 KJ mole^{-1} (36,42,43) but the mode and mechanism of rotation, *ie.* whether the ligand is rotating completely or oscillating through some part of a circle, and the effect of the *cis* ligands on this rotation, have not yet been fully character- ized for these chiral sulphoxide - chiral olefin complexes (42,43). Since the olefin is not observed to rotate to a position which puts the phenyl ring on the same side as the

cis Cl atom it would appear that some gain in stabilization energy is made which counteracts the nonbonded interactions. This increased stabilization could arise from three sources: an $O\cdots H$ interaction between the sulphoxide and an H atom on the olefin, crystal packing forces, or an attractive force arising from the overlap of the π orbitals of the phenyl rings. An $O\cdots H$ interaction would still be possible after a 180° rotation about the Pt-olefin bond, but in either case hydrogen bonding to an olefin is not generally accepted as significant (117). Determining the effects of crystal packing forces is much more difficult but in terms of simple contact between molecules, a visual examination of the molecular packing (Figure 3.4) and analysing inter-molecular distances seems to indicate no unusual nonbonding interactions which would serve to determine the observed configuration.

The structures of a variety of purines, pyrimidines, nucleotides, nucleosides and nucleic acids (118,119) all show overlapping or layering of phenyl rings in their solid state structures. These species all contain polar hetero-atoms in the aromatic rings or attached to the rings. Similar structures are observed when unsubstituted aromatics, that is those without heteroatoms present, interact with aromatic rings with polar sites (120) or when purines and pyrimidines interact with metal-Schiff base complexes (121). However, when the structures of unsubstituted aromatics are

examined, for example anthracene (122), the characteristic herring bone packing pattern is observed with no overlap between molecules in the cell. The forces and energetics involved in these interactions have not been fully characterized but are generally ascribed to dipole-dipole forces (118).

It is not possible, at the present time, to calculate accurate energies for these types of interactions because the energies involved ar not large (about 4 to 8 KJ mole^{-1}) and the errors inherent in the calculations are on the same order of magnitude. There have been attempts to apply molecular orbital calculations to determining the interaction energies between atoms in a chiral complex (123) but other authors feel (41,124) such calculations should be treated with caution as a result of the bias which can be introduced into the calculations by the choice of starting parameters or method of calculation.

Thus the best that can be said at the present time is that we feel there is sufficient precedent for postulating the presence of an attractive interaction between the two overlapping rings of the styrene complex which contributes to the preferred structure observed in the solid state. It is tempting to suppose that the diastereoisomer ratio in solution is affected, if not determined, by this inter-ring interaction. This extrapolation is supported by the observation, based on a manipulation of molecular models,

that if the configuration at the olefin is changed to S

the two phenyl rings cannot be put in a similar orientation

to that observed for the R diastereoisomer without

prohibitively close H atom contacts between the olefin and

the sulphoxide methyl group.

5.2 Geometry of the Metal - Olefin Interaction

For the purposes of comparison, drawings (which

include the relevant bond distances), of the Pt-olefin

unit of the styrene and methyl-butene complexes are pre-

sented in Figure 5.1. The dotted line from the Pt atom to

the carbon-carbon double bond represents the mean co-

ordination plane defined by the Pt, two Cl and S atoms.

Three points chosen for purposes of comparison are:

  i) for the styrene ligand the bisector of the

      olefin double bond has 'slid' well out of

      the mean coordination plane,

  ii) the substituted carbon atom of the olefin

      is tilted away from the Pt atom in each

      case, although this may not be a crystallo-

      graphically significant displacement, and

  iii) neither olefin is coordinated perpendicular

      to the mean square plane but are tilted

      several degrees off perpendicularity.
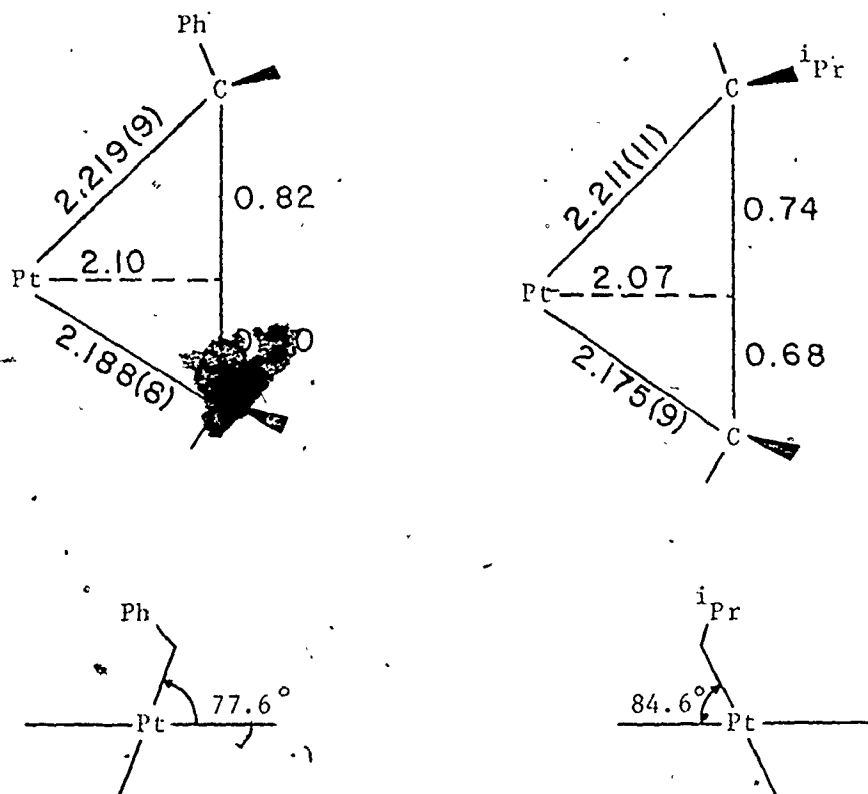
Figure 5.1   Geometries of the Pt-olefin units

The 'sliding' of an olefin ligand so that the
bisector of the vinylic bond is not in the mean square
coordination plane is a commonly observed phenomenon which
is suggested to have both steric and electronic factors
(37,125).   A valence bond approach was proposed from a
study of three Pt-styrene complexes in which the styrene
ligand was substituted with electron donating and with-
drawing groups (125).   The contributing structures were
suggested to be those depicted in Figure 5.2.

$$
\begin{array}{ccc}
\underset{\substack{| \\ H_2C \!\!-\!\! Pt^-}}{\overset{\displaystyle G}{\underset{}{CH^+}}}
&
\underset{\substack{| \\ H_2C \!\!-\!\! Pt^-}}{\overset{\displaystyle G^+}{\underset{}{CH}}}
&
\underset{\substack{\| \\ H_2C \longrightarrow Pt}}{\overset{\displaystyle G}{\underset{}{CH}}}
\\
(a) & (b) & (c)
\end{array}
$$
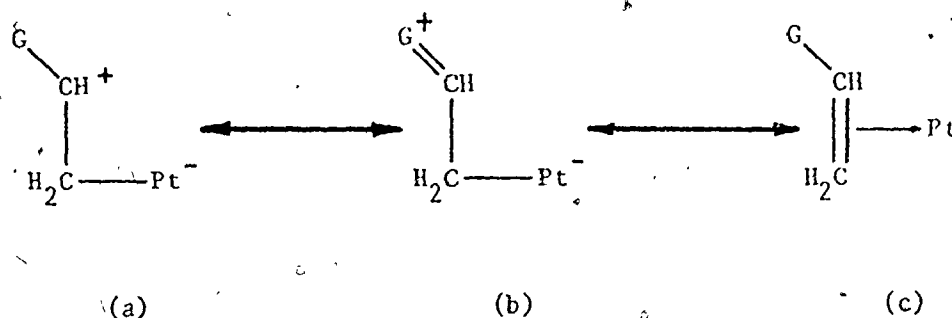
Figure 5.2   Contributing Structures of a Valence Bond
             Approach to the Pt-olefin bond

The argument used was that an electron donating substituent
on G would tend to stabilize structures (b) and (a) over
that of (c) with the result that the bisector of the double
bond would move out of the coordination plane.   The obser-
vations appeared to support this analysis.   However, by
analogy if the substituent (G) is more electron donating
than a phenyl ring (such as an alkyl group) then structure
(a), certainly, and perhaps (b) will be stabilized relative
to (c).   This would imply that the bisector of the olefinic
bond in the methyl-butene complex should be at least as far
out of the mean coordination plane as that of the styrene
ligand.   This is not observed, and in fact the two vinylic
carbons of the ligand are almost equidistant from the
coordination plane.   Thus it would appear that as yet there
is no satisfactory model which will explain the various

aspects of sliding olefins.

Tilting of the C-C double bond axis in the Pt-C-C
plane such that one carbon is farther from the Pt atom than
the other (point ii) may occur, again, as a result of both
electronic and steric effects. The electronic component
is suggested to arise from a destabilization of the olefin
π^* orbitals by the presence of the olefin substituent (126).
The energy of the π^* orbitals will, according to this theory,
be raised by the inductive effect of the substituent on the
olefin which results in a decrease in the back donation from
the metal d orbitals to the antibonding olefin orbitals
thereby weakening (lengthening) that Pt-C bond. Alternatively,
the nonbonded interactions between the olefin substituent
and the Pt atom and the *cis* ligands could result in the
tendancy for the olefin to tilt so the substituted carbon
is away from the metal atom. Using either of these approaches
the observation should be that monosubstituted olefins will
generally be tilted such that the substituted vinylic carbon
will be farther from the metal atom, whereas for the
symmetrically disubstituted olefins there should be no
significant tilt of the axis of the double bond away from
the metal atom. For a selection of square planar Pt-olefin
complexes (Pt-ethylene (113), Pt-styrene (Chapter 3,125),
Pt-(3-methyl-1-butene)(Chapter 4), Pt-(*trans*-2-butene)(110)
and Pt-(1-butene)(110) these observations appear to hold,
however not all of these structures are determined with
sufficient precision to enable detection of small differences

in the Pt-C distances with any confidence.

The twisting of the olefinic double bond away from the perpendicular to the mean coordination plane (point iii) is closely related to the phenomenon of olefin rotation introduced in Chapter 1. While extended rotation about the metal - olefin σ bond appears to be strongly influenced by both electronic and steric factors (37,41,42), it has been suggested that slight twisting of the olefin from the perpendicular is the result of nonbonded interactions between the olefin substituents and the *cis* ligands (37). This twisting of the olefin observed in the solid state has also been used to rationalize the differences in Pt-H nmr coupling constants for the geminal hydrogens of monosubstituted olefins (42). Thus it would appear that the preferred configuration in both the solid state and in solution is one in which the olefin is twisted by at least several degrees from the perpendicular. Although this olefin twist has been ascribed solely to steric factors there may be some evidence of electronic effects as well. Five crystal structures of Pt(II) complexes containing optically active coordinated olefins have been published and a projection of the coordination plane for each of these complexes is shown in Figure 5.3. The complexes a - c all have the R absolute configuration at the asymmetric carbons and in each case the olefin is twisted in the same fashion and by an average of 15°. However, for the S olefins (complexes d and e) the olefin is twisted in the opposite fashion. It is interesting
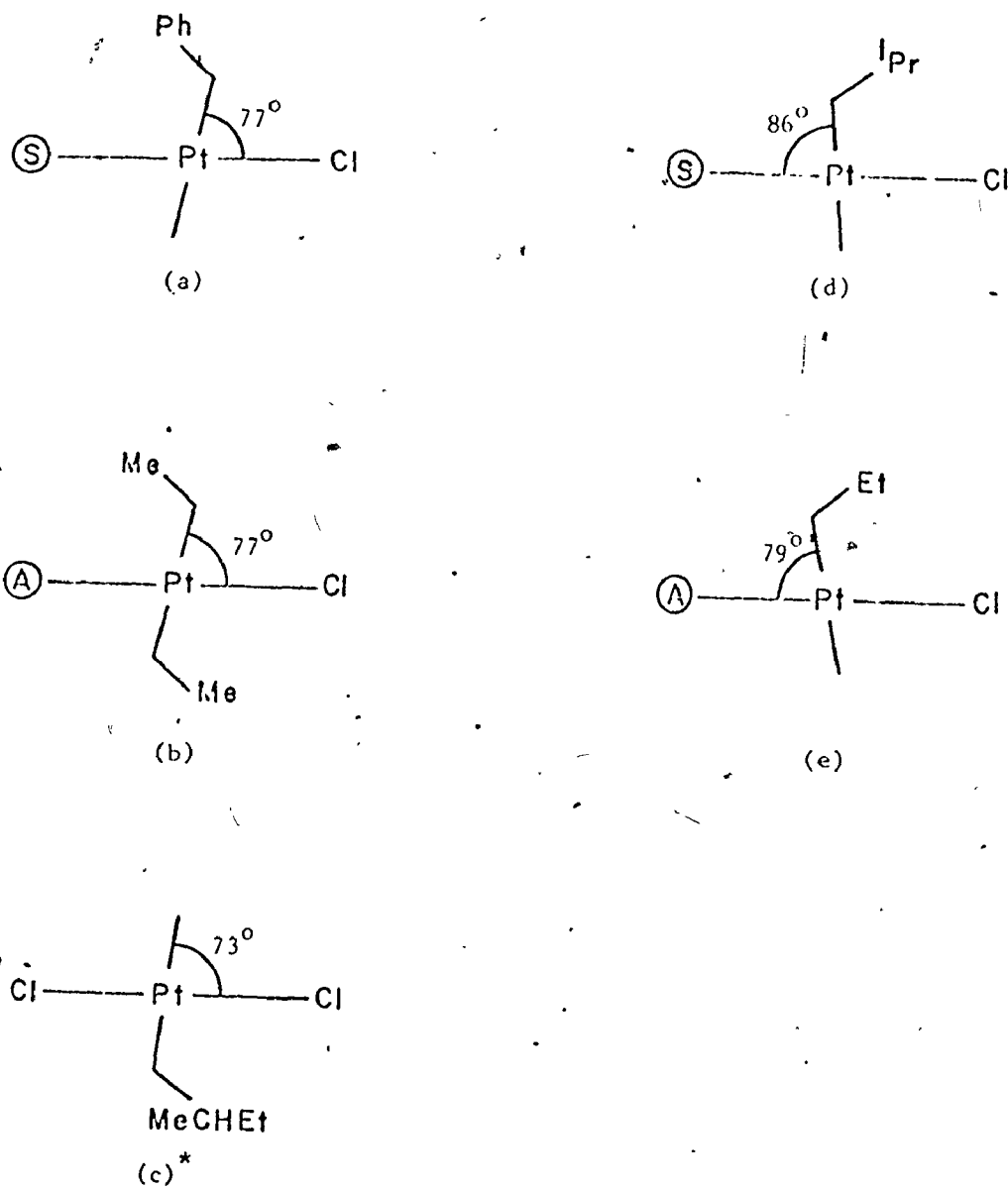
Figure 5.3 Drawings of olefin twist with respect to mean coordination plane. (S) = (S)-methyl-p-tolyl-sulphoxide, (A) = (S)-α-methylbenzylamine.

* Olefin *trans* to A .

to speculate as to whether this arrangement of the vinylic
carbons affects the observed CD spectrum in a similar manner
to that proposed for the puckered saturated five-membered
rings typified by metal -(1,2-propanediamine) complexes.
A projection of one of these metal-ligand rings is shown
below, viewed from the metal atom.
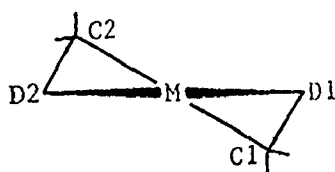
When the ligand is in this particular stereochemical
arrangement (C1 down and C2 up) then the ring is referred
to as defining a left-handed helix and therefore in the
λ conformation (15). It has also been proposed that when
the donor atoms D1 and D2 are displaced in opposing senses
from the coordination plane the helicity resulting from the
displacement may also act as a source of asymmetry (17).
In an analogous fashion the line formed by the double bond
in the Pt-olefin complexes can be used to define a right or
left-handed helix. Thus it could be said that complexes
a - c (Figure 5.3) all contain 'λ' metal - olefin conforma-
tions while complexes d and e have the opposite or 'δ'
conformations. It would be of interest to determine if all
structures containing only R (or S) olefins had only 'λ'
(or 'δ') metal - olefin conformations and what, if any, the
effect on the circular dichroism spectra of these complexes
was as a result of this olefin twist or helicity.

Unfortunately there is insufficient circular dichroism and crystallographic data available in the literature to test this theory since the crystal structures of even all those complexes which have had their CD spectrum recorded have not been done. Further crystallographic and circular dichroism studies on these types of complexes with a view to refute or verify this idea will be required before any definite conclusions can be drawn.

5.3 Circular Dichroism of Metal - Olefin Complexes

Since the study of asymmetric complexes containing optically active olefins is a relatively recent development there has been no extensive theoretical investigation into the effect on the circular dichroism spectrum displayed by these complexes and the nature of the asymmetric sites. However some investigation has been carried out into discovering a rule which would permit the use of Cotton effects to determine the chirality of these species. An empirical approach was developed by Scott et.al. (28,127) who determined that the absolute configuration of a series of simple cyclic and acyclic monoolefin complexes of Pt(II) could be related to the sign of the CD band associated with the second d-d transition of the Pt manifold (see section 2.3.3). It has been proposed, in reference to octahedral Co complexes and later extended to square planar Pt(II) complexes (21,128), that for a metal atom in an asymmetric complex the lowest energy d-d transition which displays circular dichroism will

be sensitive to the absolute configuration of the perturbing

sites coordinated to that metal atom. For the Pt(II)

complexes examined by Scott this diagnostic CD band appears

at approximately 370 nm depending on the ligand field

strengths of the ligand donor atoms. The correlation which

was found between absolute configuration at the olefin and

the sign of the diagnostic CD band could be expressed in

terms of a "quadrant" rule. This rule related the spatial

disposition of the groups attached to the double bond to

the sign of the diagnostic CD band and is shown diagramatically

in Figure 5.4.
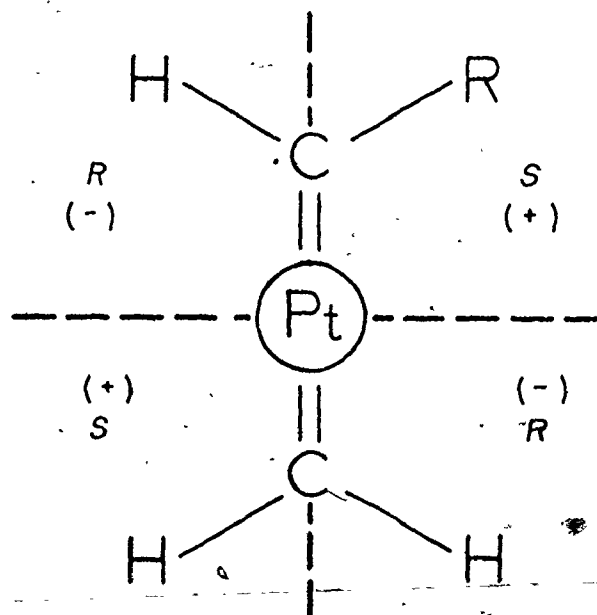
Figure 5.4 Spatial delineation of the quadrant rule.

Positive and negative absorptions, indicated by the + and -

signs, for the diagnostic CD band correspond respectively,

to S and R absolute configuration at the coordinated olefin.

The circular dichroism spectra and quadrant rule projections for *cis*-dichloro((*S*)-methyl *p*-tolylsulphoxide) ((*R*)-styrene)platinum(II) and *cis*-dichloro((*S*)-methyl *p*-tolylsulphoxide)((*S*)-3-methyl-1-butene)platinum(II) are presented in Figures 5.5 and 5.6 respectively. The styrene complex exhibits a negative band while the methyl-butene complex shows a positive band centered at 340 nm, which, according to the quadrant rule, implies the two olefins have *R* and *S* absolute configurations, respectively. This prediction of the rule is supported by the same absolute configurations being determined crystallographically (Chapters 3 and 4).

One of the major assumptions included in the formulation of the quadrant rule requires that the asymmetry of the other ligands about the Pt atom does not interfere with the effect of the chirality at the olefin on the circular dichroism exhibited by the d-d transition. This assumption was tested for the Pt-olefin complexes containing an asymmetric mono-dentate amine (28,127) and found to hold. The same is not true for the chiral sulphoxide complexes (43), a result of the donor sulphur atom chirality being able to affect the chiroptical properties of the platinum chromophore more directly. However, it was determined (43) that the magnitude of the contribution from the S atom did not outweigh that of the olefin and hence the quadrant rule based on the second d-d transition was still applicable.

In this chapter we have considered the geometrical

Figure 5.5 CD spectrum and quadrant rule projection

for $Cl_2Pt\left[(CH_3(O)S(C_6H_4CH_3)\right](CH_2=CHC_6H_5)$
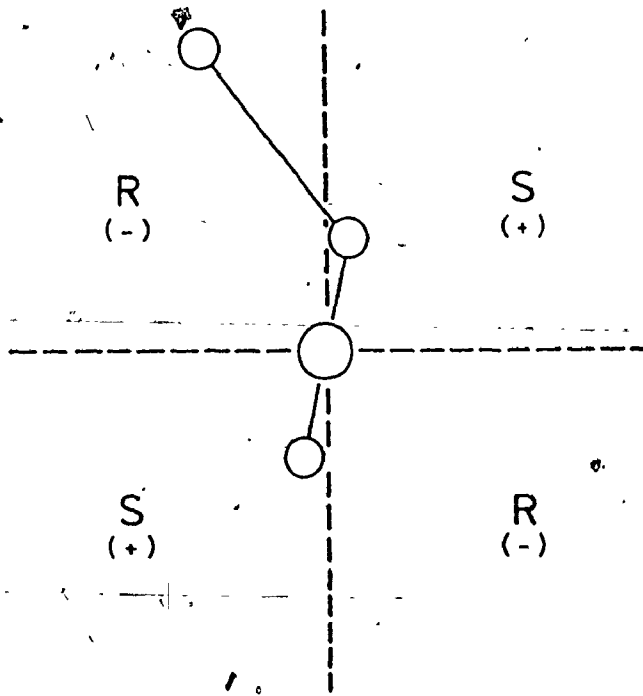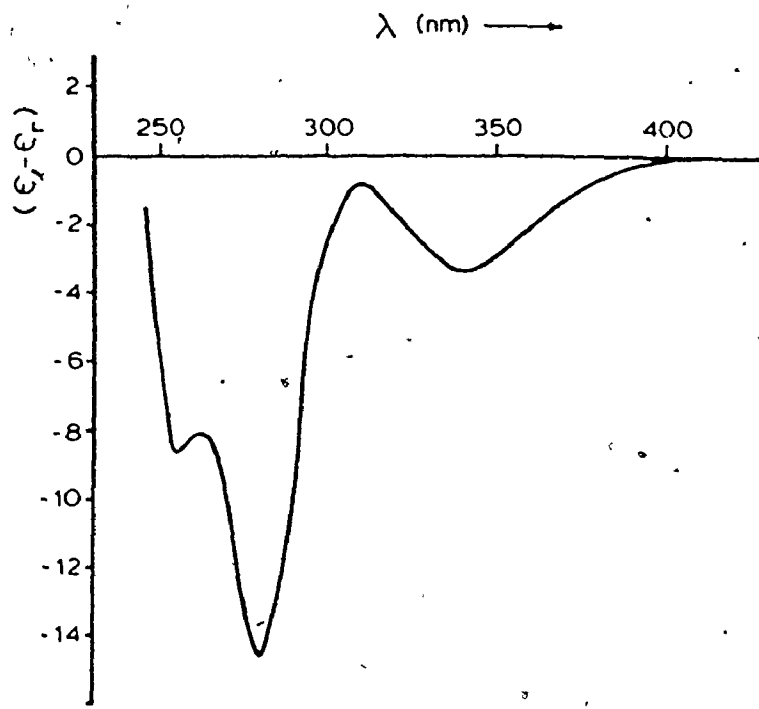
Figure 5.6   CD spectrum and quadrant rule projection for
$Cl_2Pt\left[(CH_3(O)S(C_6H_4CH_3)\right](CH_2=CHCH(CH_3)_2)$
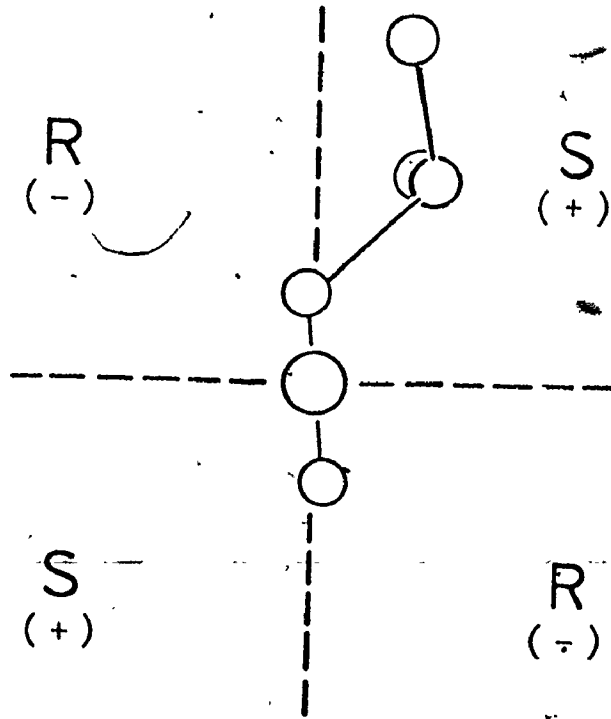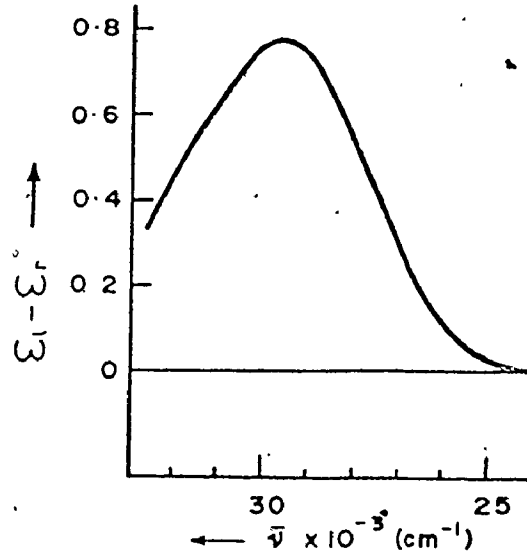
nature of the Pt-olefin unit in two similar structures by
comparing three specific aspects of this geometry. Each
of these aspects appears to be controlled by both electronic
effects and nonbonded interactions (steric effects). Indeed
it is difficult if not impossible to know where one effect
leaves off and the other begins. As was pointed out in
Chapter 1, understanding the nature of the metal - olefin
bond will have major implications with respect to the chemistry
in which this interaction plays a part. As yet this know-
ledge is not fully available even for the more easily
studied systems, such as Pt-olefin complexes. In more
intricate situations, for example when centers of asymmetry
are present, the observations very often must merely be
accepted since the present model can not explain them. A
specific example will illustrate this. In the Pt-olefin
complex containing a chiral sulphoxide and a prochiral olefin,
such as those described in Chapters 3 and 4, it was found
that the nmr spectrum of the R olefin is usually temperature
dependent whereas that of the S olefin is not (43). This
observation is ascribed to the continued rotation of the S
olefin at low temperatures while the rotation of the R
olefin is essentially stopped on the nmr time scale. In
addition it has been observed that the barrier to olefin
rotation is sensitive to the steric bulk of the non-halide
cis ligand in cis-$[Cl_2Pt(II)L(olefin)]$ complexes (42). The
commonly accepted model for olefin rotation in these complexes
certainly does not predict these observations and indeed can

not adequately rationalize them.

The combined use of crystallography and the asymmetry of prochiral olefins as probes to study the metal - olefin interaction will undoubtably provide a solid base of information on which to build a more satisfactory theory, and permit a better understanding of the origins of observations on metal - olefin complexes.

CHAPTER 6

THE CRYSTAL AND MOLECULAR STRUCTURE AND ABSOLUTE CONFIGURATION OF (1,5-CYCLOOCTADIENE)-(-)$_{589}$-2,3-BIS(DIPHENYLPHOSPHINO) BUTANERHODIUM(I) PERCHLORATE, A TETRAHYDROFURAN SOLVATE

6.1 Introduction

The rhodium hydrogenation catalysts discussed in Chapter 1 are postulated to be dihydride rhodium phosphine species, $[Rh(bisphosphine)(H)_2(S)_2]^+$ where S is a solvent molecule which is displaced by an incoming substrate molecule. Since these catalytically active species do not lend themselves to storage they are usually generated *in situ* from some catalyst precursor. The precursor used for the rhodium-(-)-2,3-bis(diphenylphosphino)butane (chiraphos) catalyst is the norbornadiene complex, $[RhNBD(chiraphos)]$ ClO$_4$ (57). This complex does not, however, form crystals of sufficient quality for crystallographic study, so an alternative complex was sought. The 1,5-cyclooctadiene (COD) complex, while not an active catalyst precursor (presumably due to the greater stability of the COD complex with respect to diolefin displacement (56)), does give crystals of excellent quality. For this reason this complex was chosen for our initial study of Rh(I)phosphine catalysts.

6.2 Experimental

Light orange crystals of (1,5-cyclooctadiene)-2,3-

bis(diphenylphosphino)butanerhodium(I)perchlorate·THF, $[$Rh$\{\pi-(C_8H_{12})\}(PPh_2CHCH_3CHCH_3PPh_2)]$ $ClO_4\cdot C_4H_8O$, were supplied by B. Bosnich and M. Fryzuk. Preliminary Weissenberg and pre-cession photography showed the crystals to be monoclinic with Laue symmetry 2/m. The systematic absences observed $0k0$ for k odd, and the requirement that an optically active species crystallize in an acentric space group, determine the space group to be $P2_1$, C_2^2, No. 4 (72).

The crystal chosen for data collection (Figure 6.1) was mounted with the long dimension of the crystal, $[0\bar{1}0]$, approximately 10° from coincidence with the diffractometer spindle axis. Cell constants and an orientation matrix were obtained from a least-squares refinement of the setting angles for 26 intense, carefully centered reflections with $24<2\theta<57^\circ$. Prefiltered $CuK\alpha_1$ radiation ($\lambda= 1.54056$ Å) was used at an ambient temperature of $20^\circ C$. Crystal and space group data are summarized in Table 6.1.

The conditions used for data collection are presented in Table 6.2. Measurement of standard reflections over the course of data collection, and an examination of crystal mosaicity, by the ω scan technique, before and after data collection, showed no significant change in crystal quality had occurred.

The intensity data were processed and the value for p in equation 2.2 was chosen to be 0.02. The results of data reduction are given in Table 6.3.
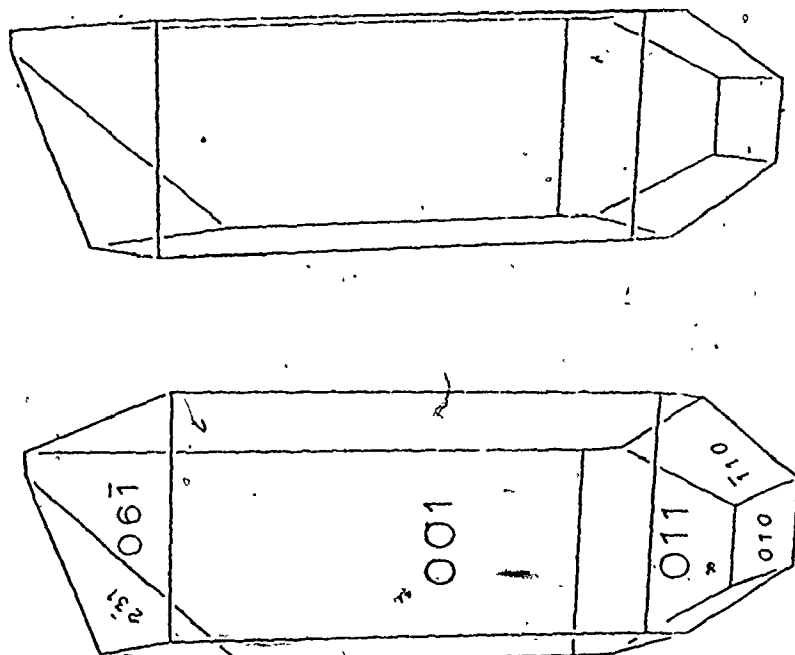
Figure 6.1 Stereoview of crystal

TABLE 6.1

CRYSTAL DATA FOR $[Rh\{\pi-(C_8H_{12})\}(PPh_2CHCH_3CHCH_3PPh_2)]ClO_4 \cdot C_4H_8O$

Formula	$C_{40}H_{48}ClO_5P_2Rh$
Fw	809.131
Crystal description	Orange prismatic needles
Systematic absences	$0k0$ for k odd
Laue symmetry	$2/m$
Crystal system	Monoclinic
Space group	$P2_1$
Cell constants	$a = 11.423(2)$ Å
	$b = 18.555(3)$
	$c = 9.950(2)$
	$\beta = 113.53(1)^{\circ}$
Cell volume	1933.5 A
Density (calculated)	1.390 g cm^{-3}
(observed)	$1.397(1)$ g cm^{-3}
Density measured by	Neutral bouyancy in CCl_4 and n-pentane
Z	2
Symmetry constraints	None
Crystal faces (9)	$\{100\}, \{001\}, \{110\},$ $\{0\bar{1}1\}, (010), (2\bar{3}1),$ $(0\bar{6}1)$
Crystal dimensions	$0.38 \times 0.22 \times 0.12$ mm
$\mu(CuK_{\alpha_1})$	51.15 cm^{-1}

TABLE 6.2

EXPERIMENTAL CONDITIONS ASSOCIATED WITH DATA COLLECTION

Radiation	$CuK_{\bar{\alpha}}$
Wavelength	1.54184 Å
Take-off angle	1.4°
% of intensity available	80%
Tube Kv,mA	40, 14
Filter	Ni foil (0.018mm) prefilter
Temperature	$20^{\circ}C$
Collimator size	1.0 mm
Aperture size	5 x 5 mm
Crystal-counter distance	33 cm
Mean ω scan width	0.08°
No. and 2θ range of centered reflections	26, $24 < 2\theta < 57^{\circ}$
Scan range; speed	1.2° for $2\theta < 110^{\circ}$, $K_{\alpha 1} - 0.7^{\circ}$ to $K_{\alpha 2} + 0.6^{\circ}$ for $2\theta > 110^{\circ}$; $2 \; min^{-1}$
Miller index range	$-13 \leq h \leq 13$, $-22 \leq k \leq 22$, $0 \leq l \leq 11$; $-14 \leq h \leq 14$; $0 \leq k \leq 23$, $0 \leq l \leq 11$ for $2\theta > 125^{\circ}$
2θ shells	$0-60^{\circ}$, $60-90^{\circ}$, $90-110^{\circ}$, $110-125^{\circ}$, $125-130^{\circ}$
Background count time	20s
Standards	200, 002, 020, 011, $\bar{2}$00; recorded every 200 reflections

TABLE 6.3

RESULTS OF DATA REDUCTION

Number of measured intensities   6772

Average Standard Change   +1%; intensity data uncorrected

The 'p' factor   0.02

Distribution of measured
intensities

$6467 > 3\sigma(I)$
$2\sigma(I) < 96 < 3\sigma(I)$
$\sigma(I) < 56 < 2\sigma(I)$
$153 < \sigma(I)$

Absorption correction method   Analytical

Data absorption corrected $6697, F^2 > 0$

Maximum, minimum transmission
coefficients   0.657, 0.393

Pairs of equivalent reflections,
and the symmetry relationship $379; hk0, \bar{h}k0$

R factor for averaging equivalent
reflections: nonabsorption corrected   —

        absorption corrected   0.014

6.2.1 Structure Solution and Refinement

For the solution and preliminary refinement only those data with $2\theta \leq 90°$ and $F^2 > 3\sigma(F^2)$ were used. The positional parameters for the Rh atom were determined from a three-dimensional Patterson synthesis. A series of least-squares refinements and difference Fourier synthesis calculations located the remaining 43 non-hydrogen atoms of the anion and cation. Refinement of atomic parameters was carried out by full matrix least-squares techniques on F as described in Chapter 2. Subsequent least-squares refinement used 6465 observations for which $F^2 > 3\sigma(F^2)$.

One cycle of full matrix least-squares refinement varying the positional and thermal parameters for the ion pair (omitting the THF of solvation) with the four phenyl rings constrained as rigid groups (D_{6h} symmetry, C-C=1.392 Å), and employing anisotropic temperature factors for the Rh, P and Cl atoms gave values of $R_1 = 0.0846$ and $R_2 = 0.1223$. At this point the enantiomeric structure was refined under identical conditions to R_1 and R_2 values of 0.0684 and 0.1024 respectively. Accordingly, this second model was used in the subsequent calculations.

In order to locate the solvent molecule, a series of difference Fourier syntheses was computed, but these revealed only a torus of electron density containing no peaks higher than 1.4 eÅ^{-3}. Since the presence of a solvent molecule had been confirmed by elemental analysis, the density determination and ^{1}H nmr results, a disordered

tetrahydrofuran molecule was postulated. Tetrahydrofuran can adopt two configurations, one with C_s symmetry, called the envelope form (I), and one having C_2 symmetry (II)(129).
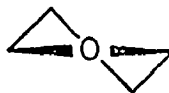
I   II

After several trials a suitable model for the electron density was achieved, employing a molecule of C_2 symmetry exhibiting twofold disorder. The second molecule, super-imposed upon the first, was rotated by approximately 180° about an axis perpendicular to the mean molecular plane. Optimal positional and thermal parameters for these atoms were obtained by including the two molecules as rigid groups, each of multiplicity 0.5, and refining the group origin, orientation angles (130) and individual isotropic thermal parameters. The parameters so obtained were not varied subsequently. One cycle of least-squares refinement on this model varying the positional and thermal parameters for all the atoms of the cation and anion, using the 3454 data with $k \geq 0$, resulted in R_1 and R_2 values of 0.0485 and 0.0644 respectively.

All 40 H atoms present in the cation were located in a difference Fourier synthesis and these positions compared

favorably to idealized positional coordinates calculated
assuming sp^2 and sp^3 coordination geometries about the C
atoms and an H-C bond distance of 0.95 $\overset{o}{A}$. The H atoms were
assigned isotropic thermal parameters 1.0 $\overset{o}{A}{}^2$ greater than
those of the atom to which they are bonded. The contribu-
tions from the H atoms, in their calculated positions,
(excluding those of the tetrahydrofuran) were included in
subsequent refinement cycles but no attempt was made to
refine their parameters.

One cycle of full matrix least-squares refinement
using the data with $F^2 > 3\sigma(F^2)$ followed by recalculation of
the H atom positions preceded the convergence of the model.
In the final two cycles of refinement all 6697 data for which
$F^2 > 0$ were used to refine 276 variables. The conditions and
results of the final cycle are presented in Table 6.4. A
statistical analysis of R_2 in terms of $|F_o|$, diffractometer
setting angles χ and ϕ, and $\lambda^{-1} \sin \theta$ showed no unusual
trends. The largest remaining peak on a total difference
Fourier synthesis calculated from the final structure factors
was 0.93(12) $e\overset{o}{A}{}^{-3}$ located near the disordered solvent
molecule.

Final positional and thermal parameters for the non-
hydrogen atoms are given in Tables 6.5 and 6.6, those for
the H atoms are in Table 6.7 and the group parameters are
given in Table 6.8. The structure factor amplitudes are
presented in Appendix 3.

TABLE 6.4

CONDITIONS AND RESULTS FOR FINAL FULL-MATRIX LEAST-SQUARES REFINEMENT CYCLE

Unique Observations	6318
Variables	276
Ratio (observations/variables)	22.9
Agreement factors R_1	0.0403
R_2	0.0505
Error on an Observation of Unit Weight	2.68 e
Maximum (parameter shift/esd)	0.98
Number of Anisotropic atoms	20
Number of H atom contributions included	40
Anomalous Scatterers	4; Rh, 2xP, Cl
Remaining Difference Fourier Peak: a) Electron density	$0.93(12)e\text{Å}^{-3}$
b) Fractional coordinates	-0.439, 0.415, -0.894
c) Associated with	Disordered THF

Final Atomic Positional and Thermal Parameters*

TABLE 6.5

Atom	x	y	z	U11	U22	U33	U12	U13	U23
Rh	1866.3(3)	3000	-124.6(3)	379(2)	385(2)	347(2)	27(2)	150(1)	-2(2)
P(1)	1528(1)	4197(1)	-629(2)	358(6)	394(7)	476(7)	-28(5)	170(6)	8(7)
P(2)	1209(1)	2894(1)	-2587(1)	387(5)	457(9)	373(5)	4(6)	173(4)	-5(6)
Cl	-2721(2)	2792(1)	669(2)	792(10)	625(11)	786(11)	-88(7)	315(9)	-26(7)
O(1)	-2909(8)	3193(4)	-628(7)	2159(68)	1210(64)	775(36)	-258(52)	590(43)	31(36)
O(2)	-3911(6)	2656(3)	733(9)	1092(45)	1317(54)	1905(74)	118(38)	882(51)	217(48)
O(3)	-2192(7)	2126(4)	666(12)	1233(53)	773(43)	3799(137)	189(39)	1260(74)	28(61)
O(4)	-1983(8)	3214(4)	1854(7)	2346(77)	1131(61)	848(39)	-592(53)	-233(47)	-12(37)
C(1)	580(5)	4322(3)	-2602(6)	473(28)	526(32)	533(31)	48(24)	175(25)	62(25)
C(2)	1154(5)	3785(3)	-3414(6)	600(33)	544(33)	466(31)	-49(26)	243(27)	29(25)
C(3)	456(7)	5896(4)	-3158(8)	942(50)	702(43)	696(44)	207(36)	212(39)	206(36)
C(4)	508(8)	3811(4)	-5086(7)	1262(63)	763(46)	537(40)	-23(42)	410(43)	101(33)
C(5)	1672(5)	2988(5)	2030(5)	772(32)	689(32)	385(23)	90(48)	290(23)	-54(39)
C(6)	1303(7)	2227(4)	2298(8)	927(49)	944(53)	691(43)	40(41)	497(40)	259(39)
C(7)	1079(7)	1680(4)	1135(8)	855(46)	703(47)	819(49)	-91(38)	453(41)	154(39)
C(8)	1762(6)	1808(3)	147(7)	675(39)	436(35)	548(37)	-9(28)	194(33)	45(30)
C(9)	3013(5)	1980(3)	568(7)	553(31)	471(31)	616(36)	142(25)	234(28)	58(26)
C(10)	3954(6)	2039(4)	2166(8)	613(36)	683(41)	693(42)	183(31)	146(33)	70(33)
C(11)	4072(6)	2752(4)	2828(7)	654(37)	1004(60)	580(38)	48(34)	36(31)	-45(34)
C(12)	2877(6)	3209(3)	2292(6)	710(35)	653(45)	575(27)	69(28)	139(26)	-52(24)

*Estimated standard deviations in this and other tables are given in parentheses and correspond to the least significant digits.

The thermal ellipsoid is given by $exp[-(B_{11}h^2 +B_{22}k^2 +B_{33}l^2 +2B_{12}hk +2B_{13}hl +2B_{23}kl)]$ and $U_{ij}=B_{ij}/(2\pi^2 a_i^* a_j^*)$ Å². The quantities

given in the table have been multiplied by 10^4.

TABLE 6.6

Final Atomic Positional* and Thermal Parameters for the Phenyl Ring Atoms

Atom	x	y	z	U11
C(21)	683(5)	4664(3)	297(6)	.0454(11)
C(22)	-581(6)	4479(3)	-56(7)	.062(2)
C(23)	-1216(6)	4748(4)	743(8)	.072(2)
C(24)	-623(6)	5191(4)	1981(7)	.068(2)
C(25)	606(6)	5384(4)	2281(7)	.071(2)
C(26)	1275(5)	5122(3)	1480(6)	.0573(14)
C(31)	3013(5)	4678(3)	-205(6)	.0493(12)
C(32)	3100(6)	5419(3)	-268(7)	.062(2)
C(33)	4293(7)	5759(4)	75(8)	.075(2)
C(34)	5372(7)	5344(4)	436(8)	.075(2)
C(35)	5291(7)	4597(4)	508(8)	.073(2)
C(36)	4115(5)	4265(3)	148(6)	.0558(14)
C(41)	-400(5)	2523(3)	-3438(6)	.0455(11)
C(42)	-970(6)	2305(3)	-4093(6)	.0576(14)
C(43)	-2206(6)	2008(4)	-5456(8)	.072(2)
C(44)	-2041(7)	1934(4)	-4571(8)	.077(2)
C(45)	-2292(6)	2166(4)	-3132(7)	.068(2)
C(46)	-1102(5)	2466(3)	-2580(6)	.0548(13)
C(51)	2215(5)	2346(3)	-3195(6)	.0456(12)
C(52)	1907(5)	1660(3)	-3754(6)	.0556(13)
C(53)	2780(6)	1236(4)	-4065(8)	.072(2)
C(54)	4002(7)	1512(4)	-3770(8)	.076(2)
C(55)	4330(7)	2180(4)	-3180(8)	.074(2)
C(56)	3460(6)	2611(3)	-2881(7)	.067(2)

*The positional parameters have been multiplied by 10^4.

TABLE 6.7.

Derived Hydrogen Atom Positional* and Thermal Parameters

Atom	x	y	z	B
H1C(1)	-261	4164	-2787	5.15
H1C(2)	2020	3923	-3162	5.05
H1C(3)	1276	5295	-2874	7.46
H2C(3)	34	5084	-4201	7.46
H3C(3)	-38	5361	-2763	7.46
H1C(4)	578	4292	-5389	7.68
H2C(4)	921	3489	-5483	7.68
H3C(4)	-361	3689	-5379	7.68
H1C(5)	992	3338	1638	5.79
H1C(6)	1972	2044	3145	7.34
H2C(6)	539	2251	2457	7.34
H1C(7)	1345	1220	1592	6.80
H2C(7)	180	1657	549	6.80
H1C(8)	1244	1760	-887	5.58
H1C(9)	3343	2084	-170	5.22
H1C(10)	3664	1714	2713	6 55
H2C(10)	4771	1893	2242	6.55
H1C(11)	4333	2699	3856	7.20
H2C(11)	4707	3015	2640	7 20
H1C(12)	2991	3711	2124	5.48
H1C(22)	-1017	4179	-871	5 95
H1C(23)	-2077	4630	481	6.80
H1C(24)	-1068	5355	2438	6.24
H1C(25)	1025	5699	3067	6.48
H1C(26)	2142	5244	1753	5.43
H1C(32)	2344	5699	-524	5.79
H1C(33)	4327	6275	93	7.09
H1C(34)	6171	5570	588	7.10
H1C(35)	6041	4312	804	6.65
H1C(36)	4048	3752	151	5.47
H1C(42)	-508	2346	-5500	5.58
H1C(43)	-2608	1855	-6443	6.69
H1C(44)	-3666	1718	-4905	6.97
H1C(45)	-2755	2123	-2516	6.12
H1C(46)	-746	2620	-1585	5.25
H1C(52)	1083	1479	-3937	5.40
H1C(53)	2553	772	-4501	6.91
H1C(54)	4587	1225	-4015	7.19
H1C(55)	5159	2363	-2978	6.80
H1C(56)	3698	3067	-2476	6.41

*The positional parameters have been multiplied by 10^4.

TABLE 6.8

Final Group Positional* and Thermal Parameters

Atom	x	y	z	B
		THF(1)		
O(6)	6142	5108	6826	21.9519
C(61)	6853	4706	6180	18.5111
C(62)	5837	4234	4855	30.3335
C(63)	4675	4742	4346	26.4661
C(64)	4809	5074	5910	26.7729
		THF(2)		
O(7)	5457	4713	4846	29.0580
C(71)	4248	4642	4946	20.6063
C(72)	4528	4464	6644	27.4673
C(73)	5776	4032	7087	34.0254
C(74)	6452	4458	6164	26.8770

*The positional parameters have been multiplied by 10^4.

6.2.2 · Determination of Absolute Configuration

The absolute configuration of the cation, determined by the Bijvoet absorption edge technique, was confirmed by refinement of both models, including recalculated H atom contributions, to convergence. The chosen model had residuals of $R_1 = 0.0403$ and $R_2 = 0.0505$ while the enantiomeric structure gave R_1 and R_2 values of 0.0726 and 0.1021 respectively. When the R factor ratio test (92) is applied to R_2, it indicates that the alternate model can be rejected at a confidence level of greater than 0.995 assuming no systematic errors in the data. Table 6.9 lists a selection of structure amplitudes for the chosen model for which F_c (hkl) and $F_c(h\bar{k}l)$ differ by more than 25%, based on the final positional parameters. The observed F_o relationships for the same reflections confirm the choice of enantiomer.

6.3 Structure Description

A perspective drawing of the cation with the atom numbering scheme is presented in Figure 6.2 and a stereoview of the overall geometry of the cation is shown in Figure 6.3. Selected bond distances and angles are listed in Table 6.10.

The Rh atom is coordinated in a square planar geometry to the diphosphine and the diene ligands. The internal geometry of the diene is quite normal with average Csp^3-Csp^3 and Csp^2-Csp^3 distances of $1.47(2)$ and $1.51(1)$ Å respectively;

TABLE 6.9

DETERMINATION OF ABSOLUTE CONFIGURATION

h	k	l	$F_c(hkl)$	F_o Relationship	$F_c(h\bar{k}l)$
$\bar{6}$	$\overline{14}$	3	6.87	<	10.25
9	4	1	5.96	<	8.59
$\overline{11}$	$\overline{11}$	2	3.44	<	4.76
6	$\bar{5}$	4	7.38	<	10.20
0	$\bar{8}$	6	11.01	<	15.17
$\overline{11}$	4	5	9.04	>	5.66
$\bar{7}$	$\overline{15}$	7	6.05	<	8.29
$\bar{3}$	$\overline{16}$	7	6.63	<	9.98
$\bar{3}$	12	2	19.58	>	12.89
0	$\bar{6}$	6	16.88	<	22.24
$\bar{2}$	9	10	2.68	>	1.84
$\bar{4}$	$\bar{5}$	7	16.49	<	21.40
$\bar{9}$	3	5	17.69	>	12.70
$\bar{1}$	$\bar{5}$	1	40.03	>	29.21

Figure 6.2 Perspective view of cation showing the
atom numbering scheme
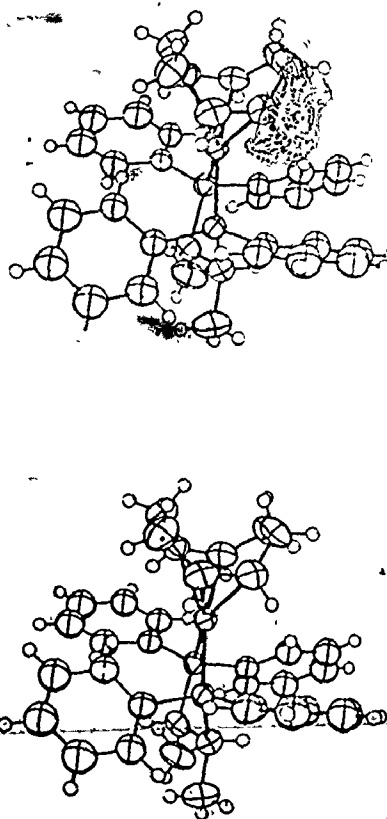
Figure 6.3 Stereoview of the cation. The thermal
parameters of the H atoms have been
reduced for clarity

TABLE 6.10

SELECTED BOND DISTANCES (Å) AND ANGLES (Deg.)

Rh-P(1)	2.275(1)	P(1)-Rh-P(2)	83.82(6)
Rh-P(2)	2.266(1)	C(5)-Rh-C(8)	80.7(3)
Rh-C(5)	2.241(4)	C(9)-Rh-C(12)	80.2(2)
Rh-C(8)	2.238(6)		
Rh-C(9)	2.247(5)	Rh-P(1)-C(1)	109.5(2)
Rh-C(12)	2.247(5)	Rh-P(1)-C(31)	111.7(2)
		C(1)-P(1)-C(21)	106.2(2)
C(5)-C(12)	1.362(8)	C(21)-P(1)-C(31)	106.7(2)
C(8)-C(9)	1.357(8)	Rh-P(2)-C(2)	110.1(2)
		Rh-P(2)-C(51)	115.5(2)
P(1)-C(1)	1.840(6)	C(2)-P(2)-C(41)	106.4(2)
P(1)-C(21)	1.801(5)	C(41)-P(2)-C(51)	106.8(2)
P(1)-C(31)	1.812(5)		
P(2)-C(2)	1.837(6)	P(1)-C(1)-C(2)	106.2(3)
P(2)-C(41)	1.824(5)	P(1)-C(1)-C(3)	115.8(4)
P(2)-C(51)	1.811(5)	P(2)-C(2)-C(1)	106.6(4)
		P(2)-C(2)-C(4)	115.5(4)
C(1)-C(3)	1.524(8)	C(6)-C(5)-C(12)	125.7(6)
C(2)-C(4)	1.527(8)	C(5)-C(6)-C(7)	117.9(5)
C(1)-C(2)	1.580(8)	C(6)-C(7)-C(8)	115.5(6)
C(5)-C(6)	1.517(11)	C(7)-C(8)-C(9)	126.5(6)
C(6)-C(7)	1.480(10)	C(8)-C(9)-C(10)	123.8(6)
C(7)-C(8)	1.500(9)	C(10)-C(11)-C(12)	116.4(5)
C(9)-C(10)	1.526(9)	C(9)-C(10)-C(11)	115.6(5)
C(10)-C(11)	1.456(9)	C(5)-C(12)-C(11)	126.6(6)
C(11)-C(12)	1.510(8)		
		C(3)-C(1)-C(2)-C(4)	-50.5(7)[a]
Cl-O(1)	1.429(6)		
Cl-O(2)	1.408(6)	O(1)-Cl-O(2)	109.5(5)
Cl-O(3)	1.378(6)	O(2)-Cl-O(3)	105.8(4)
Cl-O(4)	1.385(6)	O(2)-Cl-O(4)	109.4(5)
		O(3)-Cl-O(4)	113.1(6)

[a] When looking from C(1) to C(2) rotating C(3) about the C(1)-C(2) axis will superimpose its image upon C(4).

and an average internal angle at the sp^3 carbons of $116(1)^\circ$.
The two coordinated C-C double bond lengths are $1.362(8)$ and
$1.357(8)$ $\overset{o}{A}$. The values determined in this structure are
comparable to the range of distances and angles observed for
this ligand in other structures (131,132). The average Rh-C
distance for the coordinated double bonds is $2.24(1)$ $\overset{o}{A}$.
The C(5)-C(12) and C(8)-C(9) double bonds are not coordinated
perpendicular to the Rh-P(1)-P(2) plane, but are tilted in
the same direction, by 13.3 and 13.9° respectively, as often
observed for coordinated double bonds. Also the C atoms of
these two double bonds are not symmetrically disposed above
and below the Rh-P(1)-P(2) plane, but rather the diene is
coordinated with C(5) and C(9) approximately twice as far
out of the plane as C(12) and C(8). A selection of least-
squares planes and distances from the coordination plane
is given in Table 6.11.

The overall conformation of the five-membered
chelating phosphine ring is δ. The absolute configurations
of the two asymmetric carbon atoms are designated S, S, which
places the two methyl groups, C(3) and C(4), in the expected
equatorial dispositions.

The Rh-P(1) and Rh-P(2) distances are $2.275(1)$ and
$2.266(1)$ $\overset{o}{A}$, respectively. These are somewhat shorter than
might be expected from other rhodium-phosphine structures
(133,134) but we are unable to comment on the significance,
if any, of this observation. The P(1)-Rh-P(2) angle of
$83.82(6)^\circ$ is comparable to values observed in other structures

TABLE 6.11

SELECTED WEIGHTED LEAST-SQUARES PLANES[a]

Plane 1   A = 0.624   B = -14.7   C = 5.35   D = -6.64[b]

C(21)	0.000(5)	C(24)	0.003(6)
C(22)	0.003(6)	C(25)	0.001(7)
C(23)	-0.005(7)	C(26)	-0.002(6)
		P(1)	0.242

Plane 2   A = -3.01   B = 0.951   C = 9.84   D = -0.674

C(31)	0.009(5)	C(34)	-0.006(8)
C(32)	-0.005(6)	C(35)	0.016(7)
C(33)	0.002(7)	C(36)	-0.015(6)
		P(1)	-0.006

Plane 3   A = 3.47   B = -16.9   C = 1.33   D = -4.88

C(41)	0.014(5)	C(44)	0.014(7)
C(42)	-0.007(6)	C(45)	0.004(7)
C(43)	-0.010(7)	C(46)	-0.016(6)
		P(2)	0.060

Plane 4   A = -0.544 B = -7.09   C = 8.61   D = -4.52

C(51)	-0.009(5)	C(54)	-0.010(7)
C(52)	0.011(6)	C(55)	0.007(7)
C(53)	-0.003(7)	C(56)	0.005(7)
		P(2)	0.181

Dihedral Angles (Deg) between Planes

Plane	Plane	Angle		Plane	Plane	Angle
1	2	57.80		2	3	81.90
1	3	24.98		2	4	28.12
1	4	30.40		3	4	53.83

Table 6.11 continued

Displacements from the Rh-P(1)-P(2) Plane (Å)

C(1)	0.437(5)	C(21)	1.155(5)
C(2)	-0.363(6)	C(31)	-1.640(5)
C(5)	0.891(6)	C(41)	1.628(5)
C(12)	-0.434(6)	C(51)	-1.222(5)
C(8)	0.427(6)		
C(9)	-0.890(6)		

[a]Distances given are displacements from the plane in Å with those without esd's related to atoms not included in the calculation of the plane

[b]The form of the plane equation is $Ax + By + Cz - D = 0$.

with five-membered chelating phosphine ligands (134,135).
The average P-C(alkyl) and P-C(aryl) distances of 1.838(2)
and 1.812(5) $\overset{o}{A}$ are normal, as is the average C-C distance of
1.54(2) $\overset{o}{A}$. The four phenyl rings have the following average
bond lengths and angles: R1(C(21)-C(26)) 1.373(8) $\overset{o}{A}$,
120.0(4)^{o}; R2(C(31)-C(36)) 1.391(6) $\overset{o}{A}$, 120.0(3)^{o}; R3(C(41)-
C(46)) 1.382(7) $\overset{o}{A}$, 120.0(4)^{o}; R4(C(51)-C(56)) 1.392(8) $\overset{o}{A}$,
120.0(4)^{o}. The ring geometries may be examined to see if
there are significant deviations from the D_{6h} symmetry often
imposed in group refinements. The C-C distances show no
systematic deviations from the mean values with the largest
difference being 2.5σ. The angles at the *alpha, ortho, meta*
and *para* C atoms have means of 118.5(2), 120.5(2), 120.1(3),
and 120.3(1)^{o}, respectively. These values indicate a signi-
ficant (4.8σ) decrease of the internal angle at the α carbon
atom of a phenyl ring from the expected angle of 120° for a
group of D_{6h} symmetry. A similar geometry is observed for
the phenyl rings in the structures of Chapters 3 and 4.

The diphosphine ligand maintains an approximate C_2
symmetry after coordination as indicated by the disposition
of the phenyl rings about the Rh-P(1)-P(2) plane. Thus the
related α carbon atoms, C(21) and C(51), are approximately
equidistant from the plane (Table 6.11) as is the pair C(31)
and C(41). It should also be noted that phenyl rings R1 and
R4, are bent towards the COD ligand with P(1)-C(21)-C(24) and
P(2)-C(51)-C(54) angles of 171.8(3) and 172.7(3)^{o}, respectively.

The corresponding angles for the other two rings are 176.6(3) and 176.5(3)°.

The geometry of the perchlorate anion is unexceptional, with an average Cl-O bond length of 1.40(1) Å. There are no close contacts to the cation which might indicate a hydrogen bonding network, for the distance of closest approach is 2.65 Å between O(3) and HC(32) on one phenyl ring. The shortest Rh-Cl and Rh-Rh distances are 5.616(2) and 9.950(2) Å, respectively. Thus the crystals are built up from discrete cations and anions, as is shown in the stereoview of the unit cell contents presented in Figure 6.4.

At the time this work was done there were no complete reports of structures of similar complexes in the literature. The only published results was a communication of the structure of an IrCOD((+)-diop)Cl complex (136). Thus, we felt that more information should be obtained about the stereochemistry of these complexes with a view to exploring the causes of the observed optical yields during asymmetric hydrogenation. An analogous complex to the one presented in this chapter was prepared and found to give high optical yields as an asymmetric hydrogenation catalyst (57). The phosphine used was (+)-1,2-bis(diphenylphosphino)propane ((+)-prophos) and the active catalyst precursor is the [RhNBD((+)-prophos)]ClO₄ complex. The results of the structural analysis of this complex are presented in the next chapter. After the work of Chapter 6 had been published as a full paper (138) and the

Figure 6.4 Stereoview of a unit cell contents. The thermal parameters
of the THF molecule have been reduced and only one of the disordered
pair have been included. The c axis runs from left to right, with the
b axis vertical

project of Chapter 7 was well underway a brief note in a
paper by Knowles *et.al.* (137) described a structure with
some similarities to our work.   To date these are the only
reports which have appeared in the literature and they will
be discussed in detail in Chapter 8.

CHAPTER 7

THE CRYSTAL AND MOLECULAR STRUCTURE OF (BICYCLO[2.2.1]HEPTA-2,5-DIENE)((+)$_{589}$-1,2-BIS(DIPHENYLPHOSPHINO)PROPANERHODIUM(I)
PERCHLORATE

7.1 Introduction

After completing the structure presented in Chapter 6, there were questions as to whether the phosphine geometry observed in the solid state could be interpreted in terms of the actual catalyst and its interactions with a substrate molecule. We felt that the more information which could be obtained about these complexes, the more confidence we could put in any extrapolations of solid state configuration to behavior in solution. Accordingly we undertook the structure of an analogous complex.

The title complex is an active catalyst precursor for the same type of asymmetric hydrogenations catalysed by the Rh(I) complex of the phosphine ((-)-chiraphos) used in Chapter 6. In this case the phosphine was prepared in the opposite chirality, and consequently gives enantiomeric reduction products, but the optical yields are still in excess of 90%. The crystals were not of good quality but as that is often the case for those structures which are interesting, the study was pursued anyway. Unfortunately a satisfactorily complete solution to this structure was not achieved.

7.2 Experimental

Dark orange-red crystals of (Bicyclo $[2.2.1]$ hepta-2, 5-diene)-1,2-bis(diphenylphosphino)propanerhodium(I) perchlorate, $[Rh\pi-(C_7H_8)(PPh_2CHCH_3CH_2PPh_2)]$ ClO_4, were supplied by B. Bosnich and M. Fryzuk as a methylene chloride solvate-containing, by analysis, a half CH_2Cl_2 per Rh atom (139). Weissenberg and precession photography showed the crystals to be monoclinic with Laue symmetry 2/m. The systematic absences observed, $h + k$ odd for hkl reflections, and the requirement that an optically active species crystallize in an acentric space group, determine the space group to be C2, C_2^3, No. 5 (72).

The crystal chosen for data collection (Figure 7.1) which had been fractured from a clump, was mounted with $[100]$ approximately $15°$ from coincidence with the diffractometer spindle axis. Cell constants and an orientation matrix were obtained from a least-squares refinement of the setting angles for 23 intense, carefully centered reflections with $23<2\theta<50°$. Prefiltered Cu K_α radiation ($\lambda=1.54184$ Å) was used at an ambient temperature of $20°C$. Crystal and space group data are summarized in Table 7.1.

The conditions used for data collection are presented in Table 7.2. Measurement of standard reflections over the course of data collection and an examination of crystal mosaicity by the ω scan technique, before and after data collection, indicated extensive crystal decomposition had
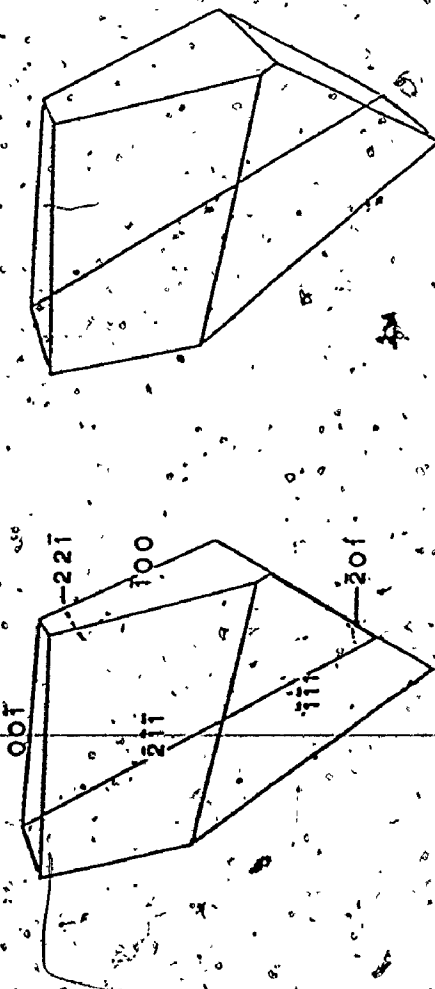
Figure 7.1. Stereoview of crystal

TABLE 7.1

CRYSTAL DATA FOR $[Rh\pi-(C_7H_8)(PPh_2CHCH_3CH_2PPh_2)]ClO_4 \cdot \frac{1}{2}CH_2Cl_2$

Formula	$C_{34.5}H_{35}Cl_2O_4P_2Rh$
Fw	749.42
Crystal description	Red-orange blocks
Systematic absences	$h + k$ odd for hkl
Laue symmetry	$2/m$
Crystal system	Monoclinic
Space group	C2
Cell constants	$a = 34.092(12)$ Å
	$b = 11.516(3)$
	$c = 20.388(6)$
	$\beta = 118.398(13)°$
Cell volume	7041.2 Å^3
Density (calculated)	1.414 g cm^{-3}
(observed)	$1.452(1)$ g cm^{-3}
Density measured by	Neutral bouyancy in CCl_4 and n-pentane
Z	8
Symmetry constraints	None, 2 formula units per equivalent position
Crystal faces (7)	100, $(\overline{1}\overline{1}1)$, $(\overline{2}01)$, $(2\overline{1}\overline{1})$, $(22\overline{1})$, $(00\overline{1})$
Crystal dimensions	$0.15 \times 0.12 \times 0.31$ mm
μ (CuK$_{\alpha_1}$)	62.29 cm^{-1}

TABLE 7.2

EXPERIMENTAL CONDITIONS ASSOCIATED WITH DATA COLLECTION

Radiation	CuK_α
Wavelength	1.54184 Å
Take-off angle	$2.7°$
% of intensity available	90
Tube Kv,mA	40, 16
Filter	Ni (0.018 mm) prefilter
Temperature	$20°C$
Collimator size	1.0 mm
Aperture size	4 x 4 mm
Crystal-counter distance	32 cm.
Mean ω scan width	$0.1°$
No. and 2θ range of centered reflections	23; $23<2\theta<50°$
Scan range; speed	$\alpha_1 - 0.6°$ to $\alpha_2 + 0.8°$; $2°min^{-1}$
Miller index range	$\pm h$, $+k$, $+l$
2θ shells	$2-60°$, $60-90°$, $90-120°$
Background count time	10s
Standards	5; 002, 400, 020, $\bar{4}00$, $11\bar{1}$; measured every 200 reflections.
No. of measured intensities	5686
Standard decay	002, -23%; 400, -17% 020, -4%; $\bar{4}00$, -14% $11\bar{1}$, -5%

occurred. The reduction in standard intensities varied from 4 to 23%, and the peak width at half-height in the ω scans increased by an average of 0.03°. In order to try and collect a better data set some 18 attempts were made to find other suitable crystals from the samples provided. These proved fruitless and were abandoned.

The intensity data were processed and the value for p in equation 2.2 was initially chosen to be 0.02 but was increased to 0.06 by the end of the refinement process.

7.3 Structure Solution and Refinement

The positional parameters for the two Rh atoms were determined from a three-dimensional Patterson synthesis. A structure factor calculation and difference Fourier synthesis revealed four peaks assignable to the P atoms. A series of least-squares refinements and difference Fourier calculations eventually resulted in locating all non-H atoms of the cation and anion. At this stage of the refinement the full matrix least-squares cycles were being run under the following conditions:

i) two Rh, four P and two Cl atoms as individual atoms having anisotropic thermal parameters;

ii) all eight phenyl rings as rigid groups (D_{6h}, C-C = 1.392 Å) with an overall temperature factor for each group,

iii) the remaining twenty C atoms of the phosphine and diene ligands as individual isotropic atoms,

iv) and the O atoms of the two perchlorate anions

as rigid groups $(T_d,$ Cl-O = 1.41 $\overset{o}{A})$ with an overall temperature factor for each group.

Two cycles on this model using 4313 observations with $F > 3\sigma(F)$ and 263 variables gave residuals R_1 and R_2 of 0.124 and 0.162 respectively.

In order to improve the agreement between F_o and F_c, decay and absorption corrections were considered. A decay correction of the form

$$CT = CT_o + 0.10(NREF)CT$$

was applied to the data, where CT is the total peak count and NREF is a function representing the percentage of time from the start of data collection. An examination of the variation in transmission coefficients, 0.416 to 0.603, showed there was little to be gained by correcting the data for absorption effects, especially in light of the crystal decomposition problems. Accordingly the data used for the subsequent refinement was not so treated.

At this time a difference Fourier was examined for evidence of any methylene chloride molecules of solvation, for the presence of half a methylene chloride per Rh atom had been postulated to account for the nmr and analytical results (139). No peaks could be found which could reasonably be fitted to the assumed geometry for CH_2Cl_2 (140) or to any disordered arrangement of this species.

Despite several attempts to locate these solvent molecules

no model could be constructed which appeared practicable, so no methylene chloride molecules were included.

Other problems were also apparent at this point in the refinement. The geometry of the cations was unsatisfactory. The C-C single bond lengths ranged from 1.26 to 1.77 Å with grossly inequivalent lengths for chemically equivalent bonds. The angles around the tertiary carbon atom, $C(2)$, of the phosphine chelate ring were abnormally large ranging from 115 to $122°$. In addition, the temperature factors were larger than would be expected for most of the atoms.

The most apparent cause of difficulty (excluding the crystal decay problems) is the presence of two supposedly independent molecules in the cell. It is observed that one molecule is approximately related to the second by $\frac{1}{2} + x$, $0.2 + y$, $\frac{1}{2} + z$ which is equivalent to an approximate two-fold axis along $3x + z + 1 = 0$, $y = -0.1$. All attempts to incorporate this symmetry into an alternate space group failed. With this sort of difficulty present it was decided to use the direct methods program MULTAN to see if a different solution could be found which would give a better refinement. There were sixteen possible solutions generated by MULTAN. Of these only that with the highest reliability index was geometrically feasible and this solution was that originally determined by the Patterson method.

Since a stereochemically reasonable model could not be obtained by the usual least-squares refinement process,

it was decided to determine if any particular data were

causing the poor agreement observed. A model was calculated

containing the norbornadiene constrained to a rigid group

geometry derived from previous structures (141,142), and

each five-membered phosphine ligand as a rigid group based

on the structure determined in Chapter 6. After a least-

squares cycle varying the parameters for the Rh atoms,

phosphine groups, norbornadiene groups, phenyl and

perchlorate groups the observed structure factors, F_o,

were examined for statistical trends with the program

RANGER. This analysis showed the 736 data with $118<2\theta<48.6°$

gave anomalously poor agreement. Two subsequent cycles

with the group restraints removed from each set of five

atoms comprising the phosphine backbone and omitting the

poorly agreeing data gave residuals of $R_1=0.092$ and $R_2=0.118$.

The resulting geometry was much more reasonable and the

large residual peaks in a difference Fourier, which had

been located near the sites of the Rh atoms, were markedly

decreased. In examining F_o and F_c for the omitted data it

was found that there were 31 reflections with particularily

poor agreement, $|(F_o-F_c)/\sigma(F_o)|\geq 15$. By dropping only these

reflections out of a least-squares refinement cycle, the

agreement factors remained the same as those calculated

when all 736 data were omitted. Examination of the 31

omitted data indicated that $F_c>F_o$ for most of the reflections

dropped. This observation may result from the presence of

secondary extinction effects, consequently an extinction

parameter was refined during the last cycle of refinement. The maximum change in F_o as a result is 8.6%. No other cause could be found for the poor agreement between F_o and F_c.

It was felt that the structure at this point represented the best model which could be achieved given the inherent problems with the data set. Refinement was not continued. The conditions and results of the final least-squares cycle are given in Table 7.3.

On the basis of the synthetic route to the ligand and the behavior of the complex during hydrogenation (57, 139), the asymmetric C atom is supposed to have the R absolute configuration. The structure was refined in this hand, but upon attempting to prove the configuration by refining the enantiomorphic structure there was no significant difference in R_2 (0.118 compared to 0.117). Thus while it is almost certain that the chiral site is R we are unable to confirm this by the anomalous dispersion of X-rays.

The final atomic positional and thermal parameters are presented in Table 7.4, while the group parameters are given in Table 7.5. The structure factor amplitudes are listed in Appendix 3.

7.4 Structure Description

A perspective view of a cation including the atom labelling scheme is presented in Figure 7.2. A stereoview showing the overall stereochemistry of a cation is given in

TABLE 7.3

CONDITIONS AND RESULTS FOR FINAL FULL MATRIX LEAST-SQUARES REFINEMENT CYCLE

Observations	4341
Variables	239
Ratio (observations/variables	18.2
Agreement factors R_1	0.0918
R_2	0.1184
Error on an Observation of Unit Weight	2.4e
Maximum (parameter shift/esd)	8.2
Number of Anisotropic atoms	8
Anomalous Scatterers	8; 2xRh, 2xCl, 4xP.
Rigid Groups (type)	2(perchlorate oxygens); 8(phenyl); 2(norbornadiene)
Extinction Coefficient	0.499×10^{-7}
Remaining Difference Fourier Peak: a)Electron density	$1.4(2) e \text{ Å}^{-3}$
b)Fractional coordinates	-0.35, -0.01, -0.35
c)Associated with	1Rh

TABLE 7.4

Final Atomic Positional and Thermal Parameters*

Atom	x	y	z	U11	U22	U33	U12	U13	U23
1Rh	3248.4(5)	-75(2)	3601(1)	649(10)	631(12)	612(11)	-14(8)	319(8)	-1(19)
2Rh	-1781.8(5)	2838	1369(1)	638(9)	614(11)	593(10)	-25(8)	347(8)	-13(9)
1P(1)	3799(2)	916(6)	3557(3)	658(30)	771(41)	550(31)	-21(28)	311(25)	-14(29)
1P(2)	3476(2)	731(6)	4743(3)	755(36)	547(34)	683(37)	-16(28)	369(30)	39(28)
2P(1)	1514(2)	914(6)	300(3)	705(30)	505(33)	654(35)	1(26)	414(27)	-18(28)
2P(2)	1868(2)	1165(6)	1285(3)	633(38)	728(40)	568(33)	-36(28)	314(26)	8(29)
1C1	1212(3)	648(8)	5334(6)	1491(61)	703(48)	1560(83)	187(46)	632(58)	77(56)
2C1	3816(3)	1208(6)	-473(5)	1466(60)	617(41)	1489(66)	-77(41)	515(50)	-59(43)
1C(1)	4020(8)	1548(22)	5002(13)	.091(7)					
1C(2)	4608(8)	1965(23)	4299(13)	.072(6)					
1C(3)	4443(11)	2465(32)	4492(20)	.160(12)					
2C(1)	734(7)	445(19)	363(12)	.076(6)					
2C(2)	1873	-218(19)	131(11)	.068(5)					
2C(3)	82	-628(23)	-639(14)	.094(8)					

*Estimated standard deviations in this and other tables are given in parentheses and correspond to the least significant digits.

The thermal ellipsoid is given by $\exp[-(B_{11}h^2 +B_{22}k^2 +B_{33}l^2 +2B_{12}hk +2B_{13}hl +2B_{23}kl)]$ and $U_{ij}=B_{ij}/(2\pi^2 a_i^* a_j^*)$ Å². The quantities

given in the table have been multiplied by 10^4.

TABLE 7.5

Positional and Thermal Parameters for the Atoms of the Rigid Groups.

Atom	x	y	z	B	Atom	x	y	z	B
1ClO4					**2ClO4**				
1O(1)	1642(6)	934(22)	5296(12)	20.1(12)	2O(1)	3414(7)	846(26)	-414(13)	19.8(9)
1O(2)	1418(6)	-124(18)	6017(8)	13.7(6)	2O(4)	4151(7)	425(29)	3(14)	26.7(12)
1O(3)	1002(6)	-191(17)	4727(8)	14.8(6)	2O(3)	3702(9)	881(29)	-1241(12)	23.6(11)
1O(4)	1887(7)	1488(16)	5359(13)	15.0(8)	2O(2)	3902(12)	2309(21)	-335(21)	34.1(23)
1Ph1					**2Ph1**				
1C(11)	3071(4)	1726(12)	4719(8)	5.5(4)	2C(11)	1172(4)	72(13)	2014(7)	6.4(5)
1C(21)	3105(4)	2921(13)	4652(8)	7.3(6)	2C(21)	1385(5)	587(11)	2726(9)	7.4(5)
1C(31)	2765(6)	3651(18)	4597(9)	6.3(5)	2C(31)	1437(5)	-250(16)	3326(6)	8.1(6)
1C(41)	2391(5)	3187(15)	4618(9)	8.5(8)	2C(41)	1434(5)	-1443(14)	3214(8)	8.7(6)
1C(51)	2357(4)	1992(16)	4677(8)	7.3(5)	2C(51)	1300(6)	-1879(10)	2582(10)	9.7(7)
1C(61)	2697(5)	1262(18)	4732(9)	7.6(6)	2C(61)	1169(5)	-1121(14)	1902(7)	6.9(5)
1Ph2					**2Ph2**				
1C(12)	3673(4)	1708(12)	2740(6)	4.5(4)	2C(12)	1964(4)	41(12)	295(8)	4.5(4)
1C(22)	3599(5)	2988(12)	2706(7)	7.4(5)	2C(22)	2029(4)	-1108(12)	536(7)	4.6(4)
1C(32)	3479(5)	3500(18)	2845(9)	8.8(6)	2C(32)	2402(5)	-1713(10)	617(8)	6.0(5)
1C(42)	3432(5)	2907(15)	1417(7)	9.4(6)	2C(42)	2711(4)	-1170(14)	455(8)	6.6(5)
1C(52)	3506(5)	1714(15)	1450(7)	7.7(6)	2C(52)	2647(4)	-21(14)	214(9)	8.3(7)
1C(62)	3626(5)	1114(18)	2111(9)	6.7(6)	2C(62)	2273(5)	585(10)	134(9)	6.2(6)

	1Ph3			
IC(13)	3635(4)	-142(15)	5541(7)	5.3(7)
IC(23)	3680(5)	336(12)	6201(9)	6.9(5)
IC(33)	3861(5)	-324(16)	6851(7)	9.0(8)
IC(43)	3995(5)	-1462(16)	6842(8)	9.8(6)
IC(53)	3958(5)	-1961(12)	6182(11)	7.4(7)
IC(63)	3778(5)	-1281(15)	5532(8)	6.2(6)
	1Ph4			
IC(14)	4276(5)	-12(14)	3688(9)	6.1(5)
IC(24)	4602(6)	349(12)	3525(9)	5.9(6)
IC(34)	4945(5)	-404(17)	3602(10)	9.4(8)
IC(44)	4961(5)	-1518(15)	3878(10)	7.9(8)
IC(54)	4635(6)	-1879(12)	4060(10)	8.8(6)
IC(64)	4293(5)	-1125(16)	3965(9)	6.4(7)
	1NBD			
IC(4)	3123(4)	-1528(15)	2791(9)	7.6(6)
IC(5)	2872(5)	-2363(10)	3046(8)	6.6(7)
IC(6)	2862(5)	-1660(14)	3680(5)	6.8(5)
IC(7)	2563(5)	-768(12)	3326(8)	5.7(5)
IC(8)	2403(4)	-946(13)	2488(6)	7.6(6)
IC(9)	2825(6)	-619(13)	2437(8)	5.8(6)
IC(10)	2395(4)	-2259(13)	2425(7)	6.9(5)

	2Ph3			
2C(13)	663(4)	2142(11)	1285(7)	4.7(3)
2C(23)	668(4)	3283(12)	1054(8)	6.0(5)
2C(33)	321(5)	4036(10)	985(9)	7.6(6)
2C(43)	-10(4)	3649(13)	1147(9)	9.0(6)
2C(53)	-5(4)	2509(14)	1378(8)	6.9(5)
2C(63)	332(5)	1755(10)	1447(8)	7.3(5)
	2Ph4			
2C(14)	1316(4)	1773(12)	-554(6)	5.6(4)
2C(24)	1186(4)	2920(12)	-558(6)	5.7(4)
2C(34)	1029(4)	3578(10)	-1207(8)	6.7(5)
2C(44)	1003(5)	3090(14)	-1852(6)	5.8(6)
2C(54)	1133(5)	1943(15)	-1848(7)	9.0(6)
2C(64)	1293(5)	1284(10)	-1199(9)	7.0(6)
	2NBD			
2C(4)	2088(5)	2429(13)	2563(8)	6.1(5)
2C(5)	2539(4)	2629(12)	2577(6)	6.5(5)
2C(6)	2416(5)	2340(12)	1765(8)	6.5(6)
2C(7)	2148(6)	3255(14)	1346(5)	5.3(5)
2C(8)	2116(5)	4068(10)	1919(8)	7.5(5)
2C(9)	1820(4)	3344(15)	2145(9)	6.5(8)
2C(10)	2573(5)	3942(13)	2592(7)	7.1(8)

The positional parameters have been multiplied by 10. The phenyl group numbering scheme is : the number preceeding the group specifies the molecule in which the group is found, the first digit in brackets is the atom number, and the second digit is the group number.

Figure 7.2 Perspective view of cation including the atom numbering scheme

Figure 7.3. Only one molecule is illustrated due to the similarity between the two molecules arising from the pseudo two-fold axis in the cell. Selected bond distances and angles associated with those atoms which were not constrained to be groups are listed in Table 7.6.

The Rh atom displays square planar coordination geometry with the double bonds of the norbornadiene oriented approximately perpendicular to the square plane. The average Rh-C(sp^2) distance to the dienes is 2.19(9) Å with values ranging from 2.11 to 2.28 Å, and the average Rh-P distance is 2.28(4) Å. Both these average distances agree reasonably well with values determined in Chapter 6. With respect to the rest of the molecular geometry it is observed that no single quantity is particularily bad and the errors are large enough to keep the values within statistical range (3σ) of the commonly accepted values for comparable distances and angles (Chapter 6, 143).

It was to examine the stereochemistry of the phosphine ligand that this structure was undertaken and although it is unfortunate that better results could not be obtained we can still evaluate the overall conformation. The methyl group on the phosphine backbone is in the expected equatorial orientation. At first glance the phenyl rings appear to have a very similar orientation to that observed in Chapter 6. However, upon closer examination it is seen that while the two rings on P(2) in each complex adopt a similar
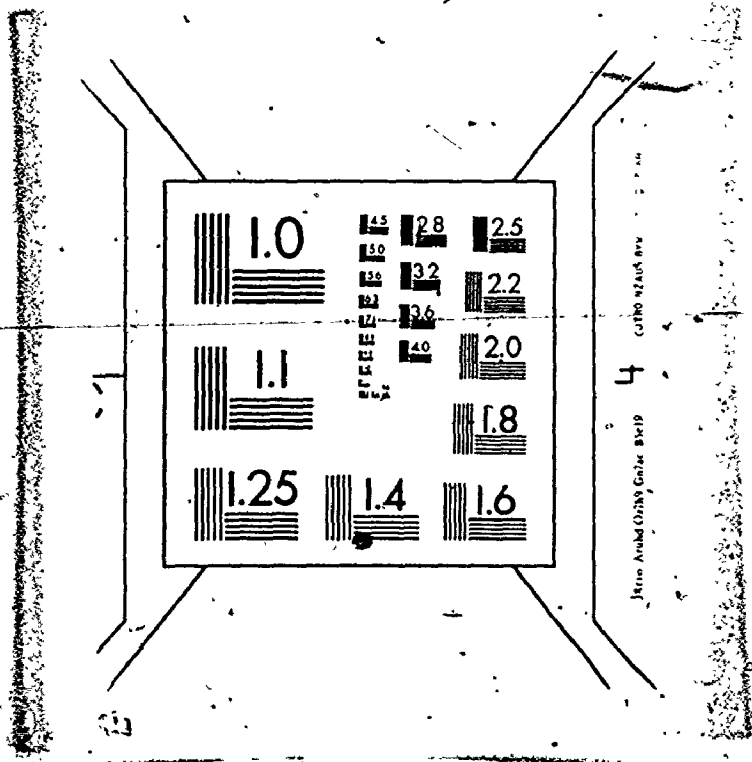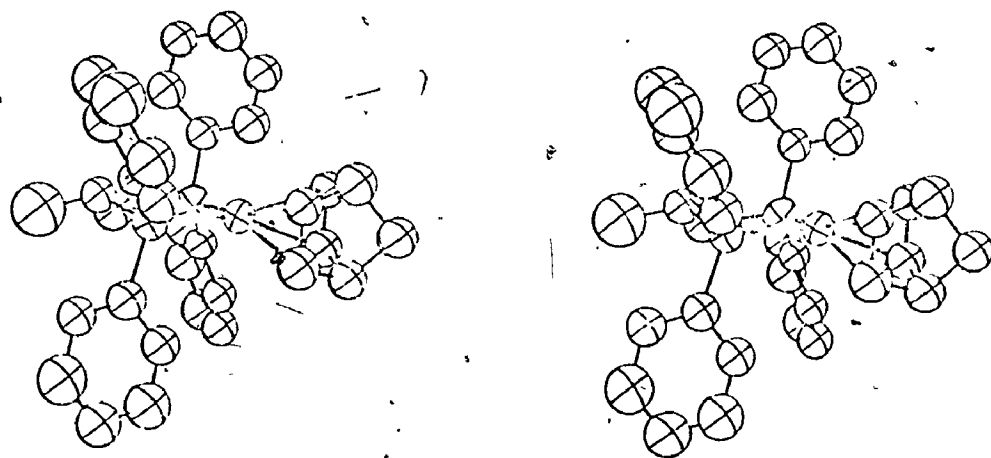
Figure 7.3   Stereoview of the cation.

TABLE 7.6

SELECTED BOND DISTANCES (Å) AND ANGLES (Deg)

Distances

Atoms	1[a]	2
Rh-P(1)	2.259(6)	2.322(6)
Rh-P(2)	2.234(6)	2.298(6)
Rh-C(4)	2.24(2)	2.20(2)
Rh-C(6)	2.28(1)	2.21(2)
Rh-C(7)	2.24(2)	2.11(2)
Rh-C(9)	2.20(2)	2.11(2)
P(1)-C(2)	1.80(2)	1.89(2)
P(1)-C(12)	1.76(1)	1.84(2)
P(1)-C(14)	1.86(2)	1.83(1)
P(2)-C(1)	1.91(2)	1.86(2)
P(2)-C(11)	1.79(2)	1.85(2)
P(2)-C(13)	1.80(2)	1.78(2)
C(1)-C(2)	1.49(3)	1.63(3)
C(2)-C(3)	1.46(3)	1.46(3)

Angles

Atoms	1	2
P(1)-Rh-P(2)	86.1(2)	82.8(2)
C(4)-Rh-C(6)	63.3(6)	65.2(6)
C(9)-Rh-C(7)	64.7(6)	68.5(6)

Table 7.6   continued

Angles

Atoms	1	2
Rh-P(1)-C(2)	108.0(7)	112.4(6)
Rh-P(1)-C(12)	117.8(5)	116.2(5)
Rh-P(1)-C(14)	113.7(6)	114.5(5)
C(12)-P(1)-C(14)	103.7(7)	102.7(7)
Rh-P(2)-C(1)	109.6(8)	111.2(7)
Rh-P(2)-C(11)	111.1(6)	114.3(5)
Rh-P(2)-C(13)	121.4(6)	115.9(5)
C(11)-P(2)-C(13)	104.7(8)	111.2(8)
P(2)-C(1)-C(2)	107(2)	109(1)
P(1)-C(2)-C(1)	114(2)	104(1)
P(1)-C(2)-C(3)	116(2)	115(2)
C(1)-C(2)-C(3)	108(2)	109(2)

[a]The columns headed 1 and 2 refer to the first and second molecules respectively.

conformation with respect to the phosphine and Rh atom, the two on P(1) orient themselves in the opposite sense from those in the other complex. Further discussion of the conformation of the phosphine ligand in these two structures will be presented in Chapter 8.

Little else need be said about this structure, other than that there are no particularily close cation-cation or cation-anion contacts and the closest Rh-Rh approach is 5.59 Å.

DISCUSSION OF THE RESULTS PRESENTED IN CHAPTERS 6 AND 7

The value of phosphine complexes of Rh as catalysts
for a variety of reactions (50,52,144-147), including hydro-
genation, hydrosilation and hydroformylation has fostered
extensive research and discussion into the mechanism of the
catalytic reaction (57,137,148). Out of this work has come
a consensus as to the overall mechanism, although the process
has proved to be a complicated one and there are many details
of the reaction which have not been fully elucidated. In
the following sections a brief discussion of the proposed
mechanism for homogeneous catalytic hydrogenation using
rhodium - phosphine complexes will be presented, as well as
a discussion of how the stereochemistry of asymmetric
chelating phosphines may control the enantiotopic discrimina-
tion displayed towards some prochiral olefinic substrates.

8.1 Hydrogenation Mechanism

The initial research studied the mechanism of
homogeneous hydrogenation catalysed by the rhodium - phosphine
complex $Rh(PR_3)_3Cl$ (53-56,150). It was determined that the
active catalytic species was a cationic dihydride, thus the
isolable complex $Rh(PR_3)_3Cl$ is not the actual catalyst but a
precursor. Recent work (56) has shown that other complexes,
such as $[Rh(diene)L_n]^+$ (where diene = a chelating diene;
n = 2 or 3 if L is a monophosphine or 1 if L = a chelating

bisphosphine), also produce active hydrogenation catalysts.
An outline of a proposed mechanism for homogeneous
catalytic hydrogenation, starting from the cationic catalyst
precursor, $[Rh(diene)L_n]^+$, is as follows.

(i) A catalyst precursor is dissolved in a suitable
solvent (for example, ethanol or tetrahydrofuran) under an
H_2 atmosphere. Oxidative addition of H_2 occurs to give a
solvated cationic dihydride species.

$$[Rh(diene)L_2]^+ \xrightarrow{H_2 \,/\, solvent} cis\text{-}[Rh(H)_2L_2S_x]^+$$
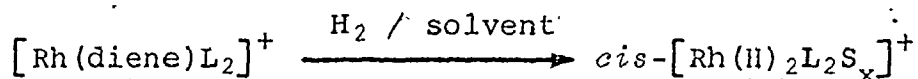
It is suggested that the coordinated diene is eliminated
from the coordination sphere by a stepwise reduction to an
alkene and then to an alkane (56). The number of solvent
molecules in the coordination sphere has not been determined,
but it is supposed that there are enough to fill any empty
coordination sites. The dienes used are commonly norborna-
diene (NBD) or 1,5-cyclooctadiene (COD) (56,57,137) and it
is observed that the initial step of diene hydrogenation to
produce the active catalyst proceeds some 100 times faster
for the NBD complex than for the COD complex.

(ii) The olefin then coordinates to the metal
dihydride complex to produce a species such as I.

R_3P ⎯ Rh ⎯ H

(structure of complex with Rh center, ligands R_3P, R_3P, H, H, S, and coordinated olefin)
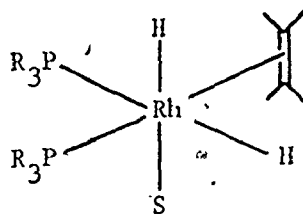
$$I$$

At present it is not known by what mechanism the hydride atoms are transferred to the olefin. There are two possible paths; a stepwise addition which would give rise to an Rh-alkyl intermediate, or the addition may be a concerted process with both hydrides being transferred simultaneously to the olefin via a five – center intermediate. Since metal – alkyl species are isolable in other systems (149) the stepwise mechanism is favored. It has been determined that H addition to the double bond occurs stereospecifically *cis* and is probably *endo* with respect to the coordinated face of the olefin (150-152).
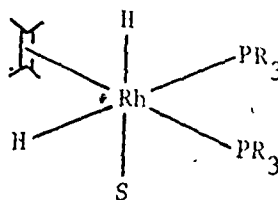
(iii) After elimination of the alkane the active catalyst is regenerated by oxidative addition of H_2 followed by coordination of another olefin molecule (56) as the process repeats.

8.1.1 Stereochemistry of Asymmetric Hydrogenation

When complex I is formed it will be as a mixture of the enantiomers Ia and Ib.
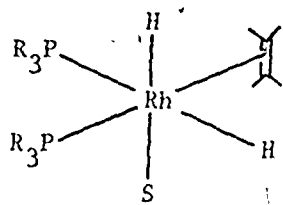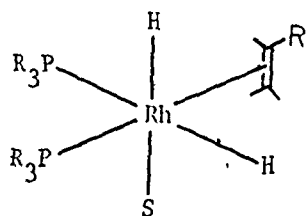
Ia   Ib
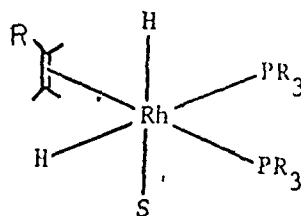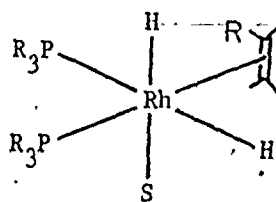
The use of a prochiral olefin as the substrate would there-
for result in two pairs of enantiomers, IIa, b and IIIa, b.

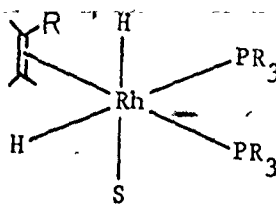IIa   IIb

IIIa   IIIb

In principle these diastereoisomers are not necessarily of equivalent thermodynamic stability. However, in practice, there would be no difference in the hydrogenation products since both R and S forms of the coordinated olefin will occur in equal amounts and, with the mechanism as postulated, the product resulting from each enantiomeric pair will be the same. Thus we need not consider the chirality at the Rh atom as influencing the distribution of the hydrogenation products.

When optically active phosphines are present in complex I then upon coordination of a prochiral olefin two diastereoisomers will be formed. Unlike the case of complexes II and III, an appreciable energy difference is now possible between the complex with the R olefin and the one containing the S olefin resulting from the interaction between the olefin and the asymmetric phosphine. If the energy of this interaction is sufficient, then a preference for either the R or S form of the coordinated olefin will be displayed. If a predominance of one diastereoisomer does exist then, since the hydrogenation step is stereospecific, an enantiomeric excess of one form of the hydrogenation product will result. This situation was appreciated by Horner et.al. (153) and Knowles et.al. (50) in the late 1960's and the first asymmetric hydrogenations using homogeneous catalysts of Rh and optically active phosphines were carried out at this time. The optical yields from these reactions were not large (from 7 to 15% depending on the system) and research

was directed towards their improvement. In these first
systems monophosphines having either chiral P or chiral C
atoms were used but, with an exception to be discussed later,
the highest optical yields occur in systems having a more
rigid ligand environment firmly bonded to the metal atom.
A chelating bisphosphine which is conformationally rigid can,
in principle, provide just such an environment about the
metal atom during the coordination and hydrogenation of the
substrate. Kagan (52) prepared (-)-2,3-O-isopropylidene-
2(R),3(R)-dihydroxy-1,4-bis(diphenylphosphino)butane
((-)-DIOP) a chelating bisphosphine which when coordinated
to Rh displays an ability to give optical yields of 70 - 80%
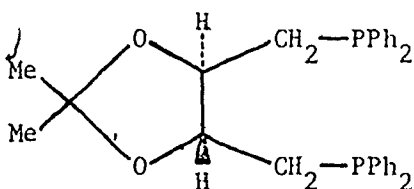
(-)-DIOP

in the reduction of β-substituted α-N-acylaminoacrylic acids
(IV) to give amino acids.
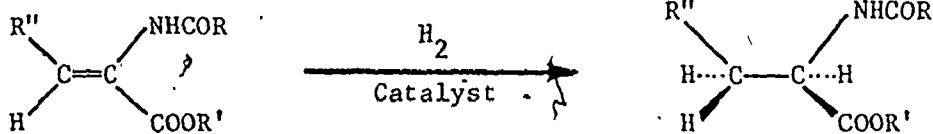
IV

Bosnich and Fryzuk (57) prepared the Rh(I) complexes of (-)-2,3-bis(diphenylphosphino)butane and (+)-2,3-bis(diphenyl-phosphino)propane and examined the ability of these ligands to discriminate towards various prochiral derivatives of IV. They found that the optical yields of the hydrogenation products ranged from 72 - 100% depending on the choice of solvent and substrate.

The question is then, *how does an asymmetric phosphine in which the chiral site is well removed from the vicinity of the metal atom, as in the above phosphines, influence the coordination mode of the incoming prochiral olefin?* Much of the research for this thesis was directed towards this problem, and a possible answer to this question will be discussed in the following sections.

8.2 Discussion of Structural Results

The structure presented in Chapter 6 and the analogous complex examined in Chapter 7 represent two of the four structures of this type which have been completed. The report of the structure in Chapter 6 has appeared in the literature as a full paper (138), that of Chapter 7 has not yet been reported, and the structures of the two others are available only as a communication (136) or as a note to an accompanying paper (137). The four phosphines, V - VIII, show distinct similarities in basic structure, as indicated in Figure 8.1, although the number and location of the asymmetric sites may differ. For V - VII the chirality is

V — S,S

VI — R
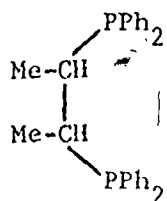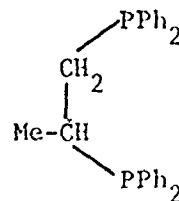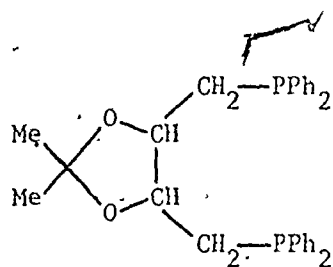
VII — R,R
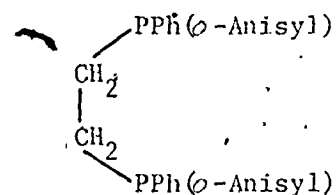
VIII — R,R (coordinated)

Figure 8.1   Four related bidentate phosphine ligands used in the structural and chemical studies

located in the backbone, while VIII has the P atoms as the asymmetric sites.   A comparison and discussion of the structural results of the Rh(I) complexes of V and VI will serve to cover several salient points regarding these complexes.

The phosphine V forms a five-membered chelate ring upon coordination to a metal atom.   Each of the carbon atoms of the backbone is substituted with a methyl group and

these serve two purposes. Firstly, the presence of these groups makes the ligand optically active, in this case S at each site, and secondly the stereochemical preference for these groups to lie equatorial with respect to the ring 'locks' the chelate ring into the δ conformation. While this is not usually a complete stereospecificity studies of similar chelating ligands show a single conformer does predominate (154) to a large extent.

The structure presented in Chapter 7 has phosphine VI as the ligand. This phosphine has only a single methyl substituent on the chelate ring and it was suggested from chemical evidence that the chiral center has the R absolute configuration and consequently the λ conformation of the chelate ring.

Constraining the chelate rings to assume either the λ or δ conformation makes the phosphine more stereochemically rigid than it would be if the backbone were not fixed into a particular conformation. This rigidity will then have an effect on the substituents on the P atoms. As can be seen in Figure 8.2a, which is a view approximately down the pseudo two-fold axis through the bisector of the P-Rh-P angle for phosphine V ((-)-chiraphos), the four phenyl groups are oriented in a quasi-axial, quasi-equatorial manner with respect to the plane of the chelate ring. The displacements of the α-C atoms of the rings from the P-Rh-P plane are given in Table 8.1 to support this assertion. With

Figure 8.2   Stereoviews of (a) the Rh-(-)chiraphos, and
(b) the Rh-(+)prophos entities.   The view is
approximately along the metal - phosphine
pseudo two-fold axis.

(a)
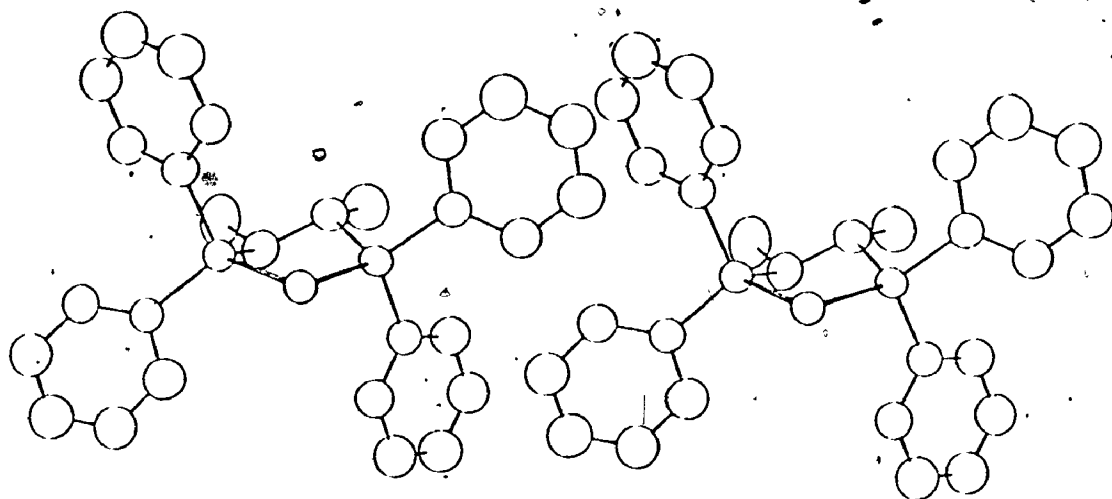
(b)
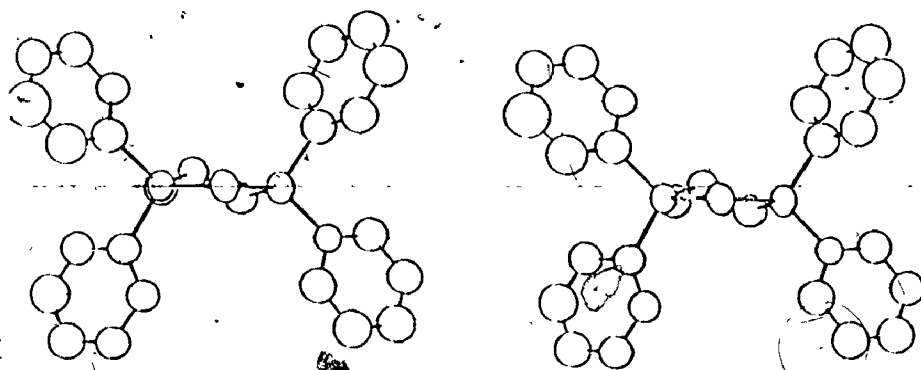
TABLE 8.1

Displacements (Å) from Rh-P-P plane in Rh-((-)-Chiraphos)

C(21)	1.155(5)		C(41)	1.628(5)
C(31)	-1.640(5)		C(51)	-1.222(5)

Displacements[a] (Å) from Rh-P-P plane in Rh - ((+)-Prophos)

C(13)	-1.28(1)		C(14)	-1.60(4)
C(11)	1.56(4)		C(12)	1.20(6)

[a] Average for equivalent atoms in both cations

the conformation of the chelate ring 'locked' this axial/ equatorial disposition of the rings can be maintained during the reaction sequence of hydrogenation.

It is also apparent from Figure 8.2a that the phenyl rings have adopted a conformation such that, alternately, a face then an edge are turned towards the coordination sites opposite the phosphine. This visualization is confirmed by an examination of the torsion angles, listed in Table 8.2, for the four atom chain from the metal to an *ortho*-carbon of each ring. A similar orientation, depicted in Figure 8.3, has been reported by Knowles (137) for a Rh(I) complex of phosphine VIII. Unfortunately, since the full structural details have not been published, no comparison of metal to ring torsion angles can be made for the two complexes.
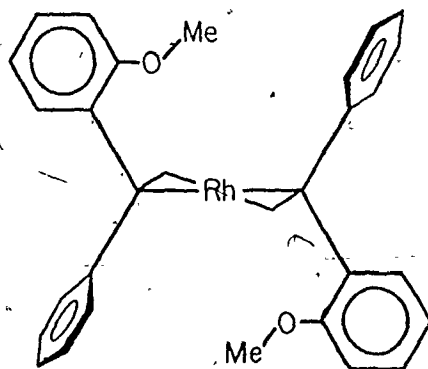
Figure 8.3 Alternating configuration for Knowles' phosphine

TABLE 8.2[a]

A. Torsion Angles[b] for Rh – ((-)-Chiraphos)

Atom Chain	Angle (deg)
Rh – P(1) – C(21) – C(22)	-66.1(5)
Rh – P(1) – C(31) – C(36)	9.2(5)
Rh – P(2) – C(41) – C(46)	10.6(5)
Rh – P(2) – C(51) – C(56)	-65.9(5)

B.   Average[c] Torsion Angles for Rh – ((+)-Prophos)

Atom Chain	Angle (deg)
Rh – P(2) – C(11) – C(21)	-99.4(5)
Rh – P(2) – C(13) – C(63)	-23.8(2)
Rh – P(1) – C(12) – C(22)	-96(5)
Rh – P(1) – C(14) – C(64)	15.1(9)

[a]The angles are listed in order of equivalent rings.

[b]A positive angle indicates a clockwise movement of atom 1 about the atom 2 to atom 3 bond to superimpose its projection on atom 4.

[c]The angle quoted is the average of the equivalent angle in each cation.

The phenyl rings in the complex of phosphine VI (Chapter 7) display a different behavior, as illustrated by Figure 8.2b and the average torsion angles in Table 8.2. The rings are almost mirror images of each other across a plane perpendicular to the mean coordination plane of the metal atom. Thus while the top rings present edges the bottom two are turned to present faces to the coordination sites opposite the phosphine. Whether this configuration represents a preferred conformation for this particular ligand or is an artifact of the molecular packing we do not know, but contrary to Knowles' assertion (137) that the IrCOD((+)-DIOP)Cl structure (136) also shows an alternating edge - face arrangement the drawing presented in that paper clearly shows an arrangement very similar to that drawn in Figure 8.2b.

The interactions which control the mutual orientation of the phenyl rings in these complexes are presumably between the H atoms on the rings and those on the substituents on the phosphine backbone. Calculation of the interaction distances when the rings of V and VI are rotated about the P-C(aryl) bond shows that these rings have very limited rotational freedom. The rings closest to the methyl groups may not rotate more than a few degrees in that direction before severe, ie. less than 2 Å, H-H interactions occur. If these rings are to rotate in the opposite direction there is some 20° before the H atoms on one ring get within 2 Å of the hydrogens on the other ring on the P atom. Should this

second ring twist to minimize the ring-ring H atom contact an interaction between the axial hydrogens on the internal C atoms of the phosphine and the H atoms on this second ring takes place. Therefore, disregarding any other effects, there is approximately 20-25° of rotational motion on either side of an equilibrium position for each ring. It is worth noting that even with this amount of freedom the rings of VI could not be set to an alternating face - edge conformation similar to that for V (Table 8.2). In the case of phosphine VIII these H atom interactions would not be as severe but it is suggested (137) that the o-methoxy groups are capable of a slight interaction with the Rh atom (Rh-0 distance of 3.7 Å) which constrains the rings to lie in the alternating edge - face arrangement.

It is interesting to note that the Rh complexes of all four of the phosphines give optical yields ranging from about 70 to 100% depending on substrate, solvent and reaction conditions (52,57,137). Thus it would appear that even if the difference in conformation of the rings persisted in solution it does not have a large effect on the enantiomer distribution. Moreover, it is apparent that the stereochemistry of the phosphine in each of these complexes must be similar in order to be consistant with the uniformly high optical yields achieved for asymmetric hydrogenation. To maintain this similarity despite the large differences between the phosphines — five- versus seven- member chelate rings, conformationally labile versus locked phosphine backbones, chiral

sites at the P atoms as opposed to once or twice removed onto the chelate ring — it is presumed that the phosphine is held quite rigidly by the variety of non-bonded interactions described above and can, therefore, provide a relatively constant ligand environment about the metal atom.

This can be contrasted to the situation which exists when monodentate phosphines are used. Several phosphines of this type which have been used are: (CH_3) $(C_3H_7)(C_6H_5)P$ (153,158), $(C_6H_5)_2$(neomenthyl)P (157), $(C_6H_{11})(C_6H_5)(CH_3)P$ (158) and $(C_6H_{11})(o$-anisyl$)(CH_3)P$ (158). The first three of these ligands are typical and give optical yields in their hydrogenations of approximately 5 to 50% depending on substrate. The fourth phosphine gives anomalously high optical yields (60 - 90%) which may imply a greater rigidity for this ligand when complexed to a Rh atom than the other monodentate phosphines examined. Since this phosphine is the analogous monodentate one to VIII it is possible that a similar interaction is taking place between the 0 atom of the o-methoxy groups and the Rh atom . thereby enhancing the stereochemical rigidity of the phosphine during the catalytic reaction. In general though there is much greater freedom for a monodentate phosphine to adopt different conformations as the ligand environment about the Rh atom changes. Indeed a crystal structure has been completed of a Rh - phosphine complex (155) in which the Rh

has adopted a tetrahedral coordination geometry in order to relieve interligand contacts rather than remain in the square planar configuration required by bidentate phosphines of which V and VI are paradigmatic.

It is apparent, in terms of the crystallographic results, that although the actual chiral sites in the coordinated phosphine may be well removed from the vicinity of the metal atom the stereochemistry of the ligand can be used to transmit an asymmetric environment to the space about the metal. This environment may then influence the coordination geometry of the prochiral olefinic substrate molecule.

8.3 Discussion of Chemical Observations

It has been suggested in the discussion to this point that it is the arrangement of the phenyl rings in these structures which is responsible for the discrimination displayed towards the face of the substrate molecule and there is direct chemical evidence which supports this view. Kagan examined the ability of Rh - ((-)DIOP) to asymmetrically hydrogenate two α-phenylacetylaminoacrylic acids (IX and X) (145). The optical yields for the R configuration of the products from IV and V were 82 and 84%, respectively. However, if the two phenyl rings on each P atom of DIOP are *orthó*
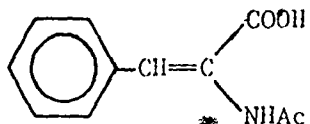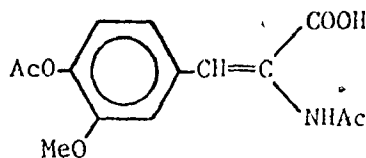
IX   X

linked the optical yields were observed to drop to 28 and

14% and the reduction gave the opposite, that is S, absolute

configuration of the products. The linking of the rings in

this fashion appears, based on molecular models, to have two

effects on the ligand stereochemistry. Firstly, the phenyl

groups are no longer able to adopt staggard conformations

about the P-C(aryl) bond but are constrained to present an

appearance of a 'flat wall' towards ligands on the opposite

side of the metal atom. Secondly, when the rings are linked

they are not as definitely axially and equatorially disposed

with respect to the coordination plane but appear to be

positioned more symmetrically out of the plane. These

stereochemical changes would support the concept that the

orientation of the phenyl rings is the major factor which

controls the optical yields of the reduction products.

Knowles came to a similar conclusion from a consideration of

the substrate geometry and how it would interact with the

arrangement of the phenyl rings he observed in the structure

of the Rh complex of VIII (137). The basic argument he presented is as follows. If the geometry of the prochiral acrylic acid substrate is Z, as depicted below, as opposed to E, it is observed (137,145) that both higher optical

$$\begin{array}{c} H \diagdown \qquad \diagup COOR \\ C == C \\ R'' \diagup \qquad \diagdown NHCOR' \end{array}$$
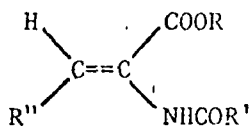
yields and faster hydrogenation rates result. If models of the Rh - phosphine complex, Figure 8.3, and the Z-isomer of the substrate are made then it is found that this isomer can coordinate more readily, given the spatial restrictions imposed by the phosphine, into the vacant Rh sites. The conclusion is that coordination of the substrate is strongly influenced by the steric interactions presented by the orientation of the phenyl groups on the P atoms.

Examination of which absolute configuration of amino acid is formed from a given chirality of phosphine further supports this assessment of the importance of the phenyl rings. Phosphine V gives R reduction products (57) while VI - VIII give S products (52,57,137). The orientations of the phenyl rings are enantiomeric for V and VIII and similar for VI and VII which is consistant with the observed distribution of product chiralities.

The discussion to this point has been limited to

those results obtained when α-N-acylaminoacrylic acid
derivatives have been used as substrates. These have been
chosen because of the excellent chemical and optical yields
obtained. It has been proposed that the presence of the
amide function in the acylaminoacrylic acids allows
additional bonding opportunities for the olefin via an
interaction between the Rh atom and the C=O group of the
amide, *ie*.
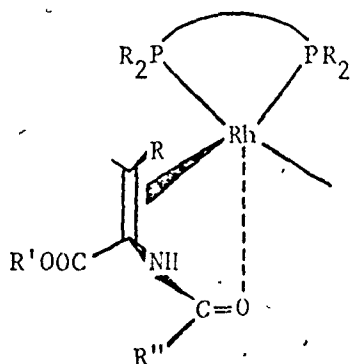
Construction of molecular models indicates that this
postulated interaction is geometrically possible. To try
and determine the importance of this supposed interaction
reactions of some substrates not containing the amide
function were explored (137,159). Kagan *et.al.* (159)
examined some enamines and enamides while Knowles *et.al.* (137)
looked at some unsaturated carboxylic acids. The *E*- and
Z-isomers of α-methyl-β-phenylacrylic acid gave optical yields
of only 1%, while an α-enol ester (below) had an enantiomeric

$$\underset{\text{Ph}}{\overset{\text{H}}{\diagdown}}C=C\underset{\text{OCOCH}_3}{\overset{\text{COOC}_2\text{H}_5}{\diagup}}$$
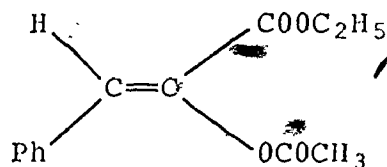
excess of 90% (137). However if various enamines, *eg.*
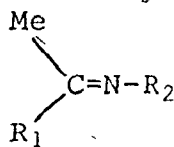
$$\underset{\text{R}_1}{\overset{\text{Me}}{\diagdown}}C=N-R_2 \qquad\qquad R_1 = \text{Ph, benzyl}$$
$$R_2 = \text{Ph, benzyl}$$

are used the optical yields all run about 50%·(159). Thus ·
it appears that the amide function (or some equivalent group)
can assist to a marked degree in determining whether the
re or si face of the substrate coordinates.

8.4 Conclusion

There is a body of persuasive crystallographic and
chemical evidence as to the importance of the substituents
on the P atoms in determining the ability of these asymmetric
phosphines to control the coordination of prochiral olefins.
It appears that the type of chirality possessed by the
phosphine, that is whether the P atoms are chiral or the
asymmetric sites are located on the backbone of the chelate
ring, is not as important as how this chirality can affect
the orientation of the phosphine substituents.

In addition to these direct ligand - ligand inter-
actions there are also electronic, solvent and other steric
effects present which can enhance or counteract the effect

of the phosphine (57,145). As these various interactions,
particularly the steric ones, become more fully understood
highly specific and efficient asymmetric catalytic synthetic
routes will become available. To this end crystallographic
studies of intermediates (or closely related complexes) in
these catalytic reactions will give valuable information
and raise questions for further investigation.

CHAPTER 9

SOFTWARE DEVELOPMENT FOR A COMPUTER AUTOMATED FOUR-CIRCLE DIFFRACTOMETER

9.1   Introduction

As was mentioned briefly in Chapter 2, in order to collect data which accurately represent the true reflection intensities, the crystal must be accurately aligned in order to relate the crystallographic cell axes to the axial system of the diffractometer.   The mathematics describing the various axial systems and orientation matrices are given in reference 159 and are summarized in section 9.1.1 as background to the subsequent sections.   Section 9.2 describes how the diffracted X-ray beam arising from a reciprocal lattice point is located in terms of the diffractometer angular settings.   This information permits the reader to appreciate how the programs discussed in section 9.3 and 9.4 serve to accurately center the diffracted ray in the counter aperture.

9.1.1   The Orientation Matrix

It is convenient to introduce an orientation matrix $\underset{\sim}{U}$ such that

$$\underset{\sim}{A}^* \equiv \underset{\sim}{U}\underset{\sim}{A}_G$$

The matrix $\underset{\sim}{U}$ (which is in general not symmetric) has nine independent elements which are related to the six cell constants and three angles describing the crystal orientation. The matrices $\underset{\sim}{A}^*$ and $\underset{\sim}{A}_G$ represent the reciprocal crystal axes

and an orthonormal axial system fixed in the goniometer head
and hence with respect to the crystal. The cell constants
may be obtained, independent of the orientation, by forming
the product of $\underset{\sim}{A}^*$ and its transpose $\underset{\sim}{A}^{*'}$

$$\underset{\sim}{G}^{-1} = \underset{\sim}{A}^*\underset{\sim}{A}^{*'} = \underset{\sim}{U}\underset{\sim}{A}_G\underset{\sim}{A}_G'\underset{\sim}{U}'$$

from which we obtain, since $\underset{\sim}{A}_G\underset{\sim}{A}_G' = \underset{\sim}{I}$ (the identity matrix),

$$\underset{\sim}{G}^{-1} \equiv \underset{\sim}{U}\underset{\sim}{U}'$$

Thus, by forming the product $\underset{\sim}{U}\underset{\sim}{U}'$, the reciprocal cell
constants and hence the direct cell constants may be obtained.

9.2 Reflection Location on a Four-Circle Diffractometer

The procedures most commonly used to determine the
orientation matrix require the accurate determination of
the angular values for a series of reflections which are
used as observations for a least-squares refinement of those
parameters (the six cell constants and three angles) necessary
to describe the crystal orientation.

The relationship between the real space of the
diffractometer and the diffraction geometry of reciprocal
space with respect to the four diffractometer angles is
shown in Figure 9.1. The point of intersection of the four
angles (at which the crystal lies) is labelled O and the
angles are labelled 2θ, ω, χ and ϕ. The point O^* is the
origin of the diffraction vector (labelled $2\theta^*$) in reciprocal
space. The sphere of reflection is represented by the circle
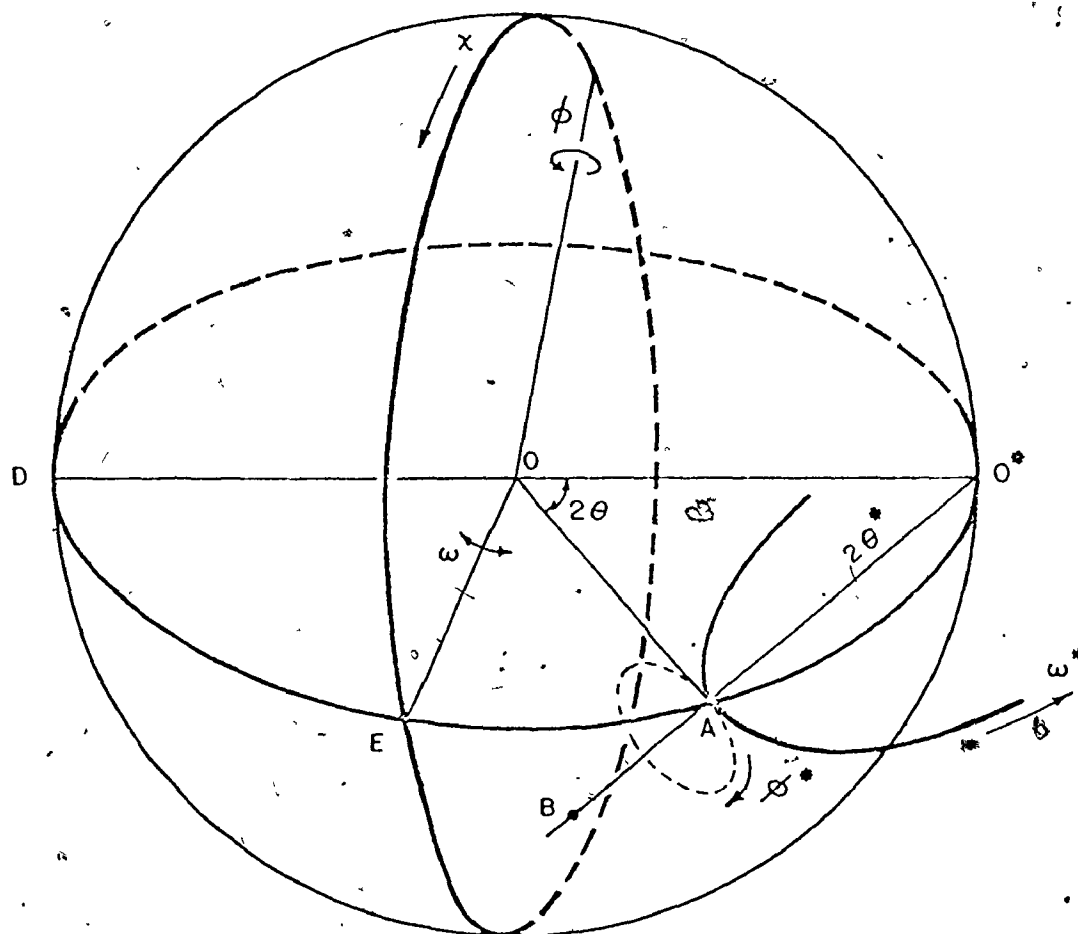
Figure 9.1   Diagram of the relationship between the
four diffractometer angles and movement
in reciprocal space.

upon which lie points D, E, A and O^*. Thus, any point A on the reciprocal lattice vector AO^* is in the diffracting position when it is coincident with the sphere of reflection. For point B to fall on the sphere of reflection 2θ must increase, and ω^* must decrease by exactly half the increase in 2θ. Rotation about χ results in the displacement of A along a circle perpendicular to the ω^* circle thus defining a sphere having radius $2\theta^*$ and centered at O^*. A rotation about the ϕ axis will cause the peak represented by A to move out of the diffraction plane along a circle which is on the surface of the sphere centered at O^*. The normal to this circle will be inclined at an angle to the diffraction plane which is determined by the χ angle. If the χ value for the reflection is zero, then the ϕ^* circle will be coincident with the ω^* circle; however, if the χ value is 90°, then the ϕ^* circle will be of zero radius and perpendicular to the ω^* circle, and rotation about ϕ will not affect the position of the diffraction vector.

Of the two software systems we have used, that supplied by Picker Corporation and P.G. Lenhert's disk oriented package (74), both implement the same algorithm to center a reflection in the counter aperture. The basic method, which is entirely automatic, keeps either ϕ or χ fixed and scans the other three angles in a specific order to determine the angular settings for maximum intensity of a diffracted beam. The procedure will be discussed in more detail in section 9.3. This approach to centering is based on the original

programs developed by Busing and Levy (73,160).

As an alternative to the Busing and Levy approach we use programs which allow all four angles to be centered individually and in any order. We feel that the flexibility of this approach serves to speed up the process of centering even a large number of reflections, not an insignificant consideration, particularily if the crystal being examined is sensitive to X-ray exposure time. From the way the computer is programed I have chosen to refer to the Busing and Levy approach as multiple angle centering and the alternative we use as single angle centering.

9.3 Multiple Angle Centering

The program written by Busing and Levy (161) has several options for the particular centering mode used and the simplest and fastest of these will be described. The program first causes ω to be step-scanned with large $(0.04°)$ then small $(0.01°)$ angle increments to horizontally position the reflection on the sphere of reflection. Then χ (or ϕ if the diffractometer is in the parallel configuration) is centered using a routine which scans the angle until the peak intensity is reduced to one-half by intersection with the aperture slits. This is done on the low and high angle sides and the peak center is taken as halfway between these limits. This can be referred to as a convergence scan. After determining the centroid of the peak with respect to χ, ω is scanned again (using both coarse and fine step-scans)

followed by a convergence scan of 2θ with adjustment of ω

to keep the crystal fixed with respect to the laboratory

reference frame. The final angles represent the position

in reciprocal space of the peak maximum, often with an

offset on ω to account for any inexactness in the position

of ϕ with respect to the diffraction plane.

'9.4 Single Angle Centering

The procedure we use and find to be an improvement

over the Busing and Levy method involves more control by

the experimenter over how each reflection is centered.

Since the data acquisition programs use the interelationships

(161) of the angles to measure the reflection intensities

with ω at zero our programs were designed to allow the

reflections to be centered with ω so set. We first

determine an approximate orientation matrix and then choose

approximately thirty relatively intense reflections having

2θ values as large as possible. After driving the angles to

the calculated peak maximum the angle ϕ is centered. This

angle is chosen first since peak centering is usually very

sensitive to small changes in this angle. The peak is step-

scanned over a range usually equal to the width of the

peak using the smallest angle increment available (0.01°).

When the maximum is found the peak is centered on χ using

a convergence scan method. This method of scanning χ is

used since the position of the peak maximum is not as

sensitive to small changes in χ. If the change in χ exceeds

about 0.2° ϕ is usually recentered. At this time the

reciprocal lattice point should lie on the diffraction

plane and all that is left is to center the counter accurately

on the peak maximum. This is done by a step-scan along 2θ.

A check can be run by a step-scan of ω to see if there is

any recentering with respect to χ or ϕ which is required,

or, the Busing and Levy algorithm may be employed. Thus,

in the best case, it takes only three angular scans to

determine the peak position whereas in the multiple angle

method six scans are the minimum.

When reflections which have χ values near $\pm 90^\circ$ are

centered it is commonly observed that it is difficult to

get an optimum value for ϕ since, as pointed out in section

9.2, a ϕ rotation at $\chi = 90^\circ$ degenerates to a simple rotation

about the diffraction vector. We find that if a large

(approximately $0.05 - 0.10^\circ$) ω offset is accepted the

changes calculated for χ and ϕ to return ω to zero are often

imprecise with respect to the position for this reflection

calculated on the basis of the refinement of the other

reflections. The problem is often circumvented by several

centerings of these reflections with changes in ϕ until ω

stays near zero. Using the single angle routines makes the

procedure faster, since ϕ can be centered using a convergence

scan followed by normal centering of χ and 2θ. The angular

setting of ω is then checked to see if the peak maximum is

on the sphere of reflection. If ω shows an appreciable

offset ϕ can be recentered followed by another check on ω.

If the final χ position is more than about 0.02 to 0.03° from the initial position the χ and 2θ angles may be recentered.

Once all the reflections have been centered the least-squares refinement of the cell constants and orientation matrix is performed, and the differences between the calculated and observed angular settings for 2θ, χ and ϕ are determined. If these values differ by more than about 1 or 1.5σ (where σ is chosen to be $0.02°$) then these reflections are recentered to determine if the first centering accurately represents the best position of the maximum. The single angle routines allow this recentering to be done very rapidly. Over the entire centering process we generally realize a significant saving of time.

It seems perversely true that when an interesting structure arises the crystal quality is often borderline and we find that we can accomodate a less than perfect crystal much better with the more flexible approach to alignment available. In particular, this method, because it requires more constant observation by the experimenter, allows one to get a "feel" for the crystal quality very quickly during the alignment process and compliments checks on crystal quality made by ω scans.

The single angle centering routines were written originally to be compatible with the operating system supplied by Picker Corporation for the FACS-1 diffractometer. The present version has been modified to interface with

Lenhert's disk operating system which is currently implemented on our diffractometer. A listing of the program routines are presented in section 9.4.1.

9.4.1 Listing of Single Angle Centering Routines

```
/ FILE: /SAR
/    SINGLE ANGLE CENTERING ROUTINES
/
/          SAVE AS /SAR:3200-3777;7600
/
          *100
LTTH,     0
LOMG,     0
LCHI,     0
LPHI,     0
COUNT,    0
PANG,     0
MODE,     0
LSCAN,    0
ANGD,     0
          0
          0
NSC,      0
ANGM,     0
          0
          0
OMGC,     0
          0
          0
CMAX,  \  TEMP1,   0
          0
          0
LIMIT,    0
          0
          0
TEMP      0
          0
          0

          *3200
/
/---ENTRY FOR ALL SINGLE ANGLE CENTERING CALLS
/      CALLED FROM SIGNAL TABLE 3
/
          JMP I FPCNT         /GP
          JMP I FCCNT         /GC
          JMP I FOCNT         /GO
          JMP I FTCNT         /GT
          JMP STEPS           /AS
/
FPCNT,    PHISCN
FCCNT,  | CHISCN
FOCNT,  | OMGSCN
FTCNT,    TTSCN
/
PHISCN, JMS PARAMS
          TAD LPHI
          DCA PANG
          TAD NSC
          SZA CLA             /CHECK IF ITS A CONVERGENCE SCAN
          JMP STPSCN          /NO, NORMAL STEP SCAN
        \ JMS I LFPT
          FGET ANGD           /HALF SIZE DELTA FOR PHI AND OMEGA
          FDIV TWO            / CONVERGENCE SCANS
          FPUT ANGD
          FPUT LANGD
          FEXT
          JMP I LCNVSC        /GO TO CONV. SCAN ROUTINE
STPSCN, JMS I ASCAN
          JMP FINIT
/
OMGSCN, JMS PARAMS
          TAD LOMG
          JMP PHISCN+2
```

```
        /
        STEPS.  JMS I LINTIN              /GET NO. OF SCAN STEPS
                DCA I SNSC               /AND STORE
                JMP I LONGA
        /
        FINIT,  CLA                      /COMMON TERMINATION POINT FOR ROUTINES
                DCA COUNT
                JMS I LSAC              /SETUP ANGLES TO CENTERED POSITION
                CUR1                    /CLOSE SHUTTER
                JMS I LPRANG            /PRINT FINAL ANGLES
                JMP I LONGA
        LSAC,SAC
        /
        PARAMS, 0
                JMS I LINTIN            /GET TIMER CODE
                DCA LCOUNT
                JMS I LGET
                DATBLK
                TAD MODE                /CHECK IF ITS A CHI SCAN
                SZA CLA
                JMP INITA               /YES -- SKIP REST OF INPUT
                TAD I SNSC
                DCA NSC                 /MOVE STEPS TO PAGE ZERO
                JMS I LINTIN            /SCAN TYPE: 0=STEP, 1=CONVERGENCE
                SNA CLA
                JMP .+3
                DCA NSC                 /ENSURE STEPS ARE ZERO FOR CONV. SCAN
                JMP INITA
        GETDEL  JMS I LENK
                JMS I LFPT
                FPUT ANGD
                FEXT
        INITA,  JMS I LINANG            /ENSURE CURRENT ANGLE POSITIONS ARE
                JMS I LWHERE            / USED IN SCANNING
                JMS I LOPSHT            /OPEN SHUTTER
                JMP I PARAMS
        DATBLK, -14                     /DATA FOR PAGE ZERO COMMON BLOCK
                DIFANG
                DIFANG+3
                DIFANG+6
                DIFANG+11
        LCOUNT, 0
                0
        SWIT,   0
                SCAN
        LANGD,  0                / APPROX 0.64
                2436
        SNSC,   6010                    /LOCATION IN XTAL PAGE FOR SCAN STEPS
                0
        /
        ASCAN,  ANGSCN
        LCNVSC, CNVSCN
        /
                *3400
        CONV,   0
                DCA IND                 /CLEAR INDICATOR
                JMS I LFPT
                FGET ONE
                FPUT SIGN               /SET STEPPING POSITIVE
                FEXT
        REPEAT, JMS I LFPT              / CONVERGENCE
                FGET ANGD
                FMPY SIGN
                FADD I PANG
                FPUT I PANG
                FEXT
                TAD MODE                /SHOULD OMEGA BE MOVED?
                SNA CLA
                JMP CHKDEL              /NO, NOT DOING 2THETA
                JMS I LFPT
                FGET ANGD
                FDIV TWO
                FMPY SIGN
                FNEG
                FADD I LONG
                FPUT I LONG
                FEXT
```

```
CHKDEL   JMS I LFPT
         FGET ANGD
         FABS
         FSUB DELMIN             /CHECK ON SIZE OF DELTA
         FEXT
         TAD HORD
         SPA CLA
         JMP I CONV              /RETURN IF TOO SMALL
         JMS I LLSAC             /SETUP ANGLES AND GET A COUNT
         JMS I LFPT              /BEGIN CONVERGENCE
         FSUB LIMIT
         FJMP TOOFAR
         FGET ONE
         FPUT SIGN
         FEXT
         TAD IND
         SZA CLA
         JMP DIVIDE              /NARROW DOWN DELTA
         JMP REPEAT
TOOFAR,  FGET ONE               /BACKUP
         FNEG
         FPUT SIGN
         FEXT
         IAC
         DCA IND                /SET INDICATOR FOR REVERSING
DIVIDE,  JMS I LFPT
         FGET ANGD
         FDIV TWO
         FPUT ANGD
         FEXT
         JMP REPEAT
LLSAC,   SAC
DELMIN,  7772
         2000
         0
IND,     0
SIGN,    0
         0
         0
/
/   GC CONVERGENCE CENTERING ROUTINE
/
CHISCN,  ISZ I LSWIT            /SET SWITCH FOR CONVERGENCE CHI SCAN
         JMS I LPARAM
         TAD LCHI
         DCA PANG
         DCA MODE
CNVSCN,  JMS I ISCAN            /GET CURRENT COUNT
         JMS I LFPT
         FGET I PANG
         FPUT HOLD
         FEXT
         JMS CONV               /CONVERGE ON UPPER ANGLE LIMIT
         JMS I LFPT
         FGET I PANG
         FPUT TEMP
         FGET I LONG
         FPUT OMGC
         FGET HOLD
         FPUT I PANG
         FGET I ADZERO
         FPUT I LONG
         FGET I ADEL
         FNEG
         FPUT ANGD
         FEXT
         JMS CONV               /CONVERGE ON LOWER ANGLE LIMIT
         JMS I LFPT
         FGET I PANG
         FADD TEMP
         FDIV TWO               /COMPUTE CENTER
         FPUT I PANG
         FGET I LONG
         FADD OMGC
         FDIV TWO
         FPUT I LONG
         FEXT
         JMP I LFIN
```

```
HOLD,   0
        0
        0
ADEL,   LANGD
/
/   GT ROUTINE FOR DECIDING ON COUNTER CENTERING MODE
/
TTSCN,  ISZ I ADEL              /CHANGE DELTA TO APPROX 1.2
        JMS I LPARAM
        TAD LTTH
        DCA PANG
        ISZ MODE                /SET MODE=1 FOR 2THETA SCAN
        TAD NSC
        SNA CLA
        JMP CNVSCN
        JMS I FSCAN
        JMP I LFIN
LFIN,   FINIT
LPARAM, PARAMS
FSCAN,  ANGSCN
LSWIT,  SWIT
/
/
        *3600
SAC,    0                       /SET ANGLES, DRIVE, & COUNT
        JMS I LSETDF
        CLA IAC                 /REQUEST FOR SLOW DRIVE
        JMS I LSTANG
        TAD COUNT
        SPA                     /GET ABS. VALUE OF COUNT TIME
        CIA
        SZA
        JMS I LCPTIM            /GO TO COUNTING ROUTINE
        JMP I SAC
LSETDF, 4400

/
/
ANGSCN, 0
        TAD COUNT
        SPA CLA                 /IF NEG. DON'T ZERO OMEGA
        JMP .+5
        JMS I LFPT
        FGET I ADZERO
        FPUT I\LONG             /START WITH OMEGA AT ZERO
        FEXT
        JMS SCAN                /START SCAN
        JMS I LFPT
        FGET CMAX
        FDIV TWO
        FPUT LIMIT              /RESET LIMIT VALUE
        FEXT
        JMP I ANGSCN

/
SCAN,   0
        TAD NSC                 /GET MULTIPLR FOR ANGLE DELTA
        CMA
        DCA KP                  /SET AS NO. SCANNING STEPS
        TAD NSC
        JMS I LFFP              /FLOAT IT
        FPY ANGD
        FDIV TWO
        FNEG
        FADD I PANG             /OFFSET ANGLE BY HALF THIS VALUE
        FPUT I PANG
        FGET I ADZERO
        FPUT CMAX               /CLEAR CMAX
        FEXT
STEP,   JMS SAC         /SET UP ANGLES & COUNT
        JMS I LFPT
        FSUB CMAX               /COMPARE CURRENT TO MAX COUNT
        FJMP ADV                /CMAX <= CURRENT COUNT
        FADD CMAX
        FPUT CMAX               /REPLACE CMAX VALUE
        FGET I PANG
        FPUT ANGM               /STORE POSITION OF MAX COUNT
ADV,    FGET I PANG

        FADD ANGD               /INCREMENT ANGLE
        FPUT I PANG
        FEXT
```

```
        ISZ KP               /TEST STEP COUNTER
        JMP STEP
        JMS I LEFT
        FGET ANGM            /SET ANGLES TO PLACE OF MAX COUNT
        FPUT I PANG
        FEXT
        JMP I SCAN           /RETURN
KP,     0
S
```

9.5 Operating System Extensions

When I began my research program the software package for our diffractometer was the original one supplied by Picker Corporation. At that time changes were implemented to allow single angle centering and a zero offset value for the angle χ. This latter option was included because we usually see a systematic difference in the measured λ values and those calculated by the program PICKTT from the least-squares refinement of the U matrix. When we implemented Lenhert's disk-based operating system the facility for the χ offset was already included so it was only necessary to interface the single angle centering routines.

The disk operating system is designed for a PDP-8 computer having at least 4K words of core memory and at least one Digital Equipment Corporation DF32 disk having 32K words of storage. Due to the manner in which the routines transfer information to and from the disk, it is necessary that each transfer be perfect every time or else the system halts. As the disk gets older, the failure rate during read/write operations tends to increase, so you can rapidly reach the point where the computer spends more time stopped than collecting data.

Thus it was necessary to modify the operating system to make it much more forgiving of parity errors while still ensuring that the data that does get transferred is correct. A new I/O routine for the disk was written which incorpor-

ated the ability to reread any information which gave a parity error. The algorithm is presented as a flowchart in section 9.5.1. Other modifications were made as the need for them became apparent, such as reducing the information from the data acquisition routines to only that necessary and typing it in a compressed form to reduce printing time and paper requirements.

9.5.1 Flowchart of Disk I/O Algorithm
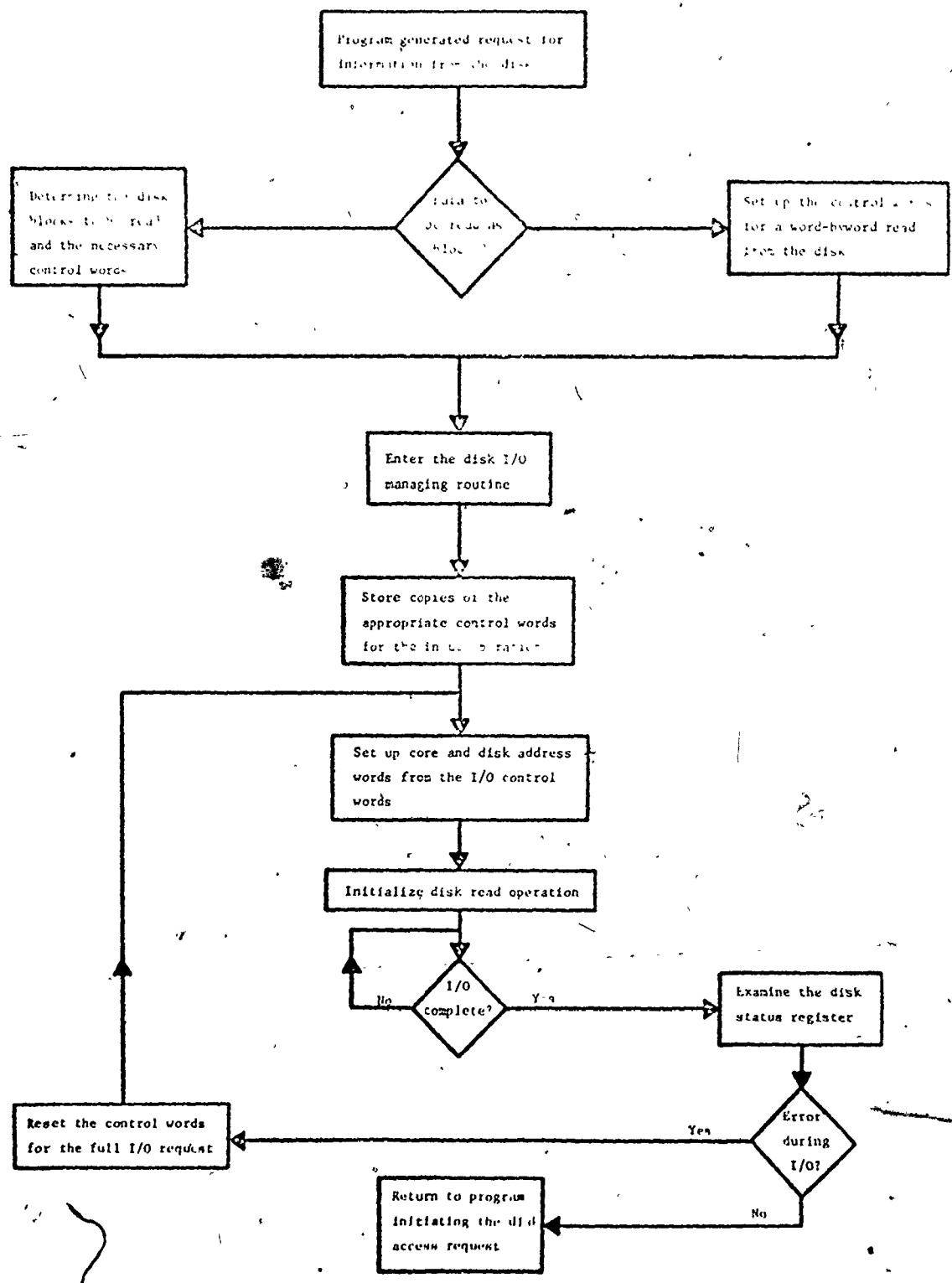
9.6 Summary

The application of computer controlled hardware to data acquisition in crystallography, or for that matter in other areas of research, has made it necessary that the researcher should be competent in the use of these machines. There must be a knowledge of how the computer is programmed to carry out its functions and how to alter this programming to introduce improvements in the algorithms. If one is forced to work within the confines of the original software then the quality of the work will probably suffer since in any advancing research field problems will be encountered which were not considered when the programs were designed. As exemplified by the programming changes discussed in this chapter, 'state-of-the-art' techniques are by definition never static but are constantly being modified to reflect new requirements. Since, this trend towards automation will likely continue it will be even more true in the future than it is now, that the researcher will be required to competently interact with and control the computers which gather and process the experimental data.

APPENDIX 1

DESCRIPTION OF COMPUTER PROGRAMS FOR

X-RAY CRYSTALLOGRAPHY

All computing was performed using the facilities of the University of Western Ontario Academic Computing Center. The two large computers available are a Digital Equipment Corporation PDP-10 and a Control Data Corporation Cyber 73/14. The program library used is comprised of versions, modified by N.C. Payne, of programs from the library of J.A. Ibers of Northwestern University, Evanston, Illinois, programs written by N.C. Payne, and others written by the author. Some of the specific programs used are described below.

1. ANGLE: used to calculate interfacial angles from optical goniometric measurements on crystals and ultimately allow face indexing. Written by J.A. Ibers.

2. AGNOST: incorporates both the Gaussian and analytical absorption correction techniques. The latter as modified from the method of de Meulanaer and Tompa by D. Cahen and J.A. Ibers.

3. BIJVOET: used to tabulate observed and calculated structure factors for Bijvoet pairs of reflections. Written by R.G. Ball.

4. EQUIV: calculates discrepancy indicies for reflections equivalent by symmetry. Written by J.A. Ibers.

5. FAME: program to calculate E's and apply Wilson statistics. Written by R.B.K. Dewar and modified by Goldberg.

6. FORDAP: a combined Fourier summation, and peak search/interpolation program. Patterson and difference Fourier synthesis were calculated with this program. Written by A. Zalkin.

7. HYDRA: used to calculate idealized positions for hydrogen atoms as determined from the geometry of attached atoms. Written by J.A. Ibers.

8. LIST: used to tabulate the final observed and calculated structure factors according to Miller indicies and print these in a form suitable for publication and deposition. Written by D. Bright and modified by N.C. Payne.

9. MULTAN: a program for direct methods solutions of crystal structures. Written by M. Woolfson and G. Germain.

10. NUDAP: calculates bond distances and angles without estimated standard deviations. Based on the comparable routines in ORFFE.

11. PICKTT: used for non-linear least-squares refinement of diffractometer setting angles to obtain unit cell parameters, their estimated standard deviations and the orientation matrix. Modified from J.A. Ibers' PICK which was derived from Hamilton's MODE1.

12. ORFFE: a modification of the Busing - Levy - Martin function and error routines used to calculate such functions as bond distances and angles with estimated standard deviations and weighted least-squares planes.

13. ORTEP2: used to prepare molecular and crystal illustrations on a computer controlled plotter. Written by C.K. Johnson.

14. RANGER: applies statistical analysis to the observed and calculated structure factors in terms of a variety of variables. Written by P.W.R. Corfield and modified by N.C. Payne.

15. RBANG: calculates rigid group orientation parameters for use in WOCLS when needed. Written by S.F. Watkins.

16. TABLE: tabulates final positional and thermal parameters for individual atoms and rigid groups in a form suitable for publication. Written by N.C. Payne

17. WOCLS: for full matrix least-squares refinement of structure parameters and structure factor calculations. Modified and revised from NUCLS by R.J. Doedans and J.A. Ibers, which in turn is a highly modified version of ORFLS by W.R. Busing and H.A. Levy.

18. WOFACA: used to process the data output from the diffractometer at the University of Western Ontario. Written by N.C. Payne.

APPENDIX 2

SUMMARY OF IMPORTANT FORMULAE

1. The general expression for a general structure factor is

$$|F_{hkl}| = (A_{hkl}^2 + B_{hkl}^2)^{\frac{1}{2}}$$

where

$$A_{hkl} = \sum_j f_j \cos 2\pi (hx_j + ky_j + lz_j)$$

$$B_{hkl} = \sum_j f_j \sin 2\pi (hx_j + ky_j + lz_j)$$

and f_j is the scattering factor for the jth atom. The phase angle is defined by

$$\alpha_{hkl} = \tan^{-1} (B_{hkl}/A_{hkl})$$

2. The function minimized in least-squares refinement is

$$\sum w(|F_o| - |F_c|)^2$$

where w is the weighting function given by

$$w = 4F_o^2/\sigma^2(F_o^2)$$

3. The agreement factors are given by

$$R_1 = \frac{\sum ||F_o| - |F_c||}{\sum |F_o|}$$

$$R_2 = \left[\frac{\sum w(|F_o| - |F_c|)^2}{\sum wF_o^2}\right]^{\frac{1}{2}}$$

4. The expression for the isotropic temperature factor, in terms of the conventional thermal parameter B, is

$$T = \exp\left[(-B/4)(2\sin\theta_{hkl}/\lambda)^2\right]$$

or, in terms of U, is

$$T = \exp\left[-U8(\pi\sin\theta_{hkl}/\lambda)^2\right]$$

where U is the mean-square amplitude of vibration in $\overset{o}{A}^2$. The general or anisotropic temperature factor expression is

$$\exp\left[-2\pi^2(U_{11}h^2a^{*2} + U_{22}k^2b^{*2} + U_{33}l^2c^{*2} + 2U_{12}hka^*b^* + 2U_{13}hla^*c^* + 2U_{23}klb^*c^*)\right]$$

where $U_{ij} = \beta_{ij}/2\pi^2 a_i^* a_j^* \overset{o}{A}^2$

5. The expression used to account for secondary extinction is that of W.H. Zachariasen:

$$F_{coor} = F_0\left[cBI_0 + \{1.0 + (cBI_0)^2\}^{\frac{1}{2}}\right]^{\frac{1}{2}}$$

where F_{coor} is the corrected structure factor, c is the extinction coefficient, B is a function taking into account the angular dependence of the extinction correction and I_0 is the observed integrated intensity.

6. The error on an observation of unit weight is calculated from

$$\left[\frac{\Sigma w(|F_o| - |F_c|)^2}{NO - NV}\right]^{\frac{1}{2}}$$

where NO and NV are the number of observations and numbers of variables, respectively.

7. Errors on difference are calculated from

$$\sigma_{diff} = (\sigma_1^2 + \sigma_2^2)^{\frac{1}{2}}$$

where σ_1 and σ_2 are the estimated standard deviations on the two quantities.

8. Errors on means

$$\sigma_m = \left[\Sigma (x_i - \overline{x})^2 / n(n-1) \right]^{\frac{1}{2}}$$

where $\overline{x}$ is the mean value of n observations of x. The standard deviation on the sample used to calculate the mean is given by

$$\sigma_s = \sigma_m \sqrt{n}$$

APPENDIX 3

OBSERVED AND CALCULATED STRUCTURE FACTORS

$(10|F_o|$ vs. $10|F_c|$ in electrons)

Complex	Microfilm Card
cis-dichloro(1-methylamino-2(*S*)- aminopropane)Pt(II)	1
cis-dichloro((*S*)methyl *p*-tolylsulphoxide)- (styrene)Pt(II)	2
cis-dichloro((*S*)methyl *p*-tolylsulphoxide)- (3-methyl-1-butene)Pt(II)	3
[(1,5-cyclooctadiene)(2,3-bis(diphenylphosphino)- butane)Rh(I)]ClO$_4$	4
[(bicyclo[2.2.1]hepta-2,5-diene)- (2,3-bis(diphenylphosphino)propane)Rh(I)]ClO$_4$	5

REFERENCES

1. F. Ciardelli and P. Salvadori, 'Fundamental Aspects and Recent Developments in ORD and CD', Eds. F. Ciardelli and P. Salvadori, Chapt. 1, Heyden and Son, 1973.

2. J.B. Biot, Bull. Soc. Philomath. Paris, 190 (1815).

3. L. Pasteur., C.R.H. Acad. Sci., 28, 477 (1849).

4. A. Cotton, Ann. Chim. Phys., 8, 347 (1896); C.R.H. Acad. Sc., 120, 989, 1044, (1895).

5. A. Werner, Ber. Deut. Chem. Ges., 1887 (1911).

6. E.U. Condon, W. Altar and H. Eyring, J. Chem. Phys., 5, 753 (1937); E. Gorin, J. Walter and H. Eyring, J. Chem. Phys., 6, 824 (1938).

7. J.G. Kirkwood, J. Chem. Phys., 5, 479 (1937).

8. W. Moffitt, J. Chem. Phys., 25, 467 (1951); W. Moffitt, R.B. Woodward, A. Moscowitz, W. Klyne and C. Djerassi, J. Amer. Chem. Soc., 83, 4013 (1961); W. Moffitt and A. Moscowitz, J. Chem. Phys., 30, 648 (1959).

9. W. Moffitt, J. Chem. Phys., 25, 1189 (1956); S. Sugano, J. Chem. Phys., 33, 1883 (1960).

10. J.A. Schellman, J. Chem. Phys., 44, 55 (1966).

11. S.F. Mason 'Fundamental Aspects and Recent Developments in ORD and CD', Eds. F. Ciardelli and P. Salvadori, Chapt. 2.1, Heyden and Son, 1973.

12. S.J. LaPlaca, I. Bernal, H. Brunner and W.A. Hermann, Angew. Chem., Int. Ed. Engl., 14, 353 (1975).

13. F.A. Cotton and G. Wilkinson, 'Advanced Inorganic Chemistry', p. 581; Third Edition, Wiley - Interscience, N.Y., 1972.

14. E.J. Corey and J.C. Bailar, J. Amer. Chem. Soc., 81, 2620 (1959).

15. Inorg. Chem., 9, 1 (1970).

16. C.J. Hawkins, 'Absolute Configuration of Metal Complexes', Chapt. 5, Wiley - Interscience, London, 1971.

17. N.C. Payne, Inorg. Chem., 12, 1151, (1973).

18. F.S. Richardson, J. Chem. Phys., 54, 2453, (1971).

19. F.S. Richardson, Inorg. Chem., 10, 2121 (1971).

20. F.S. Richardson, Inorg. Chem., 11, 2366 (1972).

21. S.F. Mason, J. Chem. Soc. (A), 667, (1971).

22. C.J. Hawkins and E. Larsen, Acta Chem. Scand., 19, 185, 1969 (1965).

23. R.A.D. Wentworth and T.S. Piper, Inorg. Chem., 4, 202, (1965).

24. J.I. Legg and B.E. Douglas, J. Amer. Chem. Soc., 88, 2697 (1966).

25. S.F. Mason, J. Chem. Soc., Chem. Comm., 856 (1969).

26. J.M. Tsangaris and R.B. Martin, J. Amer. Chem. Soc., 92, 4255 (1970).

27. J.A. Tiethof and D.W. Cooke, Inorg. Chem., 11, 315 (1972).

28. A.I. Scott and A.D. Wrixon, Tetrahedron, 27, 2339 (1971).

29. B. Bosnich and J. MacB. Harrowfield, J. Amer. Chem. Soc., 94, 3425 (1972).

30. S.F. Mason and R.H. Seal, J. Chem. Soc., Chem. Comm., 331 (1975).

31. 'Absolute Configuration of Metal Complexes Determined by X-Ray Analysis', Ed. Y. Saito, 1972.

32. S.F. Mason, 'Fundamental Aspects and Recent Developments in ORD and CD', p. 196, Ed. F. Ciardelli and P. Salvadori, Heyden and Son, 1973.

33. K.R. Hanson, J. Amer. Chem. Soc., 88, 2731 (1966). Under Hanson's rules the pro- nomenclature refers to a four coordinate center which becomes chiral upon replacement of one of the pair of identical ligands. Our use is an extension of the terminology to cover olefins which are able to become chiral upon coordination.

34. F.R. Hartley, Chem. Rev., 69, 799 (1969).

35. J.H. Nelson and H.B. Jonassen, Coord. Chem. Rev., 6, 27 (1971).

36. F.R. Hartley, Angew. Chem., Int. Ed. Engl., 11, 596 (1972).

37. S.D. Ittel and J.A. Ibers, Adv. Organomet. Chem., 14, 33 (1976).

38. M.J.S. Dewar, Bull. Soc. Chim. Fr., 18, C71 (1951).

39. J. Chatt and L.A. Duncanson, J. Chem. Soc., 2939 (1953).

40. K.S. Wheelock, J.H. Nelson, L.C. Cusachs and H.B. Jonassen, J. Amer. Chem. Soc., 92, 5110 (1970).

41. N. Rosch, R.P. Messmer and K.H. Johnson, J. Amer. Chem. Soc., 96, 3855 (1974).

42. J. Ashley - Smith, Z. Douek, B.F.G. Johnson and J. Lewis, J. Chem. Soc. (Daltons), 128 (1974).

43. H. Boucher, Ph.D. Thesis, University of Toronto, Toronto, Canada, 1975; H. Boucher and B. Bosnich, J. Amer. Chem. Soc., 99, 6253 (1977).

44. G. Paiaro and A. Pannunzi, J. Amer. Chem. Soc., 86, 5148 (1964).

45. R.S. Cahn, C.K. Ingold and V. Prelog, Angew. Chem., Int. Ed. Engl., 5, 385 (1966).

46. A. Pannunzi, A. DeRenzi and G. Paiaro, J. Amer. Chem. Soc., 92, 3488 (1970).

47. D. Hollings, M. Green and D.V. Claridge, J. Organomet. Chem., 54, 399 (1973).

48. D.P. Craig, L. Radom and P.J. Stiles, Proc. Roy. Soc., Lond., A343, 11 (1975).

49. B. Bogdanovic, Angew. Chem. Int. Ed. Engl., 12, 954 (1973).

50. W.S. Knowles, M.J. Sabacky and B.D. Vineyard, J. Chem. Soc., Chem. Comm., 10 (1972); J. Chem. Soc., Chem. Comm., 1445 (1968).

51. J.D. Morrison, R.E. Burnett, A.M. Aguair, C.J. Morrows and C. Phillips, J. Amer. Chem. Soc., 93, 1301 (1971).

52. H.B. Kagan and T.P. Dang, J. Amer. Chem. Soc., 94, 6429 (1972).

53. B.R. James, 'Homogeneous Hydrogenation', Wiley - erscience, N.Y. 1973.

54. M.M.T. Kahn and A.E. Martell, 'Homogeneous Catalysis by Metal Complexes', Academic Press, N.Y. 1974.

55. F.J. McQuillin, 'Homogeneous Hydrogenation in Organic Chemistry', D. Reidel, Holland, 1976.

56. R.R. Schrock and J.A. Osborn, J. Amer. Chem. Soc., 98, 2134 (1976).

57. M.D. Fryzuk and B. Bosnich, J. Amer. Chem. Soc., 99, 6262 (1977).

58. J.M. Bijvoet, A.F. Peerdeman and A.J. VanBommel, Nature, 168, 271 (1951).

59. J.M. Bijvoet, Endeavor, 71 (1955); A.F. Peerdeman, 'Anomalous Dispersion', Chapt. 1, Ed. S. Ramaseshan and S.C. Abrahams, IUCr, Munksgaard, Copenhagen, 1975; R.W. James, 'The Optical Principles of the Diffraction of X-Rays', Chapt. IV, Cornell University Press, N.Y. 1965.

60. D. Coster, K.S. Knol and J. Prins, Z. Phys., 63, 345 (1930).

61. Y. Okaya and R. Pepinsky, Phys. Rev., 103, 1645 (1956).

62. D.A. Buckingham, L.G. Marzilli and A.M. Sargeson, J. Amer. Chem. Soc., 89, 825 (1967).

63. J.R. Gollogly and C.J. Hawkins, Inorg. Chem., 8, 1168 (1969).

64. L.J. DeHayes and D.H. Busch, Inorg. Chem., 12, 1505 (1973).

65. D.A. Buckingham, L.G. Marzilli and A.M. Sargeson, Inorg. Chem., 7, 915 (1968).

66. M. Saburi, Y. Tsujito and S. Yoshikawa, Inorg. Chem., 9, 1476 (1970).

67. L.E. Erickson, M.D. Erickson and B.L. Smith, Inorg. Chem., 12, 412 (1973).

68. B. Bosnich and E. Sullivan, Inorg. Chem., 14, 2768 (1975).

69. T.C. Furnas, 'Single Crystal Orienter Manual', General Electric Co., 1957.

70. M.J. Buerger, 'X-Ray Crystallography', J. Wiley and Sons, N.Y. 1965.

71. M.J. Buerger, 'The Precession Method', J. Wiley and Sons, N.Y. 1964.

72. 'International Tables for X-Ray Crystallography', Vol. I, sect. 4.3, Kynoch Press, Birmingham, England, 1962.

73. W.R. Busing and H.A. Levy, Acta Crystallogr., 22, 457, (1967) and references therein.

74. P.G. Lenhert, J. Appl. Crystallogr., 8, 568 (1975).

75. 'International Tables for X-Ray Crystallography', Vol. IV, sect. 3.5, Kynoch Press, Birmingham, England, 1974.

76. ibid., Vol. III, sect. 2.2, 2.3 (1962).

77. ibid., Vol. I, sect. 4.7 (1962).

78. U.W. Arndt and B.T.M. Willis, 'Single Crystal Diffracto-metry' p. 174, Cambridge University Press, 1966.

79. 'International Tables for X-Ray Crystallography', Vol. II, sect. 5.2, Kynoch Press, Birmingham, England, 1962.

80. L.E. McCandlish, G.H. Stout and L.C. Andrews, Acta Crystallogr., A31, 245 (1975).

81. J. DeMeulenaer and H. Tompa, Acta Crystallogr., 19, 1014 (1965).

82. 'Crystallographic Computing', pp. 255-296, Ed. F.R. Ahmed, IUCr, Munksgaard, Copenhagen, 1970.

83. A.D. Booth, Proc. Roy. Soc., Lond., A188, 77 (1946).

84. 'International Tables for X-Ray Crystallography', Vol. I, sect. 4:5, Kynoch Press, Birmingham, England, 1962.

85. A.L. Patterson, Z. Krist, A90, 517 (1935).

86. M.J. Buerger, 'Vector Space', J. Wiley and Sons, N.Y., 1959.

87. D.T. Cromer and J.T. Waber, Acta Crystallogr., 18, 104 (1965).

88. R.F. Stewart, E.R. Davidson and W.T. Simpson, J. Chem. Phys., 42, 3175 (1965).

89. D.T. Cromer and D. Liberman, J. Chem. Phys., 53, 1891 (1970).

90. G.H. Stout and L.H. Jensen, 'X-Ray Structure Determination', Macmillan, Toronto, Canada, 1968.

91. M.J. Buerger, 'Contemporary Crystallography' McGraw-Hill, N.Y., 1970.

92. W.C. Hamilton, Acta Crystallogr., 18, 502 (1965).

93. 'International Tables for X-Ray Crystallography', Vol. II, sect. 5.4, Kynoch Press, Birmingham, England, 1962.

94. R.W. James, 'The Optical Principles of the Diffraction of X-Rays', Chapt. VI, Cornell University Press, N.Y. 1965.

95. W.H. Zachariasen, Acta Crystallogr., 23, 558 (1967).

96. J.L. Lawrence, Acta Crystallogr., A30, 454 (1974).

97. T. Ueki, A. Zalkin and D.H. Templeton, Acta Crystallogr., 20, 836 (1966).

98. D.W.J. Cruickshank and W.S. McDonald, Acta Crystallogr., 23, 9 (1967).

99. G. Gilli and D.W.J. Cruickshank, Acta Crystallogr., B29, 1983 (1973).

100. A.J.C. Wilson, 'Anomalous Dispersion', p. 325, Ed. S. Ramaseshan and S.C. Abrahams, IUCr, Munksgaard, Copenhagen, 1975.

101. G.H.W. Milburn and M.R. Truter, J. Chem. Soc.(A), 1609 (1966).

102. J. Iball, M. MacDougall and S. Scrimgeour, Acta Crystallogr., B31, 1672 (1975).

103. H. Ito, J. Fijita and K. Saito, Bull. Chem. Soc. Japan, 40, 2584 (1967).

104. D.S. Martin, M.A. Tucker and A.J. Karsman, Inorg. Chem., 4, 1682 (1965); ibid., 5, 1298 (1966); D.S. Martin, J.G. Foss, M.E. McCarville, M.A. Tucker and A.J. Karsman, ibid., 5, 491 (1966).

105. R.P. Messmer, L.V. Interrante and K.H. Johnson, J. Amer. Chem. Soc., 96, 3847 (1974).

106. J. Chatt, G.A. Gamlen and L.E. Orgel, J. Chem. Soc.,
486 (1958).

107. G. Paiaro, Organomet. Chem. Rev., A6, 319 (1970).

108. R. Palumbo, A. DeRenzi, A. Pannunzi and G. Paiaro,
J. Amer. Chem. Soc., 91, 3844, 3879 (1969).

109. R. Eisenberg and J.A. Ibers, Inorg. Chem., 4, 773
(1965).

110. E. Benedetti, P. Corradini and C. Pedone, J. Organomet.
Chem., 18, 203 (1969); C. Pedone and E. Benedetti,
ibid., 29, 443 (1971); S. Merlino, R. Lazzaroni and
G. Montagnoli, ibid., 30, C93 (1971); C. Pedone and
E. Benedetti, ibid., 31, 403 (1971).

111. U. DelaCamp and H. Hope, Acta Crystallogr., 26, 846
(1970).

112. B. Dahlen, Acta Crystallogr., B30, 642 (1974).

113. J.A.J. Jarvis, B.T. Kilbourn and P.G. Owsten, Acta
Crystallogr., 27, 366 (1971).

114. Lj.-Man. Muir and K.W. Muir, Inorg. Chim. Acta, 10, 47
(1974).

115. R. Melanson and F.D. Rochon, Can. J. Chem., 53, 2371
(1975) and references therein.

116. A. Pannunzi and G. Paiaro, J. Amer. Chem. Soc., 88,
4843 (1966).

117. W.C. Hamilton and J.A. Ibers, 'Hydrogen Bonding in
Solids', W.A. Benjamin, N.Y., 1968.

118. C.E. Bugg, J.M. Thomas, M. Sundaralingam and S.T. Rao,
Biopolymers, 10, 175 (1971).

119. E. Subramanian, J. Trotter and C.E. Bugg, J. Cryst.
Mol. Struct., 1, 3 (1971).

120. S.C. Wallwork, J. Chem. Soc. (A), 494 (1961).

121. D.J. Szalda, L.G. Marzilli and T.J. Kistenmacher, Inorg.
Chem., 14, 2076, 1686 (1975).

122. D.W.J. Cruickshank, Acta Crystallogr., 10, 504 (1957).

123. S. Shinoda, Y. Sudo, Y. Yamaguchi, T. Iwayanagi and
Y. Saito, J. Organomet. Chem., 121, 93 (1976).

124.   R.F. Fenske, Prog. Inorg. Chem., 21, 179. (1976).

125.   S.C. Nyberg, K. Simpson and W. Wong-Ng, J. Chem. Soc.
       (Daltons), 1865 (1976).

126.   R. Mason and G.B. Robertson, J. Chem. Soc. (A), 492
       (1969).

127.   A.D. Wrixon, E. Premuzic and A.I. Scott, J. Chem. Soc.,
       Chem. Comm., 639 (1968).

128.   P. Corradini, G. Paiaro, A. Pannunzi, S.F. Mason and
       G.H. Searle, J. Amer. Chem. Soc., 88, 2863 (1966).

129.   K.O. Hodgson and K.N. Raymond, Inorg. Chem., 11, 171
       (1972).

130.   S.J. LaPlaca and J.A. Ibers, Acta Crystallogr., 18,
       511 (1965).

131.   M.R. Churchill and S.A. Bezman, Inorg. Chem., 11,
       2243 (1972).

132.   P.A. Tucker, W. Schutcher and D.R. Russell, Acta
       Crystallogr., B31, 592 (1975).

133.   T.E. Nappier, D.W. Meek, R.M. Kirchner and J.A. Ibers,
       J. Amer. Chem. Soc., 95, 4194 (1974) and references
       therein.

134.   M.C.Hall, B.T. Kilbourn and K.A. Taylor, J. Chem. Soc.
       (A), 2539 (1970).

135.   J.A. McGinnety, N.C. Payne and J.A. Ibers, J. Amer.
       Chem. Soc., 91, 6301 (1969).

136.   S. Brunie, J. Mazan, N. Langlois and H.B. Kagan, J.
       Organomet. Chem., 114, 225 (1976).

137.   B.D. Vineyard, W.S. Knowles, N.J. Sabacky, G.L. Backman
       and D.J. Weinkauff, J. Amer. Chem. Soc., 99, 5946 (1977).

138.   R.G. Ball and N.C. Payne, Inorg. Chem., 16, 1187 (1977).

139.   B. Bosnich and M.D. Fryzuk, private communication.

140.   'Tables of Interatomic Distances and Configuration in
       Molecules and Ions', p. M108, Special Publication No. 11,
       The Chemical Society, London, 1958.

141.   J.M. Manoli, A.P. Gaughan and J.A. Ibers, J. Organomet.
       Chem., 72, 247 (1974) and references therein.

142. C. Potvin, J.M. Manoli, G. Pannetier, R. Chevalier and N. Platzer, J. Organomet. Chem., 113, 273 (1976).

143. J.A.J. Jarvis and R. Whyman, J. Chem. Soc., Chem. Comm., 562 (1975).

144. 'Homogeneous Catalysis II', Adv. Chem. Ser. #132, Ed. D. Forster and J.F. Roth, Amer. Chem. Soc., Washington, 1974.

145. H.B. Kagan, Pure and Appl. Chem., 43, 401 (1975).

146. R.J.P. Corrin and J.J.E. Moreou, J. Organomet. Chem., 120, 337 (1976).

147. I. Ojima, T. Kogure, M. Kumagi, S. Horiuchi and T. Sato, J. Organomet. Chem., 122, 83 (1976).

148. R. Glaser and J. Blumenfeld, Tettrahedron Lett., 29, 2525 (1977).

149. B.R. James, 'Homogeneous Hydrogenation', p. 327 - 347, Wiley - Interscience, N.Y., 1973.

150. J.A. Osborn, F.H. Jardin, J.F. Young and G. Wilkinson, J. Chem. Soc. (A), 1711 (1966).

151. P. Abley, F.J. McQuillin, J. Chem. Soc., Chem. Comm., 1503 (1969).

152. B.R. James, 'Homogeneous Hydrogenation', p. 214, Wiley - Interscience, N.Y., 1973.

153. L. Horner, H. Siegal and H. Buthe, Angew. Chem., Int. Ed. Engl., 7, 942 (1968).

154. L.E. Erickson, J.E. Sarneski and C.N. Reilly, Inorg. Chem., 14, 3007 (1975) and references therein.

155. P.B. Hitchcock, M. McPartlin and R. Mason, J. Chem. Soc. Chem. Comm., 1367 (1969).

156. R. Glaser, Tetrahedron Lett., 25, 2127 (1975).

157. W.S. Knowles, M.J. Sabacky and B.D. Vineyard, Ann. N.Y. Acad. Sci., 172, 232 (1970); reference #50; 'Homogeneous Catalysis II', Adv. Chem. Ser., #132, p. 274, Ed. D. Forster, J.F. Roth, Amer. Chem. Soc., Washington, 1974.

158. H.B. Kagan, N. Langlois and T.P. Dang, J. Organomet. Chem., 90, 353 (1975).

159. 'International Tables for X-Ray Crystallography',
     Vol. IV, pp. 276 - 277, Kynoch Press, Birmingham,
     England, 1974.

160. W.R. Busing, R.D. Ellison, H.A. Lery, S.P. King and
     R.T. Roseberry, ORNL report #4143, U.S. Atomic Energy
     Commission, 1968.

161. 'International Tables for X-Ray Crystallography',
     Vol. IV, pp. 278 - 279, Kynoch Press, Birmingham,
     England, 1974.